VEÐURSTOFA ÍSLANDS

Report
03019

Hrafn Guðmundsson

Analysis of radiosonde observations above Iceland since 1946 – data processing and interpretation

A thesis accepted by the University of Iceland for the degree of Master of Science in Geophysics

VÍ-ÞJ01
Reykjavík
April 2003

Contents

List of Figures

List of Tables

Útdráttur

Fjallað verður um úrvinnslu, greiningu og túlkun háloftagagnanna frá Keflavík. Gefin verður nákvæm framsetning á eiginleikum þeirra og aðferðarfræði úrvinnslu. Þá verða niðurstöður greiningarinnar kynntar og þær túlkaðar með hliðsjón af veðurfari á norðurhveli jarðar.

Háloftaathuganir frá Keflavík hafa verið gerðar að jafnaði tvisvar á sólarhring síðan 1946, að undanskildu tímabilinu 1946-70 þegar mælt var fjórum sinnum á sólarhring. Notast verður við tímabilið 1952-00 til að greina og túlka leitni (trend) eðlisþátta í lofthjúpi yfir Íslandi og tengsl hennar við Norðurheimskautssveifluna eða Arctic Oscillation (AO). Staðsetning Íslands hentar einkar vel til að greina merki frá AO og þar með að staðfesta þá leitni í veðra- og heiðhvolfinu sem sést hefur síðastliðna þrjá áratugi. Vegna legu landsins greinast merki AO best þar og staðfesting hnattrænna breytinga í staðbundnum breytingum veðra- og heiðhvolfs verður auðveldari.

Abstract

The structures of the leading modes of variability in the extratropical circulation in both hemispheres are deep and zonally symmetric. These annular structures are associated with geopotential height perturbations of opposing signs in the polar cap region and in the surrounding zonal ring centered near 45° latitude. Referred to as the Arctic Oscillation (AO) in the Northern Hemisphere (NH), it provides a connection between seemingly unrelated weather patterns and evident trends observed in recent decades. As a consequence, the AO may represent an excellent proxy for anthropogenic influences on a global scale. Climate models show that the observed AO trends can be induced by an increase in greenhouse gases and/or ozone depletion alone.

The AO's amplitude in the meteorological fields is maximized in the atmosphere over Iceland. Therefore, the Keflavik radiosonde station provides a unique opportunity for detecting the AO signal (which is global by nature) and evaluating its real local effect (natural or man-made) on climate.

The wintertime climate over Iceland has in recent decades developed toward stronger westerlies, a colder stratosphere, and lower geopotential heights at all levels. These trends are all related to a deeper, stronger and longer lasting stratospheric polar vortex. The development of the AO above Iceland confirms that the AO trends are the main cause for these climatic changes.

Inngangur

Háloftaathuganir frá Keflavík hafa verið framkvæmdar að jafnaði tvisvar á sólarhring síðan 1946 að undanskildu tímabilinu 1952-70 þegar mælt var fjórum sinnum á sólarhring. Nær öll háloftagögnin eru til á tölvutæku formi, utan tímabilanna 1946-51 þar sem mikið vantar af mælingum og 1946-72 þar sem vantar mælingar fyrir ofan 100 hPa. Þessi gögn eru til sem frumgögn á Veðurstofu Íslands og National Climatic Data Center, en á eftir að forvinna. Háloftagögnin hafa nú í fyrsta skipti verið sérstaklega greind í heild sinni og gerð aðgengileg í gagnagrunni Veðurstofu Íslands.

Háloftagögnin frá Keflavík henta einkar vel til að staðfesta þá leitni í veðrahvolfi og heiðhvolfi sem sést hefur síðastliðna þrjá áratugi og tengist hugsanlega athöfnum mannsins. Kemur hún fram aðallega á miðlægum breiddargráðum og heimskautssvæðunum og lýsir sér í fallandi þrýstingi, kólnun heiðhvolfs og styrkingu pólhvirfilsins. Nýlegar niðurstöður sýna fram á að þrýstingsfallið tímabilið janúar til mars og vindstyrksaukning vestlægra vinda á miðlægum breiddargráðum frá yfirborði til neðra heiðhvolfs yfir vetrarmánuðina, megi nær eingöngu rekja til jákvæðrar leitnar Norðurheimskautssveiflunnar eða Arctic Oscillation (AO). Einnig sýna sömu niðurstöður að svæðisbundin formgerð á leitni ýmissa eðlisfræðilegra kennistærða og sveifluvídd (eða merki) þeirra í AO eru nánast eins. Þetta hefur í för með sér að hámarksleitni vindstyrksins og mættishæðar liggur beint fyrir ofan Ísland. Skilgreiningin á AO byggir á normuðum yfirborðsþrýstingi eins og Norður-Atlantshafssveiflan (NAO) gerir, en þess ber að gæta að skilgreiningin á AO nær yfir stærra svæði og tengist veðurfari yfir öllu norðurhvelinu norðan við $\sim$20°N breiddargráðar, en skilgreiningin á NAO er takmörkuð við veðurfar á Norður-Atlantshafi.

Að frátaldri árstíðasveiflunni er AO meginsveiflan í lofthjúpi norðurhvels jarðar og jafnframt eins konar eiginháttur lofthjúpsins. Þar með stjórnar AO loftstraumum norðurhvels og hefur t.d. áhrif á Íslandslægðina. Talið er líklegt að sú leitni sem mælst hefur í AO undanfarna þrjá áratugi megi að hluta rekja til mannsins og að hluta til náttúrulegra sveiflna. Ekki er þó vitað hvor þátturinn er mikilvægari.

Jafnvel þótt AO skilgreiningin byggi á yfirborðsþrýsting[1], þá sjást merki hennar greinilega í heiðhvolfinu á veturna. AO er því ekki bara bundin við veðrahvolfið, sem undirstrikar mikilvægi víxlverkunar milli veðrahvolfs og heiðhvolfs. Nýlegar rannsóknir benda til þess að heiðhvolfið geti haft mikil áhrif á veðurfar við yfirborð jarðar, og þá sér í lagi í gegnum eiginhátt lofthjúpsins AO.

Fyrstu niðurstöður úr greiningu Keflavíkurgagnanna staðfesta þá afgerandi leitni í hnattrænum breytingum á þrýstingi, hita, vindi og raka frá

[1] AO er stundum skilgreind út frá þrýstingi (eða mættissviði þrýstingsflata) í nokkrum lögum veðra- og heiðhvolfs, sem gefur svipaða niðurstöðu og þegar notast er eingöngu við þrýstingssviðið við yfirborðið.

yfirborði og upp í neðri hluta heiðhvolfs sem sést hefur undanfarna áratugi í tengslum við AO. Þau ferli sem talin eru stuðla að þeirri veðurfarsleitni sem mælst hefur síðastliðin 30 ár og hugsanleg tengsl þeirra við AO eru meðal annars ræddar.

Við byrjum á því í fyrsta kafla að ræða um veðurfar norðurhvels í tengslum við pólhvirfilinn og AO. Eiginleikar pólhvirfilsins og ferli sem eru talin geta haft áhrif á hann og skýrt m.a. leitni samkvæmt mælingum síðustu áratuga eru ræddir. Merki AO á norðurhvelinu er síðan skoðað og það tengt ýmsum veðurfyrirbærum og leitni veðurfars á öllu norðurhvelinu. Síðan er lagður grunnur að því hvernig AO merkið fyrir ofan Ísland er fundið með háloftagögnunum í Keflavík. Í öðrum kafla er greint frá og ræddir eiginleikar háloftagagnanna. Einnig verður sagt frá aðferðafræði gagnaúrvinnslunnar og útreikningum. Í lok kaflans er lagt mat á óvissu mælinganna og marktækni niðurstaðnana. Í þriðja og síðasta kafla verða niðurstöður verkefnisins settar fram. Við munum sýna fram á að dægursveiflur eru óverulegar. Síðan verður þróun veðurfars síðan á sjötta áratug aldarinnar skoðuð. Við hefjumst loks handa við að greina AO merkið í lofthjúpnum fyrir ofan Ísland. Að lokum ræðum við helstu niðurstöður verkefnisins og framtíðarhorfur.

Introduction

Climate change is a subject that has received increasing attention in recent years. Main concerns pertain to the extent of anthropogenic influence on the climate, reflected most dramatically in the greenhouse effect and ozone depletion. Climate studies rely on extensive daily global observations. Consequently, data processing and analysis are essential before any assessments and interpretations can be made concerning climatic development. Ultimately, to confirm the influential factors involved or responsible for particular climatic processes, climate modelling and data assimilation are inevitable.

An important factor in the daily global upper air observation system is the global radiosonde network. The global radiosonde system dates back to the 1940s and now includes more than 2300 stations each usually conducting two observations per day. It is widely used in climate studies as well as in real time weather forecasting.

This study aims at analysing and relating the processes in the atmosphere over Iceland in the second half of the 20th century to climate change in the Northern Hemisphere. We have used data from the Keflavik radiosonde station in Iceland. In the process, the data has been made more accessible to the scientific community.

Recent studies have revealed interesting processes in the Northern Hemisphere related to the greenhouse gas increase and ozone depletion. Their previously unappreciated connection and the dramatic climatic trends the last three decades is a realization of a major climatic mode of variability. It has an important consequence for the propagation of tropospheric planetary wave energy into the stratosphere through the stratosphere-troposphere coupling scheme. Even though the understanding of many climatic processes has improved greatly in recent years, it still remains unclear how much of the trends can be attributed to anthropogenic forcing and how much to natural variability. With the Keflavik radiosonde data we get a new opportunity to assess how global climate trends are reflected regionally in meteorological field variables from the surface up to the lower stratosphere. The main contribution of this study to the subject of climate change is the establishment of a remarkably clear direct linkage between recent hemispheric meteorological trends, possibly related to human activities, and regional changes in the lower atmosphere (Homosphere) over Iceland. This has not been achieved before.

In chapter 1 we discuss the climatological structure of the Northern Hemisphere in relation to the polar vortex and the Arctic Oscillation, and outline our methodology in the detection of the AO signal. In chapter 2 the properties of the Keflavik radiosonde data are represented together with the data processing procedure and the estimation of radiosonde measurement precision. In chapter 3 the results in our analysis of the Keflavik radiosonde data are given. Finally, in chapter 4 we summarise the main results in this study and give a brief discussion on there significance.

Chapter 1

The climatological structure of the Northern Hemisphere

A main climatological features during the winter at high latitudes and polar regions in both hemispheres are called polar vortexes. Owing their existence to the meridional temperature gradient, they are characterized by annular shapes in the geopotential height and zonal wind centered at the poles, which amplify with altitude. Therefore, in the cold seasons when the meridional temperature gradient is largest, the polar vortex is strongest with extreme cold conditions in the stratosphere and strong subpolar westerlies from the surface up to the stratosphere. The polar vortex strength and position can vary considerably from year-to-year, having pronounced affects on ozone depletion, winter storm tracks, troposphere-stratosphere coupling, and sudden warmings, to name a few processes of importance. In the last three decades, the polar vortex has exhibited a significant trend towards a stronger, longer prevailing vortex, associated with the strengthening of the stratospheric jet and the cooling of the stratosphere. While the polar vortex has strengthened, the troposphere has been warming. As observational and theoretical studies indicate a dynamical coupling between the stratosphere and the troposphere, it is believed that these trends may be related. Moreover, these trends are closely related to changes in atmospheric circulation, which are manifested by a gradual reduction in high-latitude sea-level pressure, and an increase in midlatitude sea-level pressure associated with one phase of the so-called Arctic Oscillation. These trends appear through a naturally occurring mode of atmospheric variability and may be linked to anthropogenic effects.

The main atmospheric variability in the Northern Hemisphere (NH), excluding the seasonal variability, has often been associated with the so-called Northern Atlantic Oscillation (NAO[1]). Designed to describe the major fluctuating component in the NH general circulation, the NAO is regionally

[1]The NAO index is usually defined as the normalized surface level pressure difference between selected locations in Portugal and Iceland.

limited to the Atlantic sector and thus not very descriptive for the entire NH. Recent studies have convincingly reasoned that there exists a more general mode of climate variability whose barotropic[2] structure exhibits a strong longitudinally symmetric (annular) component that extends from the surface to the stratosphere in middle and high latitudes. Called the Arctic Oscillation[3] (AO), in contrast to the extensively documented Antarctic Oscillation[4] (AAO) in the Southern Hemisphere (SH), it is superimposed on the polar vortex and is responsible for controlling the climate in the NH. In the past 30 years, this mode has exhibited a trend that seems larger than its natural background variability, and may be related to human influences on stratospheric ozone and/or atmospheric greenhouse gas concentrations.

In this chapter we start in section 1.1 by describing the climatological seasonality of the wind, temperature and humidity fields from the surface to the lower stratosphere. In section 1.2 we discuss the characteristics of the polar vortex. Furthermore, we specify the processes that are thought to affect the polar vortex and are likely to explain the recent observed trends. In section 1.3 we uncover the properties of the leading mode of variability in the NH. Termed the AO, we examine its signature in the geopotential height, surface air temperature, zonal-mean temperature and zonal-mean zonal wind. Also, the important role of the AO in the stratosphere-troposphere scheme is discussed. We note the remarkable similarities in the AO signature and the climate trends in the last 3 decades and discuss the possibilities of an anthropogenically induced AO. Finally, we outline our methodology in the detection of the AO signal over Iceland.

1.1 Seasonality in climate

Before we present the climatological trends and changes, it is instructive to capture the climatological mean structure and seasonal variability of the meteorological variables of interest. The climatological mean values from the Keflavik radiosonde data presented in the following diagrams are based on the period 1973-00 between 1000 and 30 hPa. This period is chosen for technical reasons, since data in the period 1952-72 is limited to 100 hPa in this study (section 2.1).

A latitude-height cross section of the longitudinally averaged (zonal-mean) zonal wind at the time of the solstices is shown in fig. 1.1[5]. We see that in both summer and winter hemispheres there are westerly (from west to east) jets in middle latitudes at an altitude of 10 km, the approximate location of the tropopause. The tropospheric jet in the winter hemisphere

[2] i.e. only variation in pressure.

[3] Sometimes called the Northern Hemisphere Annular Mode (NAM).

[4] Sometimes called the Southern Hemisphere Annular Mode (SAM).

[5] All figures in this chapter are based on the Keflavik radiosonde data, unless stated otherwise.

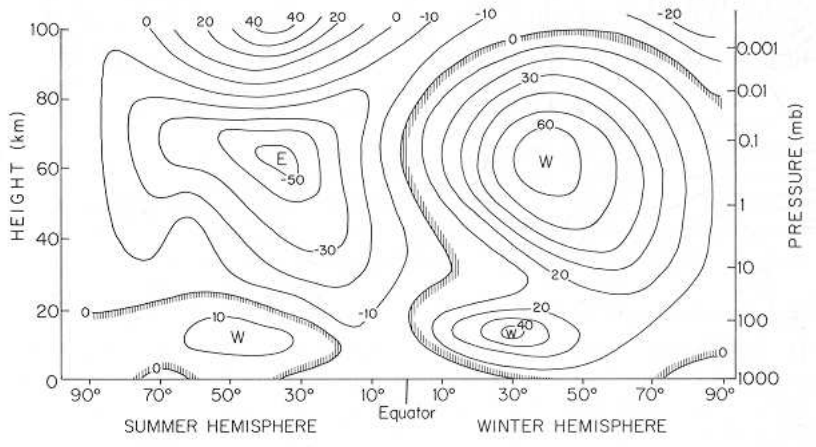

Figure 1.1: Meridional cross section of longitudinally averaged (zonal-mean) zonal wind in meters per second at the time of the solstices. Positive zonal winds denote flow from west to east (westerly flow). [From Wallace and Hobbs (1977)]

is considerably stronger than the one in the summer hemisphere, which is in accordance with the climatological monthly mean zonal wind and wind speed in fig. 1.2. The stronger winds are associated with the matched pair of mesospheric jets at 60 km, where at middle latitudes the wind undergoes a dramatic seasonal reversal between winter westerlies and summer easterlies (from east to west). In our forthcoming discussion, we will see that the main variability in the NH climate, after the seasonal variability, is associated with a close to symmetric structure of the zonal wind in midlatitudes, centered around the polar cap. We have to keep in mind that this "annular" structure is far from being perfectly symmetric, where the asymmetric features are thought to arise both from land-sea contrasts and from the topographical anomalies like the Rocky Mountains, the Tibetan Plateau and the Ural Mountains (Smagorinsky, 1953). As a consequence, the zonal-mean meteorological fields will always differ somewhat from the fields over Iceland. The comparison between these two fields will however deepen the understanding of the strong connection between the meteorological fields over Iceland, and at the same time the Atlantic sector, with the general circulation in the NH climate.

Fig. 1.2 depicts the seasonal variation of the wind speed, zonal wind, temperature and specific humidity from the surface to the lower stratosphere over Iceland. The wind speed and zonal wind show similar features and both increase with altitude in the troposphere, with approximately the same rate. The wind shows large variations in the stratosphere, which is related to the formation, in Aug-Dec, and destruction, in Feb-Apr, of the stratospheric polar vortex. Comparing the wind speed to the zonal wind, we see that the polar vortex is mainly westerly (positive contour lines in the zonal wind contour plot) and after the complete destruction of the polar

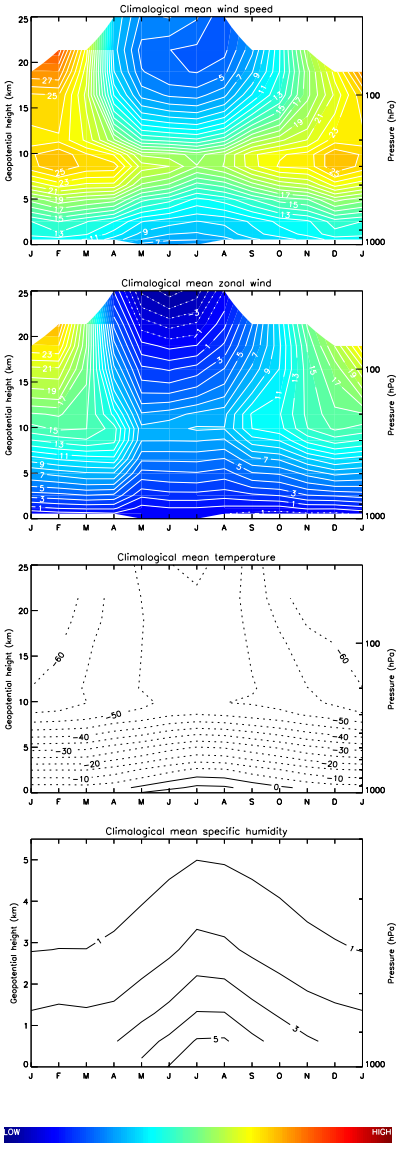

Figure 1.2: Seasonality of the climatological monthly mean wind speed, zonal wind, temperature and specific humidity for 1973-00 between 1000 and 30 hPa (except specific humidity between 1000 and 500 hPa). Contour intervals are 5 °C (-5, 0, 5, ...) for temperature, 1 m/s (-1, 0, 1, ...) for zonal wind and wind speed and 1 g/kg (-1, 0, 1, ...) for specific humidity. Dotted contour lines denote negative values. Positive zonal wind values denote westerly flow, and vice versa.

vortex in the warm months the wind is mainly easterly (negative contour lines in the zonal wind contour plot) above approximately 20 km. This is also dipicted when the zonal wind fraction of the wind speed is examined (fig. 1.3), where we see that the zonal wind is the defining component of the polar vortex and of the weak easterly winds in the summer stratosphere. The zonal wind is therefore most important in the stratosphere in the 7 cold months period Sep-Mar and 2 warm months period Jun-Jul, reaching more than 80% above approximately 15 km in the former and above approximately 23 km in the latter. Furthermore, the predominant zonal wind flow is westerly, except in the summer stratosphere and near the the surface. However, although the wind speed and zonal wind decrease rapidly with lower altitude in the troposphere, it is apparent that the zonal flow fraction of the wind speed decreases also, diving down to about 10% at the surface. The zonal flow fraction is also low in the transitional periods in the stratosphere (between the buildup and breakdown of the polar vortex.).

The formation and destruction processes of the polar vortex seem both to have a downward development in the climatological monthly mean, i.e. first appearing in the upper atmospheric levels. However, the destruction process is much more dramatic and appears to penetrate the entire troposphere, mainly affecting the zonal flow (the Apr-May contour slopes), which is evident in both fig. 1.2 and 1.3. One could point out that seasonal variations might explain this effect since the solar radiation is increasing fast in this period. If

this where true, we would also expect to see a similar effect of zonal wind decrease in the autumn. There is evidence of this in two steps occurring in Aug-Sep and in Oct-Nov in the upper troposphere above approximately 5 km, but virtually disappears in the lower troposphere. Therefore, we conclude that the zonal wind changes in the Aug-Sep period is seasonally induced and affects only the upper troposphere, while the changes in the Apr-May period are seasonally and stratospherically induced and affects the entire troposphere. This is convincing evidence of the stratosphere-troposphere coupling where stratospheric processes can have substantial effects on the tropospheric climate. Although the seasonality of the wind is mainly seen in the stratosphere, there is a considerable difference in the winter to summer wind speed in the troposphere, where the climatological difference is about 5 m/s. The cold-warm seasonal destruction of the wind speed is the following:

- Lower stratosphere: $\sim 80 - 90$ %
- Tropopause: ~ 30 %
- Surface: $\sim 40 - 50$ %

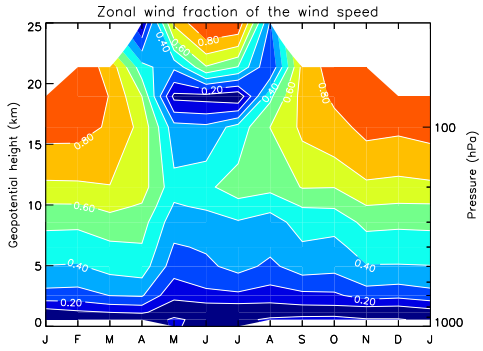

Figure 1.3: Seasonality of the climatological monthly mean zonal wind fraction of the wind speed based on data in the period 1973-00 between 1000 and 30 hPa. Contour intervals are 0.1 (0, 0.1, ..., 1).

A notable feature is the strong wind belt at the tropopause seen in the wind speed (jet stream). This is where the winds are strongest after the breakdown of the polar vortex. In addition, after the breakdown of the polar vortex the zonal wind decreases considerably at the tropopause relative to the wind speed. This means that meridional transport is predominent in the warm months at the tropopause. Finally, we see that January is on average the coldest month in the stratosphere, in agreement with the strong polar vortex at the same time, and July and August are the warmest months, which is also reflected in the specific humidity (fig. 1.2).

1.2 The polar vortex

1.2.1 Spatial and temporal properties

The climatological structure of isobaric surfaces in the stratosphere, extending from high latitudes to the polar caps, is characterized by deep, zonally symmetric or "annular" structure of the isobaric surfaces. Induced by the thermal contrasts between the polar and midlatitude regions (meridional temperature gradient), this annular structure is responsible for maintaining the westerly winds through the thermal wind equation (see section A.1 for the derivation)

$$\frac{\partial \mathbf{V}_g}{\partial \ln p} = -\frac{R}{f}\mathbf{k} \times \nabla_p T \tag{1.1}$$

and is referred to as the polar vortex. Fig. 1.4 shows the climatological wintertime 50 hPa height field for 1958-97 and pictures a near annular shape of the stratospheric polar vortex. From this figure we see that the climatological depth (or amplitude) of the wintertime polar vortex at the 50 hPa level is about 1 km, with the maximum depression over the polar caps and extending to middle latitudes. This can be interpreted as the mean maximum depth of the polar vortex at 50 hPa since the polar vortex is strongest in the wintertime. Furthermore, from fig. 1.5 (left) it is evident that the climatological seasonality of the 50 hPa geopotential height over Iceland is approximately 1.4 km and the meridional pressure gradient changes signs over the warm seasons (values above the horizontal line), signifying the complete destruction of the polar vortex at that time. We therefore conclude that the amplitude of the seasonal variability of the polar vortex is approximately the same as its wintertime climatological depth. This is in accordance with the polar vortex being completely dissipated in the warm seasons.

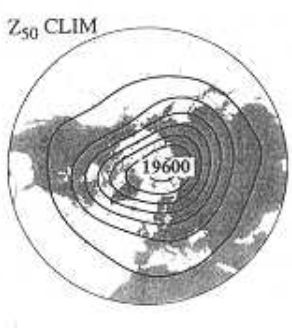

Figure 1.4: Climatological wintertime (Nov-Apr) 50 hPa height field for 1958-97. Contour interval is 150 m. [From Thompson and Wallace (1998)]

As for the geopotential height, the polar vortex has a distinct seasonality reflected in the temperature and zonal wind fields. Shown in fig. 1.5 (right) are the temperature, in black, and zonal wind, in red, at 50 hPa over Iceland. We see from the climatological zonal wind variability that the polar vortex five month buildup period is in Aug-Jan. Starting in mid-August, the zonal wind speed reaches its maximum speed of more than 30 m/s in mid-January. This amounts to a buildup speed between 6-7 m/s per month. The most notable feature of the zonal wind in the buildup period, is the ridge like shape centered around November, which signifies a sudden slow-down when the buildup process is half way through.

The climatological lifetime of the polar vortex peak is approximately two months, centered around the Jan-Feb period. However, there seems to be a characteristic depression in this period, which may signify the high occurrences of an early semi-breakdown at the end of January and a late recovery at the beginning of February. Late February marks the beginning of the polar vortex abrupt breakdown, lasting little more than two months in the period Feb-Apr, which is about half the time of the buildup process. This amounts to a breakdown speed of approximately 15 m/s per month. The polar vortex is completely destroyed in late April. The zonal wind at 50 hPa is easterly for a little more than three months in the warm period May-Aug. The temperature variability is consistent with the development of the polar vortex, reflecting cold conditions when the polar vortex is strongest. Moreover, the temperature minimum and zonal wind maximum coincide in mid-January. Apart from being more dynamic in the cold months, the temperature seems to have two distinct warm peaks on both sides of January, which are centered at early December and mid-February. These peaks most likely reflect the increase in sudden warming events, which are usually referred to as early (before January) and late (after January) sudden warmings. Assuming that this is a correct hypothesis, we can state that sudden warmings in the lower stratosphere are most likely to occur in early December and in mid-February. Furthermore, these warm peaks are likely the cause of the November ridge and the late-January early semi-breakdown of the zonal wind.

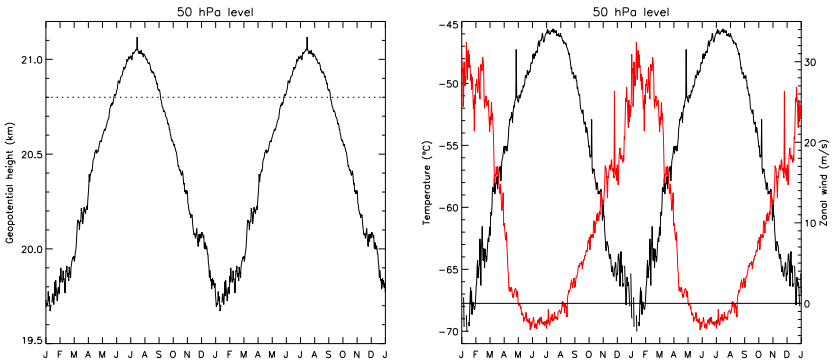

Figure 1.5: Seasonality of the climatological daily mean 50 hPa geopotential height (left), temperature (right) and zonal wind (right, red) for the period 1973-00. Note that the annual cycle is repeated for clearity The horizontal line in the figure at left indicates the annual-mean, tropical (20°N-20°S) 50 hPa height. Values below this line indicate an equator-pole gradient consistent with westerly flow, and vice versa. Positive zonal wind values denote westerly flow, and vice versa. The apparent peak occurs in 25th of November 1999 and is an error in the wind measurements

1.2.2 Processes affecting the polar vortex

The main elements affecting the polar vortex, due to human and/or natural variability, are:

- Greenhouse gas (GHG) concentration
- Ozone depletion
- Upward planetary wave propagation from the troposphere to the stratosphere
- Major volcanic eruptions
- Sudden warmings
- Stratospheric water vapor

All these elements have shown trends that contribute to a stronger polar vortex.

The recent increase in GHG concentrations is due to human activity and is reflected in the well known global warming dilemma. Although this is the main consequence of GHG buildup there are other subtle processes inherent. The main GHGs are CO_2 and H_2O. Since CO_2 is chemically inert, it is eventually homogenized by atmospheric motions up to 100 km altitude (homosphere). H_2O is also chemically inactive, but unlike CO_2, it is constantly being formed and destroyed in large regions around the globe, and consequently never becomes homogenized in the atmosphere. The high CO_2 concentration traps the heat radiated from the earths surface and consequently less heat reaches the overlaying stratosphere, which cools and thereby strengthens the polar vortex. Furthermore, the so-called cooling-to-space (direct thermal emission to space) is greatly enhanced since the radiation at stratospheric levels can more easily escape into space without being blocked by dense GHGs, which is the case in the troposphere. As a consequence, the radiative emission rate to space is proportional to the density of stratospheric GHGs. Therefore, stratospheric GHGs further contribute to the stratospheric cooling.

Recent studies have emphasized the GHG and ozone coupling and supported a stronger connection than previously thought (Shindell et al., 1998). With the buildup of CO_2 and other GHGs, the stratosphere gradually cools. Using model simulations, Shindell et al. (1998) have suggested that these cooling changes are largest in the upper stratosphere, well above the region of peak O_3 concentrations. This cooling of the upper stratosphere would lead to slightly higher concentrations of O_3 at that location due to the temperature dependence of the chemical reaction rates of several key reactions. But this effect has been masked by depletion of upper stratospheric O_3 driven by the release of industrial CFCs[6]. However, more importantly, Shindell et al.

[6]CFCs (chlorofluorocarbons) where commonly used in refrigerants, foams, spray propellants, etc. The CFCs are relatively inert species in the lower atmosphere and are transported upward without being destroyed. When the reach the middle stratosphere they decompose into free chlorine atoms (Cl) and other components under the influence

(1998) show that increasing concentrations of GHG may currently be leading to colder, more stable stratospheric polar vortex in winter, accelerating the chemical removal of lower stratospheric O_3 at high latitudes. Their calculations indicate a continuation of decrease in the total column abundance of O_3 in the Arctic vortex for the next 15 years, after levels of stratospheric chlorine begin to decline. The ideal conditions for rapid ozone loss are low temperatures[7], high concentrations of ClO and long periods of daylight. However, since ozone is a GHG, reduced ozone during the polar night slightly reduces the radiative cooling of the polar stratosphere, thus slightly counteracting the effects of GHGs. In spring, however, reduced ozone and increased GHGs both act in the same direction, strengthening and stabilizing the polar vortex.

Climate models, that account for stratospheric dynamics, have verified that increasing GHGs have significant influences on the propagation of planetary waves from the troposphere into the stratosphere (Shindell et al., 1999). The meridional temperature gradient near the tropopause increases as the tropics and midlatitudes warm, while the high latitudes cool, enhancing the zonal wind at these levels. This results in a deflection of high-latitude wave energy away from the lower stratosphere. The zonally-averaged vertical circulation is then enhanced, with greater rising motion in the polar latitudes and descent between 40° and 55°N, continuously from the surface to the middle stratosphere, in accordance with the deep barotropic nature of the Arctic Oscillation (section 1.3. This results in a cooling northward of about 55°N, and a warming at lower latitudes, and a corresponding increase in the westerly zonal wind around 55°N from the surface up to about 1 hPa. The net result is a strengthening polar vortex aloft, while the enhanced zonal circulation at the surface leads to a greater advection of warm marine air onto land, and of cold continental air over the oceans. Thus stratospheric dynamics modulates the propagation of tropospheric energy, in addition to altering the stratospheric energy budget itself. Since the strengthening of the polar vortex is associated with the decrease in Arctic surface level pressure (SLP), which again is in association with anomalies in surface air temperature (SAT), these results suggest that the stratosphere can influence climate at the surface by modulating energy propagation out of the troposphere (Shindell et al., 1999).

Major volcanic eruptions contribute to further dynamical cooling of the stratosphere at polar regions and thereby the strengthening of the polar vortex (Kodera, 1994; Kodera and Yamazaki, 1994). Volcanic aerosols injected into the stratosphere lead to extra heating in the stratosphere, especially at

---

of solar ultraviolet radiation. The free Cl atoms can then react with the ozone leading to ozone destruction.

[7]Whenever the temperatures fall below 195 K, the so-called heterogeneous reactions are triggered. This means that the formation of polar stratospheric clouds or supercooled sulphate aerosol commences, substantially enhancing the ozone depletion.

low latitudes, by absorbing solar radiation or long-wave radiation from the earth, and as a result, a negative meridional temperature gradient is created in the stratosphere at lower latitudes, enhancing the westerlies.

As mentioned above, a strong polar vortex is characterized by a cold pool of wintertime stratospheric air over the polar region. This cold pool is highly variable in the NH and often disappear completely for periods of a few weeks during midwinter, associated with an abrupt rise in temperature. These warming events are known as stratospheric sudden warmings. Therefore, sudden warmings weaken or completely dissipate the polar vortex. The recovery of the polar vortex after a sudden stratospheric warming is largely a radiative process and is relatively slow. Shindell et al. (1998) show that temperature and wind changes induced by the increasing GHG concentrations alter planetary-wave propagation in their model, reducing the frequency of sudden warmings in the NH. This results in a more stable Arctic polar vortex, with significantly colder temperatures in the lower stratosphere and concomitantly increased ozone depletion. Shindell et al. (1998) also find that the Arctic ozone loss is extremely sensitive to a reduction in the frequency of sudden stratospheric warmings, since fewer sudden warming events mean colder temperatures that promote enhanced ozone reduction.

It seems that the stratospheric cooling over the last few decades can be linked completely to anthropogenic influences through the GHG increases and ozone depletion, and as such provides one of the best pieces of evidence for anthropogenic cause to climatic change. However, de F. Forsters and Shine (1999) have showed that increases in stratospheric water vapor may be capable of causing as much of the observed cooling as ozone loss does. Since the reasons for the stratospheric water vapor increase are neither fully understood nor well characterized, their findings casts doubts on whether the cooling of the lower stratosphere can yet be fully attributable to human influences.

1.2.3 Trends

In the last three decades the polar vortex has strengthened substantially (Zurek et al., 1996; Kodera and Yamazaki, 1994). This is associated with the cooling trend in the stratosphere (Angell, 1988, 1991, 1999), which is observed to be greatest in winter (Angell, 1988). Trends toward increasing GHG, decreasing stratospheric ozone, reduced frequency of sudden warmings, increasing stratospheric water vapor and decreasing upward planetary wave energy to the stratosphere are all contributing to a colder stratosphere and thereby to a stronger more stable polar vortex. The main processes that are responsible for the strengthening of the polar vortex are likely a combination of many, both natural and anthropogenically induced.

1.3 Annular modes in the extratropical circulation

In recent decades the NH wintertime climate has undertaken drastic changes reflected in major weather patterns from the surface to the lower stratosphere. These climatic changes are reflected for example in the increase in wintertime storminess in the northeastern Atlantic and the North Sea (Marshall and Kushnir, 1997), warming of the high-latitude lower troposphere over the Eurasian and North America continents (Thompson et al., 2000), cooling of the lower troposphere over Greenland, eastern Canada and Labrador (Thompson et al., 2000), cooling of the lower stratosphere over the polar cap region (Angell, 1988, 1991, 1999; Thompson et al., 2000), a reduction in total column ozone poleward of 40°N (Thompson et al., 2000), significant decrease in the Arctic sea ice (Wang and Ikeda, 2000), strengthening of the subpolar westerlies from the surface to the lower stratosphere (Thompson et al., 2000) and precipitation increases over northern Europe, Alaska, northern Mexico, and central China, and the decreases over central North America, southern Europe, and eastern Asia (Thompson et al., 2000). It is believed that all these trends can be linked, at least in part, with a trend in a main internal mode of climatic variability in the extratropical NH called the Arctic Oscillation (AO) (Refer to Kerr (1999) for a short introduction to the AO). The first decisive definition and description of the NH annular mode and the AO index was given by Thompson and Wallace (1998). They showed that the NH annular mode (or the AO index) has exhibited a trend toward higher positive amplitude (or positive polarity), which in turn induces the weather patterns and trends that are seen in observations.

1.3.1 The AO signature

Superimposed on the polar vortex is the AO, which is apparent in all seasons throughout the troposphere and extends up to the stratosphere in the wintertime when its amplitude is greatest (Thompson and Wallace, 2000; Baldwin and Dunkerton, 1999). This signal is best seen in the wintertime SLP field, which is coupled to strong fluctuations at the stratospheric levels on the intraseasonal, interannual and interdecadal time scales, and can be interpreted as the surface signature of modulations in the strength of the polar vortex aloft. Apart from the seasonal variability, the AO is the leading mode of climatic variability in the NH. The AO is characterized by deep, zonally symmetric or "annular" structure of the isobaric surfaces, with geopotential height perturbations of opposing signs in the polar cap region and in the surrounding zonal ring centered near 45° latitude. Fig. 1.6 depicts the NH annular mode structure in the wintertime mean 10, 30, 50, 100, 200, 300, 500, 700, and 1000 hPa height anomaly fields.

The variations at the stratospheric levels and in the mean SLP field are dominated by zonally symmetric barotropic, meridional seesaw in the at-

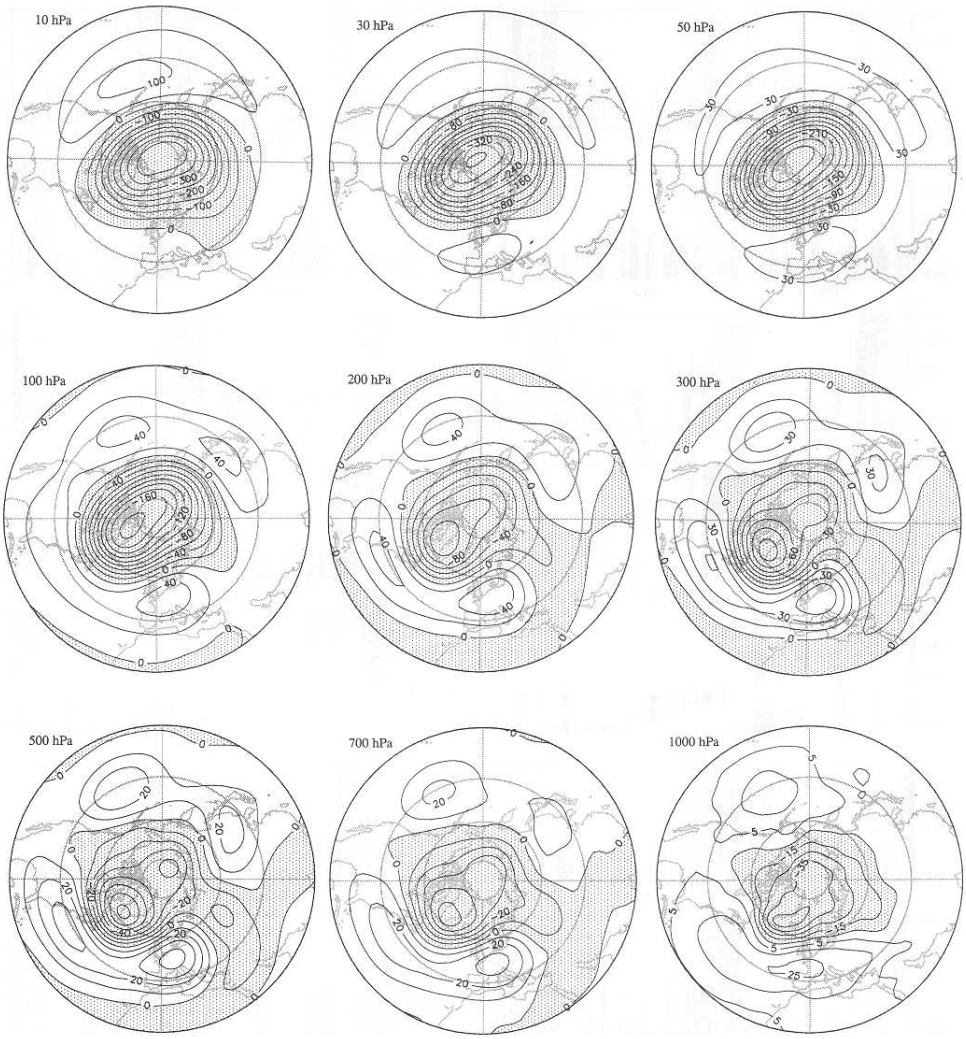

Figure 1.6: Signatures of the Arctic Oscillation (AO) at 10, 30, 50, 100, 200, 300, 500, 700, and 1000 hPa based on Dec-Feb means for the period 1958-1997. Each panel is produced by regressing the AO index with geopotential. Contour values are meters, corresponding to a one standard deviation anomaly in the AO index. The contour interval of the 1000 hPa panel is $\pm 5, \pm 15, \ldots$ for ease of comparison with Thompson and Wallace (1998, 2000). The AO index used is based on the leading EOF of a deep layer of the wintertime stratosphere-troposphere, represented by five geopotential fields at 1000, 300, 100, 30 and 10 hPa, using 90-day low-pass-filtered data north of 20°N in the period 1958-97. [From Baldwin and Dunkerton (1999)]

mospheric mass between the Arctic and the midlatitudes that amplifies by a factor of ~ 5 from the surface to the lower stratosphere according to Thompson et al. (2000). Due to its isobaric annular shape, resembling to the polar vortex structure, the AO is comparable to an oscillating drumhead, which alters the strength of the polar vortex. However, unlike the drumhead in which the fluctuations tend to be periodic, AO-related climatic fluctuations are irregular and occur on wide range of time scales. The AO is a substantial portion of seasonal variability as seen when compared to the amplitude of the polar vortex, or about 50% of the total variance of the 50 hPa geopotential height according to Thompson and Wallace (1998) (Compare the AO amplitude at 50 hPa in fig. 1.6 with the climalogical mean wintertime amplitude at 50 hPa in fig. 1.4).

The AO signal is extracted from climatic data using the so-called empirical orthogonal function (EOF) analysis, sometimes referred to as the principle component analysis (see Wilks (1995) and Peixoto and Oort (1992) for extensive mathematical representation of the method). However, there is not a unified method in extracting this signal. Thompson and Wallace (2000) apply the EOF analysis on monthly mean NH SLP data, poleward of 20°N, for the period 1958-97 to obtain this leading mode. It is important to realize that the AO is not just the leading mode of the surface, and not just of the winter months. Baldwin (2000) even claim that it is possible to obtain the AO without the EOF analysis. Baldwin and Dunkerton (1999) point out that the AO signal is extremly robust, since it may be recovered using a veriety of data levels and techniques, and it is not sensitive to the number of months included in the winter season. In their analysis, the AO pattern is identified as the leading EOF of a deep layer of the wintertime stratosphere-troposphere, represented by five geopotential fields at 1000, 300, 100, 30 and 10 hPa, using 90-day low-pass-filtered data north of 20°N. The AO index is then defined as the the daily time series of the first EOF mode (often called the EOF time series), where the positive values of the index correspond to negative height anomalies over the polar cap, and vice versa. Once the AO index has been produced, it is possible to extract the AO signal by regressing it with a particular field[8]. This was done for the height field in fig. 1.6. For clarity, we should note that the regressional maps all represent the AO pattern of a particular field corresponding to a positive polarity of the AO of one standard deviation. In our study we use the AO index as defined by Thompson and Wallace (2000) and obtain it via the internet at: *http://jisao.washington.edu/data/annularmodes/Data/ao_index.html*

[8]Equivalently, The calculation of the first EOF mode for a particular meteorological field would also represent the AO signature (or amplitude) for that field. Fields regressed on the annular mode (AO index) and their first EOF mode are both referred to as the AO signatures in the specific field.

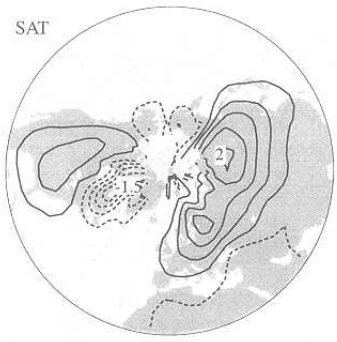

Figure 1.7: Surface air temperature regressed upon the standardized monthly time series of the annular modes (the AO index) for Jan-Mar. Contour intervals are 0.5°C (-0.75, -0.25, 0.25, ...). [From Thompson and Wallace (2000)]

The AO pattern is not only seen as a barotropic structure in the geopotential as shown in fig. 1.6. The AO index also exhibits distinct signatures in temperature and wind fields. These signatures can be obtained by regression of the AO index with the fields (A similar result is obtained by calculating the difference between periods of high and low AO index as in Hartmann et al. (2000)). The AO index exhibits a distinct baroclinic[9] signature confined to the troposphere (fig. 1.7). Thompson and Wallace (1998) have argued that the barotropic and baroclinic signatures are components of a single modal structure, in which the baroclinic features are induced by horizontal temperature advection by the zonally symmetric component of the flow acting upon the large east-west thermal contrasts at high latitudes during the NH winter. The induced baroclinic signatures are, contrary to the barotropic, reflected in a zonally asymmetric SAT distribution as seen in fig. 1.7. The positive polarity of the wintertime AO is associated with positive SAT anomalies throughout high latitudes of Eurasia and much of North America, and negative anomalies over extreme eastern Canada, North Africa, and the Middle East. This zonally asymmetric pattern of SAT anomalies is evident throughout the year except during the NH summer months according to Thompson and Wallace (2000).

The AO signature of the zonal-mean zonal wind has a distinctive meridional dipole structure with a center of action around 40°N (fig. 1.8b). In terms of the climatological zonal-mean zonal flow pictured in fig. 1.1, we see that for high AO polarity, the tropospheric jet is displaced poleward of its climatological position, vertical shear in the high latitude troposphere and lower stratosphere is increased. In the subpolar region the westerlies strengthen from the surface to the lower stratosphere for a high AO polarity, with a maximum centered around 55°N in the lower troposphere, tilting poleward with height to ~ 65°N in the upper troposphere-lower stratosphere. This signature is reflected in the correlations between the AO index and the zonal-mean zonal wind in fig. 1.8a, where the maximum correlation is centered around 55°-65°N in the troposphere and stratosphere.

The AO signature of the zonal-mean temperature is characterized by a deep polar temperature anomaly extending from the upper troposphere to the middle stratosphere, with a weaker compansating anomaly south of

[9] i.e. variations in pressure and temperature.

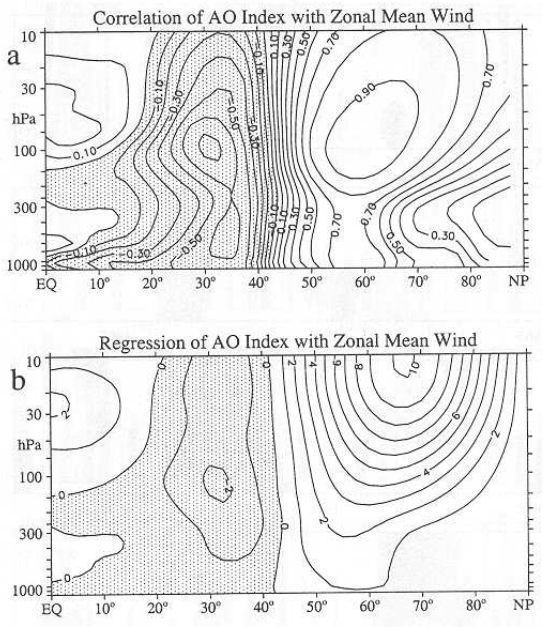

Figure 1.8: (a) Correlations between zonal-mean zonal wind and the AO index during Dec-Feb. The minimum correlation is -0.72, and the maximum is 0.96. (b) Same as fig. 1.8a, except regression between zonal-mean zonal wind and the AO index. Contour intervals are meters per second, corresponding to a one standard deviation anomaly in the AO index.[From Baldwin and Dunkerton (1999)]

$\sim 50°$N (fig. 1.9). In the tropics the anomaly is confined to the stratosphere. Therefore, the high AO polarity deepens the wintertime stratospheric polar vortex, making it colder and increasing the meridional temperature gradient, which enhances the subpolar westerlies as pictured in fig. 1.8b.

It becomes clear from the above discussions that radiosonde stations located in the latitudinal band 55°-65°N, is conveniently located for the purpose of AO detection. Moreover, the Keflavik radiosonde station, in which this study is based on, is not only in this important latitudinal band, but also located in the Atlantic sector amidst the persistant Icelandic low and in the path of the storm tracks. It is also evident from the amplitude of the AO in the height field in fig. 1.6, that its annular barotropic structure is symmetric about the polar cap in the stratosphere. However, this signal becomes increasingly tilted toward the Atlantic sector at lower altitudes in the troposphere and eventually, at the surface, the maximum AO amplitude is approximately over Iceland. These apparent asymmetric features introduced in the lower tropospheric AO signature and the tilt toward the Atlantic sector is a consequence of land-sea contrasts and topographical anomalies. The station therefore lies at the heart of the AO dynamics, where the eddy forcing due to stationary waves is most important (Limpasuvan and Hartmann, 1999b). In addition, stratosphere-troposphere coupling is best reflected over

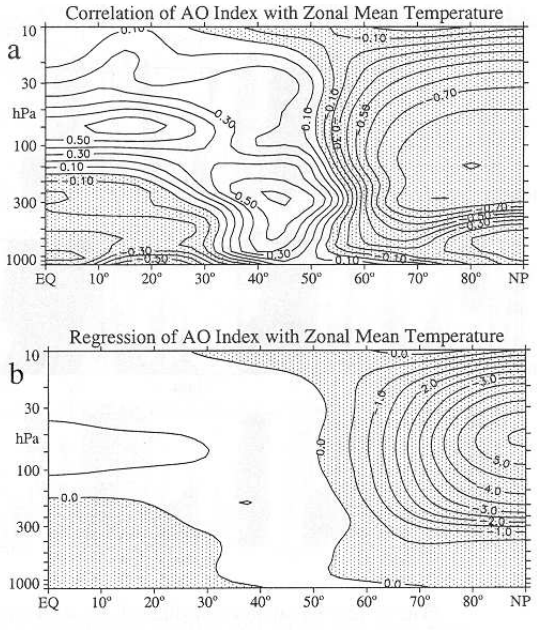

Figure 1.9: (a) Correlations between zonal-mean temperature and the AO index during Dec-Feb. The minimum correlation is -0.90, and the maximum is 0.65. (b) Same as fig. 1.9a, except regression between zonal-mean temperature and the AO index. Contour intervals are meters per second, corresponding to a one standard deviation anomaly in the AO index.[From Baldwin and Dunkerton (1999)]

the North Atlantic and Europe (Baldwin and Dunkerton, 1999).

Until recently, the stratosphere has been ruled out as an important factor in the tropospheric climate and only thought of as insignificant when it comes to weather forecasting. The AO has opened a new perspective in the stratosphere-troposphere coupling scheme and both upward and downward wave propagation have been varified in recent studies. The upward wave propagation from the troposphere to the stratosphere is well known. In the high AO phase, the poleward displacement of the tropospheric jet and the increasing high latitude wind shear from the surface to the lower stratosphere, which in turn ducts the planetary wave activity equatorward and therefore it is less likely to propagate into the stratosphere and disturb the polar vortex (Limpasuvan and Hartmann, 1999b). Shindell et al. (1999) have even suggested that the stratosphere influences climate at the surface by modulating energy propagation out of the troposphere. However, direct feedback in the opposite direction was usually thought negligible until recently. Downward propagation of stratospheric disturbances into the troposphere has been observed in data and simulated in general circulation models. Findings based on studies of volcanic effects on the atmosphere where the first clues indicating that downward propagation from the stratosphere to the troposphere is of any importance. Kodera (1994); Kodera and Yamazaki (1994) have

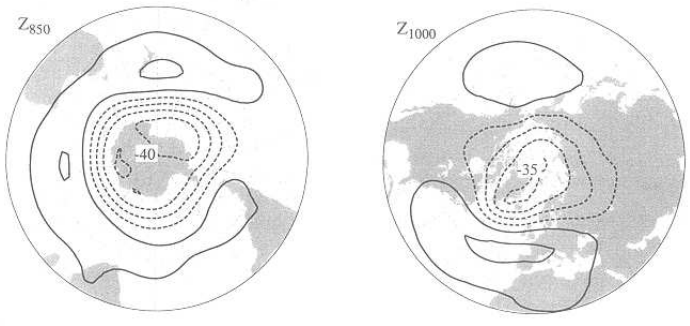

Figure 1.10: Lower tropospheric geopotential height (at 850 hPa in SH and 1000 hPa in NH) regressed on the standardized indices of the annular modes, the AO (right) and its SH counterpart, the AAO (left). [From Thompson and Wallace (2000)]

confirmed that stratospheric anomalies induced by volcanic aerosols in the stratosphere tend to propagate downwards into the troposphere producing considerable changes. Baldwin and Dunkerton (1999) show that AO anomalies typically appear first in the stratosphere (at 10 hPa or above) and propagate downward in approximately 3 weeks, resulting in changes to the storm tracks and strength of the midtropospheric flow, especially over the North Atlantic and Europe. Using a method known as piecewise potential-vorticity (PV) inversion, Hartley et al. (1998) show that stratospheric dynamics and its feedback on the troposphere are more significant for climate modelling and data assimilation than was previously assumed. Using the fact that surface cyclones tend to be steered by the 500 hPa flow and typically move at $\sim 1/3$ the speed of the 500 hPa wind, Baldwin and Dunkerton (1999) show that the difference between two positive and negative AO extremes at the 500 hPa level suggest dramatic difference in the location of storm tracks and surface cyclone activity.

The AO has a counterpart in the SH called the Antarctic Oscillation (AAO). Thompson and Wallace (2000) use monthly data to show the similarity between NH and SH annular modes in the geopotential height at the surface. In fig. 1.10 we see there striking resemblance in meridional scales and amplitude, which are predominantly zonally symmetric (the AAO structure somewhat more so). Both exist year-round in the troposphere and amplify up into the stratosphere during the active seasons (January-March in the NH and November in the SH) when the zonal flow is conducive to strong planetary wave-mean flow interaction. Due to land-sea contrasts in the NH, the annular modes in the NH appear less symmetric in structure compared to the modes in the SH. Parts of the NH annular ring over land masses are still missing, but Thompson and Wallace (2000) put that down to obstacles like Rocky Mountains and the Tibetan Platean and to temperature contrasts between land and sea that can disrupt weather patterns. Also, high land-sea contrasts promotes planetary wave propagation, which is reflected in the

more dynamic and longer lasting active seasons in the NH (section 3.4).

It should be kept in mind that the observed structure, amplitude, and time scale of both the AO and AAO in the troposphere are free annular modes, internal modes of tropospheric variability that will occur in the absence of any external forcing. This has been verified with climate model simulations with the climatological sea surface temperature distribution (Shindell et al., 1999; Limpasuvan and Hartmann, 1999a,b; Graf et al., 1998). Since the annular modes are a natural atmospheric response, it is likely that they can change minor perturbations into major climate shifts. This could explain how modest stratospheric forcing can lead to significant response in the tropospheric annular modes that is supported by strong dynamical feedbacks within the troposphere. Therefore, it is likely that the dynamical linkage between annular variability in the troposphere and stratosphere are very strong and changes above and below the tropopause influences the behaviour of the annular modes at all levels.

1.3.2 Recent climate trends associated with high AO polarity

Various indices related to the NH annular mode, including the AO index, have exhibited a pronounced drift toward the high index polarity during the past few decades that appears to be unprecedented in the historical record, which is reflected in patterns of e.g. SLP, geopotential height, and SAT trends[10]. These trends are clearly reflected in the color spectrum of the monthly AO index time series in fig. 1.14 and in the Jan-Mar mean of both AO and NAO index time series in fig. 1.15.

As we mentioned above, recent climatic trends that have been observed are nearly all, if not all, associated with the trend observed in the AO index. Thompson et al. (2000) calculate various trends for the 30-year period 1968-97 and partition them into linearly congruent[11] and linearly independent (or residual) components. Using this method they conclude that:

- virtually all of the Jan-Mar geopotential height falls over the polar cap region,
- virtually all of the strengthening of the subpolar westerlies from the surface to the lower stratosphere,
- ∼50 % of the Jan-Mar warming over the Eurasian continent,

[10]The AAO has also shown a trend toward its high index state in recent years (Thompson et al., 2000)

[11]The components of the trends that is linearly congruent with the monthly AO index is estimated by regressing monthly values of the particular time series onto the AO index, and then multiplying the resulting regression coefficient by the linear trend in the AO index.

- ∼30 % of the Jan-Mar warming over the NH as a whole,
- ∼40 % of the Jan-Mar stratospheric cooling over the polar cap region,
- and ∼40 % of the March total column ozone losses poleward of 40°N

are linearly congruent with the AO, or equivalently, can be explained by the recent trend exhibited by the AO index. Therefore, the trends in the annular modes should be reflected best in the geopotential height falls and the subpolar westerlies. Since Iceland is situated virtually at the center of the maximum amplitude of the AO, reflected in the geopotential in fig. 1.6 and in the zonal-mean zonal wind in fig. 1.8b, it is safe to say that with the Keflavik radiosonde data we have a grandstand for detecting the AO signature and the trends associated with it. Also, implicitly included in the above results is the remarkable similarity between recent climate trends and the structure of the annular modes in the month-to-month variability. This is pictured in fig. 1.11, where trends in the 1000 and 50 hPa geopotential heights, SAT, precipitation, zonal-mean zonal wind and zonal-mean temperature are shown (Compare this figure with the annular modes in fig. 1.6, 1.8b and 1.9b).

To summarise, we list the main climatic processes associated with a high wintertime AO period:

- Colder stratosphere
- Stronger polar vortex
- Enhanced reduction of ozone in springtime
- Decrease in stratospheric sudden warmings events
- Warming over the Eurasian and North American continents
- Cooling over Greenland, Labrador and eastern Canada
- Increasing cyclonic activity in the Atlantic sector
- Storm track displacement
- Strengthening of the westerlies from the surface to the lower stratosphere
- Decrease in Arctic sea ice

As mentioned before, the stratospheric cooling has been fully established. The trend toward high AO polarity results in geopotential falls over the polar caps and thereby colder conditions aloft in the upper troposphere and the lower stratosphere. This in turn increases the meridional temperature gradient and thereby enhances the zonal wind flow, strengthening the wintertime

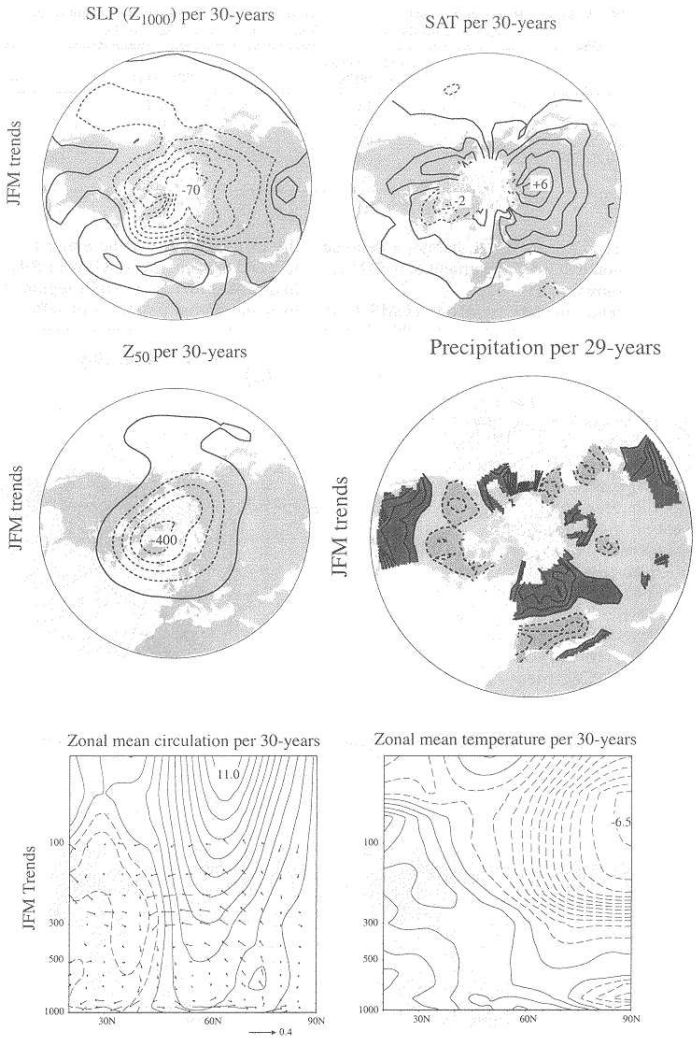

Figure 1.11: Linear Jan-Mar trends in (top, left) SLP expressed as 1000 hPa geopotential height, Z_{1000}, (top, right) 50 hPa height, Z_{50}, (middle, left) SAT, (middle, right) precipitation, (bottom, left) zonal-mean zonal wind, and (bottom, right) zonal-mean temperature. All trends are based on the 30-year period 1968-97, except the precipitation on the 29-year period 1968-96. The vectors in the zonal-mean zonal wind is the meridional circulation. For the precipitation contour, dark shading indicates increased precipitation of at least +10%; light shading indicates reduced precipitation of at least -10%; the zero contour line is omitted. Negative contours are dashed. Contour intervals are 15 m (30 yr)$^{-1}$ (-22.5, -7.5, +7.5, ...) for SLP, 100 m (30 yr)$^{-1}$ (-150, -50, +50, ...) for Z_{50}, 1 K (30 yr)$^{-1}$ (-1.5, -0.5, +0.5, ...) for SAT, 10% (29 yr)$^{-1}$ (-10, 10, 20, ...) for precipitation, 1 ms^{-1} (30 yr)$^{-1}$ (-1.5, -0.5, +0.5, ...) for zonal wind, and 0.5 K (30 yr)$^{-1}$ (-0.75, -0.25, +0.25, ...) for zonal-mean temperature. [From Thompson et al. (2000)]

polar jet. Associated with the high AO polarity are fewer sudden warming events, since these events cause the AO index to rapidly become negative followed by a slow recovery (Baldwin and Dunkerton, 1999). The horizontal flow associated with a high AO polarity induces a characteristic SAT distribution which results in a warming over the Eurasian and North American continents and cooling over Greenland, Labrador and eastern Canada.

1.3.3 Perturbation of the AO; Anthropogenically and/or naturally induced AO

As of yet, the controlling mechanism behind the low frequency variability of the AO is not understood. Since the AO is a highly robust mode of climate variability, it is believed that minor perturbations of anthropogenic origin can easily tip the AO in such a manner that major climatic shifts result.

Kodera (1994); Kodera and Yamazaki (1994) offer evidence that the volcanic aerosols injected into the stratosphere induce weather patterns similar to high AO climate patterns. Volcanic aerosols are thought to produce a stronger polar vortex in the winter stratosphere, as mentioned in section 1.2.2. They also state that after major volcanic eruptions, the following winter has stronger zonal-mean zonal winds in the polar region but weaker around 40°N. This dipole type anomaly in the middle and higher latitudes extends from the stratosphere to the troposphere and resembles the AO induced dipole structure of the zonal-mean zonal winds seen in fig. 1.8b. In addition, their results show an AO like SAT signature induced by a major eruption.

Shindell et al. (1999) have stated that the AO trend is anthropogenically induced through GHG emissions in model simulations and changes in ozone concentrations are not necessary to simulate the observed climate trends. They further claim that a realistic representation of the stratosphere in models is needed to simulate the AO trend. This is however a ground for debate since other studies have simulated the AO trend without a detailed stratospheric represention in models (Fyfe et al., 1999). Fyfe et al. (1999) also simulate the AO trend in response to aerosol forcing. To add to the confusion, Gillett et al. (2000) claim that their model exhibits no systematic AO trend in response to GHG, sulphate aerosol, or ozone forcing. However, their model might not resolve the stratosphere in enough detail and therefore rendered as unsufficient to simulate the AO trend according to Shindell et al. (1999). Gillett et al. (2000) go even further and claim to be able to reject the hypothesis that the observed change in temperature is explained solely by the observed AO change and other internal variability in annual, Dec-Feb and Mar-May means. This implies that there is an important component of the temperature response to these anthropogenic forcings which is distinct from that associated with the AO. This is also in accordance with the results of Thompson et al. (2000), who claim that $\sim$50 % of the Jan-Mar warming

over the Eurasian continent can be attributed to the AO trend.

1.3.4 Active and inactive seasons

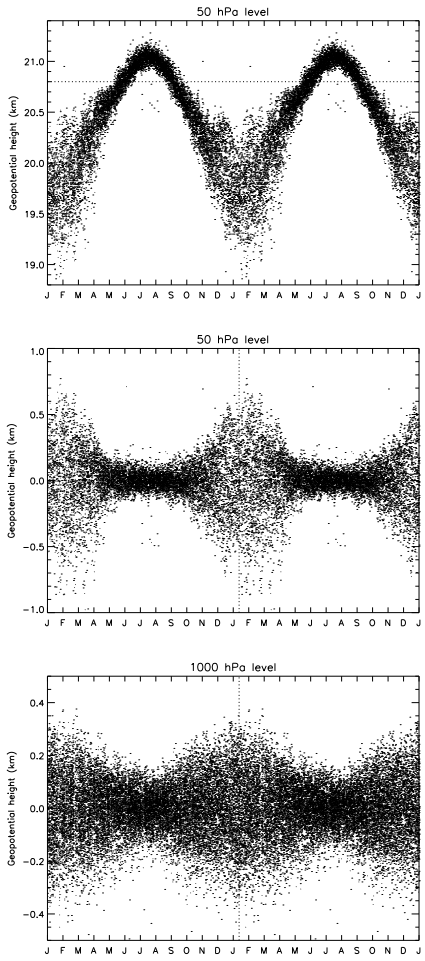

Figure 1.12: Scatter plots of the daily mean geopotential height at 50 and 1000 hPa for 1973-00 (50 hPa) and 1946-00 (1000 hPa) plotted as a function of calander day. Note that the plots have different scales and the annual cycle is repeated. In the top panel, the horizontal line indicates the annual-mean, tropical (20°N-20°S) 50 hPa height. Values below this line indicate an equator-pole gradient consistent with westerly flow, and vice versa. The vertical line in the middle and bottom panels is located approximately where the polar vortex is at its climatological peak strength.

An important feature in the Thompson and Wallace (2000) analysis is the realisation of the seasonally varying climatology of the annular modes. The division of the seasons in active and inactive seasons forms the framework of their analysis. The annular modes are evident throughout the year in the troposphere, but amplify with height into the polar lower stratosphere in the active season period marking the period when tropospheric and stratospheric coupling is at its peak. Thompson and Wallace (2000) show that the active season for the NH is in the three month period Jan-Mar, contrary to only a one month period November in the SH. Due to greater land-sea contrasts in the NH compared to the SH, the active seasons in the NH are much more dynamic and longer lasting, powered by topographically induced planetary waves. The scatterplots for the Keflavík radiosonde in fig. 1.12 confirm these conclusions, showing an obvious annual march in the variance, with higher amplitudes in the cold-season months. The middle and bottom panel show daily anomalies for the 50 and 1000 hPa height field. In the top panel we see the daily values of the 50 hPa height field and the annual mean 50 hPa height of the Tropics. Since the 50 hPa height field in the Tropics never departs much from its

annual-mean value, the points are indicative of the meridional gradient in the 50 hPa height field: points below the line are indicative of an equator-pole gradient consistent with westerly flow, and vice versa. We can therefore conclude that the variance is largest when the westerly polar vortex is strongest and when the vortex is easterly the variance is relatively small. In other words, the active season corresponds to months in which the flow is westerly in the lower stratosphere. If the seasonality of the variance is a manifestation of planetary wave-mean flow interaction, the observed seasonality is consistent with the fact that in the active season, planetary waves propagate more easily from the troposphere to the stratosphere. Based on these results, Thompson and Wallace (2000) define the following active and inactive seasons for the NH:

1. Active season, strong westerly vortex: January-March (JFM).

2. Inactive season, weak or easterly vortex: June-August (JJA).

In their analysis they conclude that the annular modes are present year-round in the lower-troposphere height field, but it is only during the stratosphere's active season that a distinct leading mode resembling the surface signature of the annular modes is recovered in the 50 hPa height field.

1.3.5 Detection of the AO signal

Since the AO signal is stronger (larger amplitude) in the atmosphere in the cold seasons and propagates only then to the stratosphere, we will focus on the Jan-Mar mean in our analysis. In fig. 1.15 we see that there is considerable difference in amplitude between the Jan-Mar and Jun-Aug mean AO. Therefore, we will expect variations in the Jan-Mar mean AO index to be reflected more strongly in the NH climate than the Jun-Aug AO index, hence AO signals over Iceland and in the NH in general should be easier to detect in the cold seasons.

We will therefore use the Jan-Mar AO mean to detect AO signals in the atmosphere over Iceland. The reason we choose the AO index rather than the NAO index is because of the regional property inherited in the definition of the AO, which connects it more deeply to the NH climate circulation. Therefore, changes in the AO value influence the entire NH climate circulation, while NAO fluctuations only apply to the subtropical midlatitudes in the Atlantic Ocean sector.

By comparing high and low AO polarity years in their climatological mean, we will see if there is any real significant influence on the climate over Iceland, which can be related to the AO index. We will also examine the trends in climate in the period 1952-00 and connect them with the AO induced climate changes. We will further varify the AO signal by selecting periods characterized with positive and negative Jan-Mar mean AO trends

and analyse the development of the main physical parameters for those periods. Agreement between the trend analysis and high and low AO polarity comparison will increase our certitude on what the real AO influences are on the climate.

The high AO polarity in the late 80s and in the 90s is unprecedented in the data record available since 1900, with a record high monthly mean value in January 1993 and in the 1989 Jan-Mar mean. This is clearly seen in the Jan-Mar mean AO index in fig. 1.15 and in the color spectrum in fig. 1.14 (red area). Even though record minimum monthly mean value occurs in February 1947, the period characterized by a predominantly low AO index polarity is in the 50s and 60s, which is also seen in the color spectrum (blue area) and the Jan-Mar mean AO index where the record minimum is in 1969.

High AO	Low AO
1903†‡	1900†
1911†	1915†
1913†	1919†
1914†	1924†
1920†	1931†
1921†	1936†‡
1928†	1940†
1938†	1941†
1943†	1947‡
1948†	1955
1949†	1958
1967	1960
1973	1963
1976	1965
1989‡	1966
1990‡	1969‡
1992	1970
1993‡	1977
1997	1979
-	1980
-	1985

Table 1.1: Years where the Jan-Mar mean AO index is above or below one standard deviation. The symbols † and ‡ denote those years not available in the data set used in this study and years with standard deviation equal or greater than two, respectively.

In our attempt to analyse the AO signal we will compare the climatological mean between the observed high and low AO polarity years in the period 1946-00. We define high and low AO polarity years those that are equal or exceed one standard deviations from the Jan-Mar mean AO index. These cases are frequent enough for the calculations of the climatological means, where we have 8 high and 13 low AO polarity years fulfilling this condition in the period 1946-00. These years are listed in table 1.1. We will have to keep in mind that above 100 hPa there is only data available for the period 1973-00 as will be discussed in section 2.1 and consequently the climatological means there will only depend on 7 years for the high AO polarity and 4 years for the low AO polarity. To certify further if the AO signal is the main climatological amplitude, apart from the seasonal variability, we select two pars of periods characterized by high and low AO polarity. First, the periods 1988-00 and 1955-71 are compared. From the 5-year running mean of the Jan-Mar mean AO index time series in fig. 1.15 and the color spectrum in fig. 1.14 it is clear that the former period is characterized by a high AO polarity and the latter period by a low AO polarity. Secondly,

Low AO	High AO	+ AO trend	- AO trend
1955-71	1988-00	1977-90	1989-00
1952-76	1976-00	1969-00	1952-69

Table 1.2: Periods characterized with high and low AO anomalies and positive and negative AO trends based on the Jan-Mar AO index.

we take advantage of the fact that the period 1952-00 devides approximately in half, as described above, in a high and low AO polarity sense, the first half 1952-76 being the low polarity and the second half 1976-00 the high polarity. Furthermore, this method uses all the available data, thereby increasing the significance of the climatological means. We will seek to establish the climatological contrasts between these par of periods and try to relate them to the difference between high and low AO polarity situations in the climate. Since the climatological mean of the periods contain years that are close to the mean AO index (i.e. neither anomalously high nor low in AO polarity), we would expect the contrasts between the high and low AO periods to be less substantial than for the high and low AO polarity years, although there should be a similar structure apparent between the two contrasts.

In our trend analysis we will start by examining the entire period available, 1952-00, between 1000 and 100 hPa and the period 1973-00 between 1000 and 30 hPa. As we have seen from the Jan-Mar mean AO index time series in fig. 1.15, the first half of the period 1952-00 is anomalously low in AO polarity and the second half is anomalously high in AO polarity. The trend over the entire period 1952-00 should therefore show similar features as seen in the climatological difference between high and low AO polarity years. Next we devide the period 1952-00 into periods characterized by a positive and negative trends. In fig. 1.15 we see that the positive Jan-Mar mean AO trend occurs mainly in the 70s and 80s, in a stepwise manner (two peaks in the 5-year running mean). However, in the 90s, the Jan-Mar mean AO index has exibited a negative trend but non the less maintained an anomalous high value since the record high Jan-Mar mean AO anomaly in 1989. In the 50s and 60s the Jan-Mar mean AO has exhibited a negative trend. It seems reasonable to devide the radiosonde data into two periods characterized by a positive and negative Jan-Mar mean AO trend. We use the record Jan-Mar mean minimum in 1969 as our deviding point and compare the positive and negative AO trend periods 1952-69 and 1969-00, respectively. In our attempt to understand the response of various physical parameters to increase and decrease of the AO index, we further devide the last part of the stepwise AO trend into the positive and negative trend periods 1977-90 and 1989-00, respectively. Table 1.2 lists the high and low AO periods and the positive and negative trend periods analysed in this study.

From the monthly mean time series of the AO and NAO in fig. 1.13 it is difficult to capture any common features between the two indexes, although

	AO JJA	NAO JFM
AO JFM	0.08	0.84
NAO JJA	0.17	0.19

Table 1.3: Jan-Mar and Jun-Aug correlations between the AO and NAO indexes. For comparison, the correlation between the AO and NAO monthly time series is 0.63.

the correlation between them is considerably high, giving a value of 0.63. It is not until we compare their Jan-Mar mean time series in fig. 1.15 that similar features reveal themselves and the correlation jumps up to 0.84. Correlations in the Jun-Aug means are very low (Table 1.3). In addition, one might expect a tendancy toward a high Jun-Aug AO polarity after a high Jan-Mar AO polarity the same year.This is however not the case judging from the correlations in table 1.3. This reflects the dynamical difference between the active and inactive seasons, with larger amplitudes in the former (especially for the AO index). Despite that there is no apparent connection between the Jan-Mar and Jun-Aug AO time indexes, this does not necessarily rule out that there is a connection between the Jan-Mar AO index and the development of the breakdown and buildup processes of the polar vortex and the strength of the summer stratospheric easterlies. Therefore, in our analysis of the high and low Jan-Mar AO years we will also present the summer months. The spectrum plots of the AO and NAO indexes show different characteristics, which is mainly caused in their Jun-Aug dissimilarities.

There are however difficulties concerning the comparison of the high and low AO periods and trend estimations, which we should mention. First of all, these periods are both rather short Secondly, the apparent large interannual fluctuations in the Jan-Mar mean AO in fig. 1.13 combined with the former difficulty, introduces a problem when selecting "trend" periods. These shortcommings must be kept in mind when trend significance is presented.

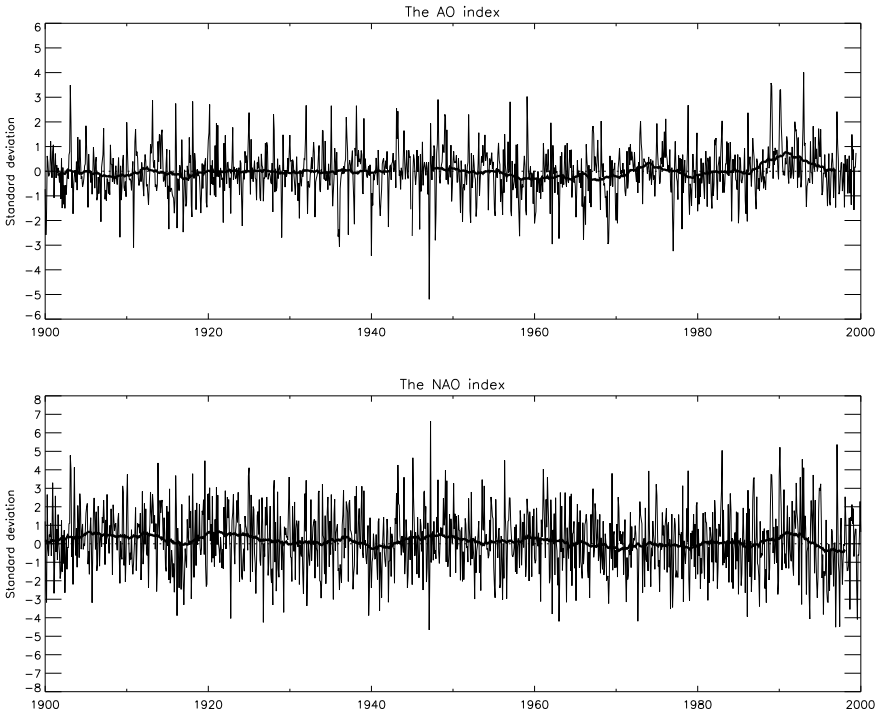

Figure 1.13: The monthly mean AO and NAO indexes. The thick line is the 5-year running mean. The correlations between the indexes is 0.63.

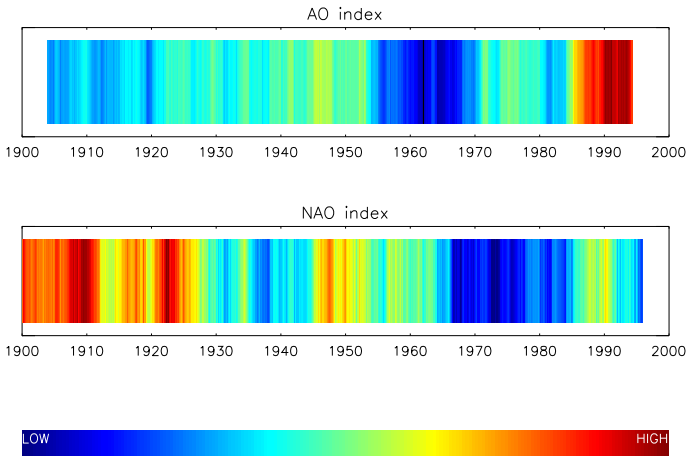

Figure 1.14: Color spectrum of the monthly mean AO and NAO indexes. The data is based on the 10-year running mean.

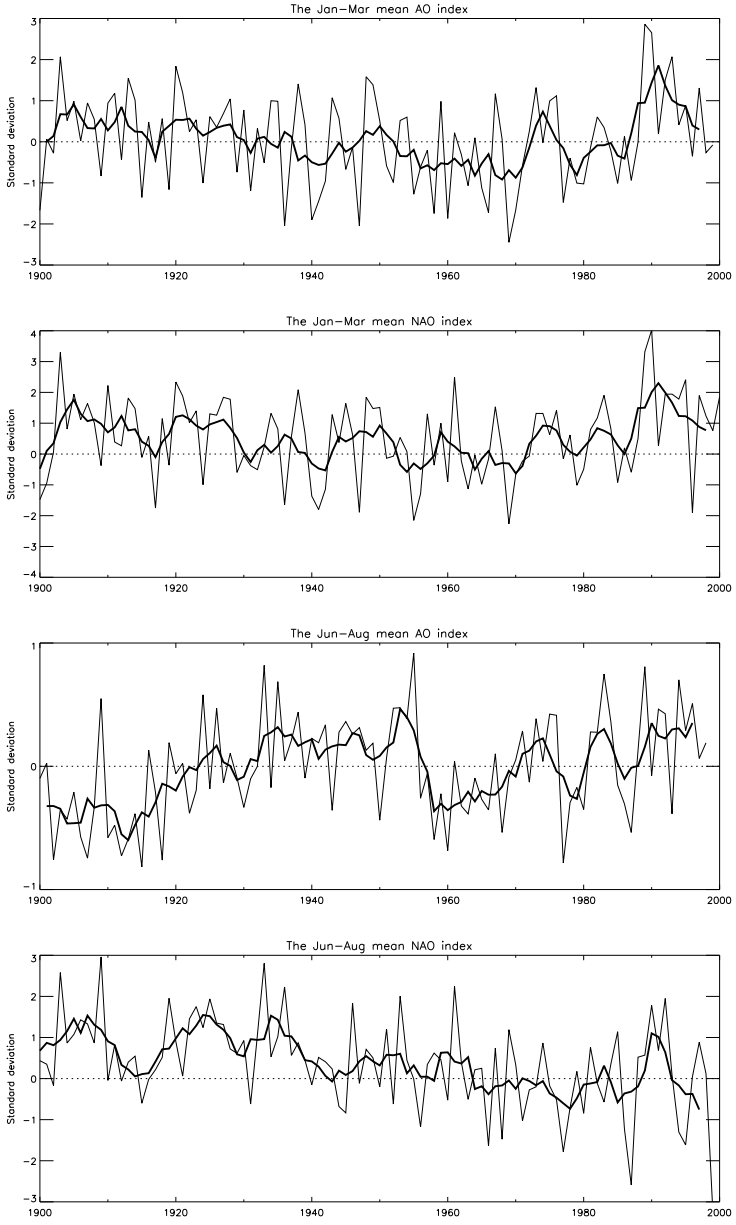

Figure 1.15: The Jan-Mar and Jun-Aug means of the NAO and AO indexes since 1900. The standard deviations are the mean standard deviations from the corresponding monthly time series. This allows easy comparison of the relative amplitudes.

Chapter 2

The Keflavik radiosonde data

The radiosonde observation station at Keflavik has been operated by the Icelandic Meteorological Office (IMO) since 1971. During the first operational years of the station, 1946 - 1952, it was operated by the United States Navy (USN). In the period 1953-71 the station was operated jointly by USN and IMO. Due to its importance in the middle of the North Atlantic the station is still partly supported financially by the USN as well as by the International Civil Aviation Organization.

Modern radiosondes are small, lightweight packages of instruments, suspended from a helium filled balloon[1] intended for upper air measurements of pressure, temperature and humidity. When the balloon is released, the apparatus rises through the atmosphere at approximately 5 ms^{-1} and eventually bursts at a height of 20-25 km, where the *terminal pressure*[2] is about 40-30 hPa. The radiosonde is then returned safely to the surface by means of a small parachute. Measurements are taken at intervals during flight and information is transmitted to the surface as a radio signal. The ground station equipment receive the signal and process the data. Wind speed and direction (see section A.4 for definition of the wind direction) can also be determined from additional windfinding equipment. Most radiosonde systems are capable of measuring wind speed and direction in which case they are sometimes called *rawinsondes*. Wind calculations are based on ascent velocity and air pressure. The device takes only about 700 cm^3 of space and weighs less than 200 g. With the advancement in technology and practice, there have been substancial improvements in measurement accuracy. This must be taken into account when discriminating between actual climate changes and changes in technique or practice (Elliott and Gaffen (1991); Eskridge et al. (1995)).

The radiosonde data from Keflavík has been obtained from three different sources:

[1] The balloon is made of natural or synthetic rubber, which expands as it ascend.

[2] Terminal pressure is the highest pressure level reached before the radiosonde becomes unfunctional, e.g. balloon explodes.

1. IRIS; The Laboratory of Environmental Physics[3], with data set period 1946-94; In old FSL format (section A.7).

2. The Icelandic Meteorological Office (IMO), with data set period 1993-00; Extracted from the IMO database.

3. The National Climatic Data Center (NCDC), with data set period 1973-98; In NCDC format (NCDC, 1998).

Hereafter, we will call these three data sets IRIS, IMO and NCDC respectively. Obtained from different sources, these data sets possess different systematic errors, which have been dealt with in the quality control and interpolation procedures.

In this chapter we start in section 2.1 by giving a detailed represention of the available Keflavik radiosonde data used in our study. In section 2.2 we document the data processing. This includes procedures such as data assimilation, error filtering, interpolating between sounding levels and calculation of mean values. Finally, in section 2.3 we evaluate the precision of radiosonde measurements and uncertainty expected in the climatic temporal means (e.g. monthly means).

2.1 Data representation

The three data sets IRIS, IMO and NCDC span the period 1946-00 with various gaps (fig. 2.1). The years 1948, 1949 and 1950 are missing entirely and there are also numerous occasions of days without any observations[4]. With the construction of the Combined data set[5] for the period 1973-98,

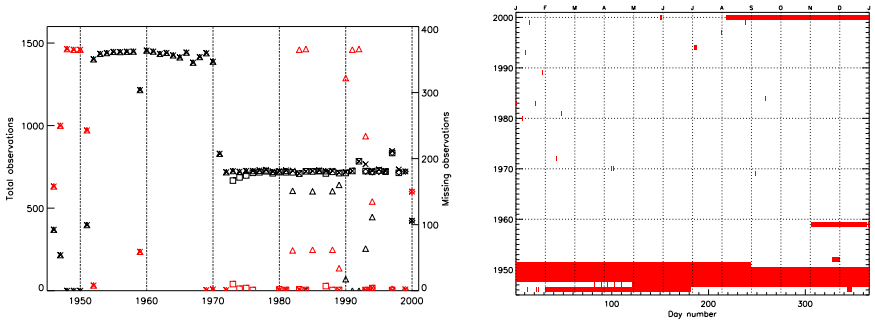

Figure 2.1: Left: Total annual observations for the IRIS data set (triangle), NCDC data set (square), IMO data set (diamond) and the Combined data set (X). Red symbols denote total number of days lacking observations (missing days). Right: Days lacking observations (missing days) shown for each year in the Combined data set. Red dots denote a missing day.

[3] An environmental research company based in Iceland.

[4] An observation denotes a single valid sounding.

[5] All time series constructed in this study are based on the Combined data set.

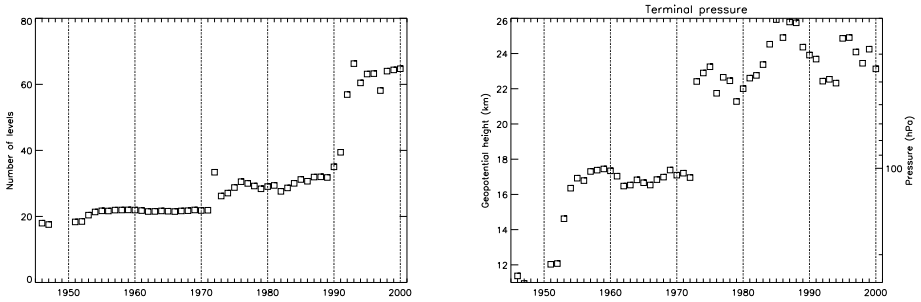

Figure 2.2: Left: Annual mean number of levels for the Combined data set. Right: Annual mean terminal pressure for the Combined data set.

where the three available data sets intersect, these gaps have been reduced. This data set is fairly exempt from large gaps after 1951 except in 1959, where all of the 59 missing days are confined to the two months, November and December (fig. 2.1, right). The Combined data set contains all the available soundings from the IRIS, IMO and NCDC data sets. Identical soundings[6] are chosen with a certain priority in mind; Soundings from the IMO data set being the first choice, NCDC the second and finally IRIS the third. In future studies, this priority should be reconsidered on the bases of the varied properties of the three data sets. The benefit from such a composition is seen in fewer gaps with missing observation days. The Combined data set is based entirely on the IRIS data set in the period 1946-72. Unfortunately, the sounding profiles in this data set are limited to approximately 100 hPa (see the terminal pressure in fig. 2.2, right). As a consequence, analysis in the lower stratosphere is confined to the period 1973-00. Observation frequencies for all the data sets are listed in detail in section A.6.

At present, there are usually twice-daily observations, conducted at times 12 and 0 Coordinated Universal Time (UTC)[7,8] (fig. 2.3 and fig. 2.4). 12 and 0 UTC daily soundings started first in 1957 (fig. 2.4). In the period 1946-1957 the observation times where scattered, the most frequent being at 3, 6, 9, 15, 18 and 21 UTC (fig. 2.5). The period the data spans can be devided into two parts depending on the total observations per day:

1. 1946-51 and 1971-00: twice-daily observations[9].

2. 1952-70: four-daily observations.

[6]Soundings recorded with identical date values (the date values being the year, month, day and hour) are called identical soundings.

[7]The UTC coincides with the Greenwich Mean Time (GMT).

[8]Surprisingly, four-daily observations were conducted in January 1992 and January and February in 1997. In these cases the additional observations where conducted at 6 and 18 UTC (fig. 2.3).

[9]With the exception of 1992 and 1997 as mentioned in the previous footnote.

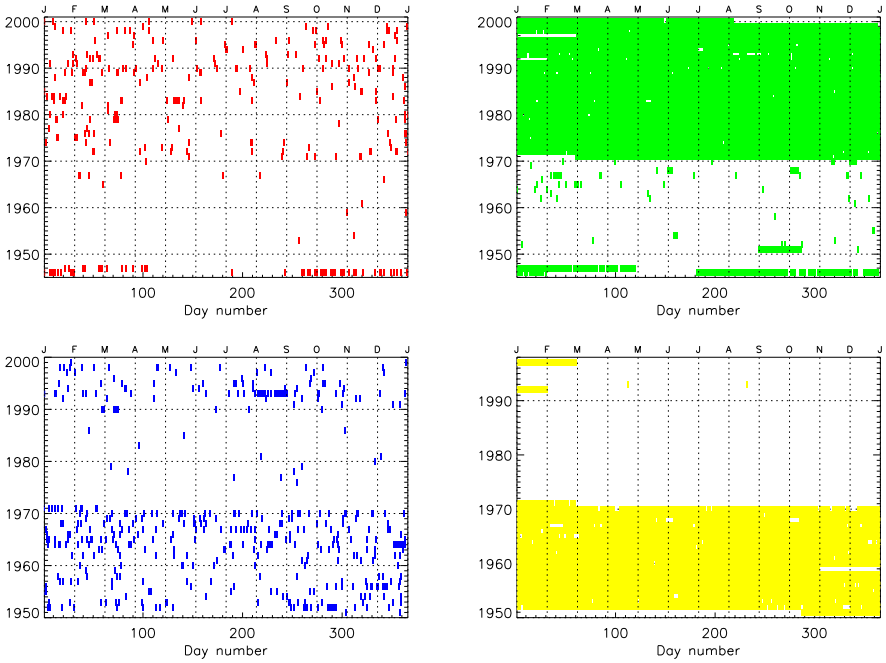

Figure 2.3: Days with one (red), two (green), three (blue) and four (yellow) observations.

The daily observations are distributed evenly for each solar day, given that there is no missing observation. There are three groups of daily UTC hour distributions used in the data set, namely 0 and 12 UTC for 2-daily observations and either 3, 9, 15 and 21 UTC or 0, 6, 12 and 18 UTC for 4-daily observations. Days with odd number of observations, namely one or three daily observations, are relatively few and are well distributed over the period of the data (fig. 2.3).

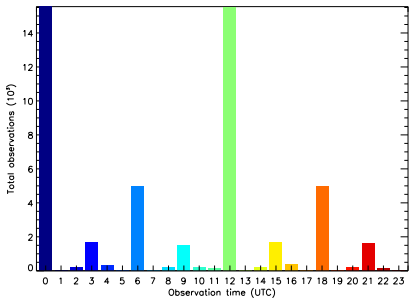

Figure 2.5: Total observations for each UTC hour in the Combined data set.

Changes in the Keflavik station height over the course of its operating period are somewhat unclear judging from the data. According to the Comprehensive Aerological Reference Data Set (CARDS) station inventory (section A.8) there have been two significant changes in the height of the station:

1. February 1962: 49 m to 58 m.
2. July 1967: 58 m to 38 m.

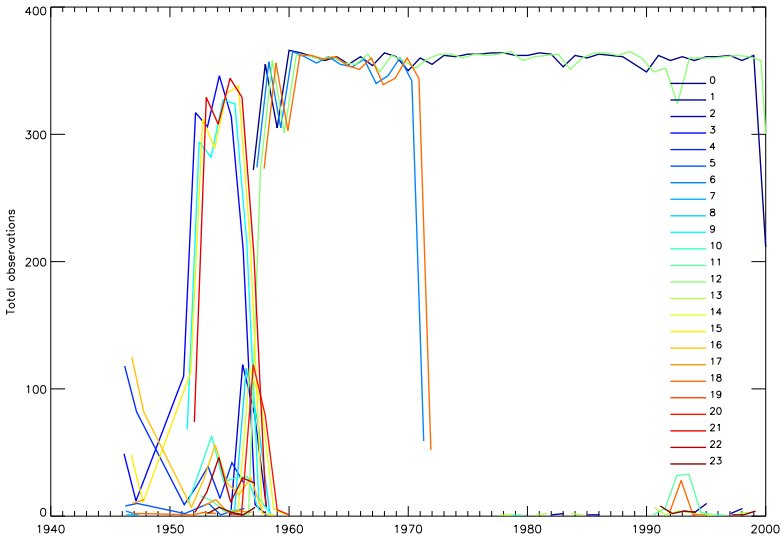

Figure 2.4: Total annual observations for each UTC hour in the Combined data set. The data is slightly offset for clarity.

However, in the IRIS data set the only height changes found where:

1. April 1947: 49 m to 57 m.
2. September 1951: 57 m to 49 m.
3. July 1967: 49 m to 38 m.

The height change at February 1962 in the CARDS data set was not found in the IRIS data set (Data for February 1962 is available in the IRIS data set.). There is a reason for questioning the height change in April 1947 since this occurs in the last observation before the gap 1948-50. The first observation after this gap is when the next height change in September 1951 occurs. In order to confirm this presumed height change we need to fill the gap 1948-50. The height change in July 1967 was found in both data sets but they do not agree on the height prior to the change. These discrepancies deserve further investigation although they will have negligible affects on our results.

2.2 Data processing

Before any calculations can take place, it is necessary to apply quality control on the entire data sets. This consists in error checking each measurement available in the database of known errors and making the necessary repairs. We will also try to replace dummy values[10], using interpolation methods

[10]Dummy values occur in data when information is either missing, not reported or not applicable. In the current data processing when dummy values are encountered, various

where applicable. There will also be cases when we desire information on a level that does not exist in the sounding. If this non-existing level or dummy value lies between two valid measured levels in the sounding, it is possible to interpolate between two adjacent measured levels to extract the desired information. Calculations of mean values must be done with care and certain requirements have to be set for each mean value to be considered valid. The requirements for this analysis are made as simple as possible in order to simplify the data processing.

2.2.1 Quality control

The process

Before any calculations can take place it is necessary to process the data. We call the data sets received from the three different sources the *original dat set* and the processed data set the *derived data set*. The data processing executed on the original data set, in order to construct the derived data set, is called *quality control*. Various corrections and error filtering procedures have been applied to the data sets. Each and every sounding is checked and fixed if necessary before being included in the derived data set. Since these data sets are originated from different sources, they contain different types of errors.

The original data set is synchronised by converting all the data to the NCDC format[11] (NCDC, 1998) and various errors eliminated in the process depending on the data set. After the derived data sets have been prepared, a new data set for the period 1973-98 is constructed, since this is where the data sets IRIS, IMO and NCDC intersect. We call this new data set INTERSECT and it contains selections of all available soundings in the data sets for this period. The so called COMBINED data set, which is used to prepare time series and our results are based on, is then composed of the IRIS data set for the period 1946-72, the INTERSECT data set for the period 1973-98 and of the IMO data set for the period 1999-00.

Known errors fixed

The errors we fix in the quality control process are the following:

1. Eliminate level duplication (Levels containing exactly the same information) in data for each sounding.

2. Eliminate levels with error of the type appearing e.g. in 3. October 1991, only found in the NCDC data set. A normal NCDC formated data level is of the form:

interpolation methods are often applicable so they can be replaced with physicaly valid values.

[11]The NCDC data set is originally in the NCDC format.

000040186358N02236W199110021200109999085000+01313-0310390350050000001

However, a level containing this sort of error is of the form:

000040186358N02236W199110031200199903301400+99-04-0089999999440909092

where at least the geopotential height is meaningless. To fix this error we note the string structure that identifies this type of error. A valid NCDC formated data level contains only two signs, a combination of plus and minus, but the line with the error has three signs. All levels having one of the eight possible combinations of three signs are therefore eliminated.

3. Eliminate levels lacking valid pressure values.

4. Eliminate levels lacking valid measurements (i.e. physical parameters apart from pressure)

5. Fix the error at 1000 hPa, only found in the IRIS data set. Normal IRIS formated (section A.7) data at 1000 hPa, which is under the surface, is of the form:

   4 1000 -30 32767 32767 32767 32767

   This is a data line in the Old FSL format that contains only dummy values, 32767, instead of valid measured physical data. However, we have a valid geopotential height 1000 hPa, which is in this case -30 m. In the IRIS data set it appears that in cases when the 1000 hPa geopotential height should be negative, the value is instead nonsense:

   4 1000 30662 32767 32767 32767 32767

   obtaining in this case the value 30662. It seems that in each case the geopotential height obtains a large value. We therefore fix this error by replacing all geopotential height values above a certain limit with a dummy value. A valid value can then usually be calculated using the interpolation methods described in section 2.2.2.

6. Eliminate soundings with invalid geopotential height in the entire profile.

7. Check for inconsistencies in duplicate pressure levels for each sounding. Any levels containing contradicting values in the physical parameters are fixed by replacing the values with dummy values. Duplicate pressure levels occur e.g. when the tropopause level is also a manditory level, like in these two NCDC formated data levels:

   000040186358N02236W199001011200199999025000+09850-5599991350279099991

   000040186358N02236W199001011200199999025000-99999-6709991350279090904

   where the 250 hPa level has contradicting temperature values. The upper data line gives the temperature value -55.9 degrees Celsius while

Error:	1	2	3	4	5	6	7	8	10
IRIS:	0(l)	-	0(l)	0(l)	12.483(l)	0(s)	0(i)	0(r)	0(s)
NCDC:	1.848(l)	2.707(l)	9.699(l)	1.204(l)	-	13(s),125(l)	0(i)	5(r)	14(l),2(s)
IMO:	9(l)	-	31(l)	827(l)	-	0(s)	3(i)	173(r)	0(s)

Table 2.1: Statistics of error occurences for the data sets IRIS, NCDC and IMO. The letters l, s, i, and r denote levels, soundings, inconsistencies between duplicate pressure levels and replacements of dummy values respectively. See section 2.2.1 for a detailed explanation of the different error types.

the lower data line gives the value -67.0 degrees Celsius. The contradiction is fixed by setting both to dummy values. The duplicate data lines then become:

000040186358N02236W199001011200199999902500+09850-999999135027909999 1

000040186358N02236W199001011200199999902500-99999-999999135027909090 4

8. Replace dummy values with valid values in duplicate pressure levels, if possible. E.g. in the duplicate data levels above, the geopotential height has a valid value of 9850 m in the upper data line but is given a dummy value in the lower data line.

9. Set maximum wind line type for each sounding. Only conducted on the IRIS data set. The maximum wind line type in missing in all soundings in the IRIS data set.

10. Eliminate soundings that have the UTC hour value greater than 23. This has been seen occurring in the NCDC data set.

Table 2.1 lists the total number of eliminated soundings and levels as a result of the error filtering for each data set used in this study. The total amount of levels eliminated from the original data sets are 28.947, which is equivalent to one year of 2-daily observations assuming an average of 40 levels per sounding.

Other errors not yet fixed

Wind measurements for parts of the years 1998 and 1999 are known to be invalid. This occurred due to technical problems in the measurement apparatus. This is not yet fixed.

Humidity conversions

The humidity in the NCDC data set is given in terms of relative humidity$r$, instead of dew point temperature T_d as in the other data sets. To make the other data sets compatible with the NCDC data set, we convertT_d to r using

the Clausius-Clapeyron equation (Refer to Bohren and Albrecht (1998) for detailed discussion and derivation of the Clausius-Clapeyron equation)

$$\frac{dp}{dT} = \frac{-s_v + s_w}{v_w - v_v} = \frac{l_v}{T(v_v - v_w)} \tag{2.1}$$

where $l_v \equiv h_v - h_w$ is the enthalpy of vaporization, and the indices v and w denote water vapor and liquid water, respectively. We then obtain

$$r = \exp\left[\frac{l_v}{R_v}\left(\frac{1}{T} - \frac{1}{T_d}\right)\right] \tag{2.2}$$

where the definition of r is

$$r = \frac{e}{e_s} \tag{2.3}$$

We can also solve for T_d

$$T_d = \frac{1}{\left[\frac{1}{T} - \frac{R_v}{l_v}\ln r\right]} \tag{2.4}$$

2.2.2 Replacing dummy values

When information is either missing, not reported, or not applicable, dummy values are used. The methods we use, to replace dummy values with valid physical data, are the following:

1. Linear interpolation with respect to height of parameters between two valid levels.

2. Interpolation of the geopotential height with the hydrostatic equation

$$p = p_0 \exp\left(-\frac{z - z_0}{H}\right) \tag{2.5}$$

With a sounding we obtain an atmospheric profile of various physical parameters. The rise time period of a radiosonde is of the order of an hour. Time scales involving horizontal motions are of the order of a day. Therefore, we can assume that the profiles represent instantaneous measurements through the atmosphere. Thus we can write $\beta = \beta(z)$, where β is some physical parameter measured in the sounding and z is the geopotential height. Since a radiosonde measures at discrete intervals[12] we have $z = (z_1, z_2, ..., z_n)$ and $\beta = (\beta_1, \beta_2, ..., \beta_n)$, where $\beta_i = \beta(z_i)$ and n is the total number of levels in the sounding.

In levels where a physical parameter is lacking, the best we can do is to assume that the parameter varies linearly with respect to geopotential height between levels. Data for a normal sounding should have all the significant

PSfrag replacements

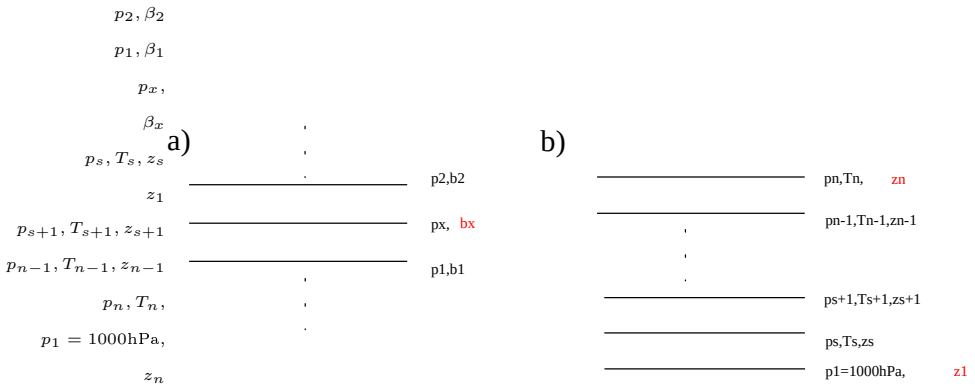

Figure 2.6: Sounding levels with missing data. (a) Pressure levels p_1, p_x and p_2 shown for a specific sounding. The corresponding parameters β_1, β_x and β_2 can be any physical parameter (including the geopotential height). β_1 and β_2 are assumed to be known and β_x unknown. (b) Same as in fig. 2.6a except for surface and top levels in the sounding. The manditory level $p_1 = 1000$ hPa is assumed to be below the surface level p_s. We also assume that the top level p_n does not have a valid geopotential height z_n.

levels[13] in its entire profile for each physical parameter. Even though significant levels could be missing for some soundings, parameters are always assumed to vary linearly between adjacent levels in our data processing.

Lets consider a level p_x, where β_x can be any physical parameter in the sounding at that level. We assume β_x is a dummy value and that there exists two levels p_1 and p_2 below and above that contain a valid measurement (fig. 2.6a). Using the hydrostatic equation (2.5) for the two layers (p_1, p_x) and (p_1, p_2) we obtain

$$\ln p_x - \ln p_1 = -\frac{1}{H_{1,x}}(z_x - z_1) \tag{2.6}$$

$$\ln p_2 - \ln p_1 = -\frac{1}{H_{1,2}}(z_2 - z_1) \tag{2.7}$$

where the scalar heights[14] for each layer can be written

$$H_{1,x} = \frac{R_d}{g_0}\frac{T_{v,x} + T_{v,1}}{2} \tag{2.8}$$

$$H_{1,2} = \frac{R_d}{g_0}\frac{T_{v,1} + T_{v,2}}{2} \tag{2.9}$$

where the subscript v denotes virtual temperature (see section A.2 for definition). Even though the scalar heights above are not in general equal, in order to simplify we will assume that the scalar height for a specified layer (p_1, p_2) is equal to the scalar height for all subsets (p_1, p_x). In other words

[12] Usually at 5 seconds intervals.

[13] The definition of a significant level is such that all parameters vary linearly with respect to the geopotential height between adjacent significant levels.

[14] The scalar height is a measure of the atmospheric depth or pressure depth, where the pressure drops off by a factor e in passing upward through a layer of depth H. For a standard atmosphere the scalar height is approximately 7 km.

we assume that $H = H_{1,2} = H_{1,x}$ for all $x \in (1,2)$[15]. Using this and the hydrostatic equation, we find that inside this layer

$$\ln p \propto z \tag{2.10}$$

Since we assume that the parameters vary linearly with respect to z (or equivalently with respect to $\ln p$) we can calculate β_x using

$$\beta_x = \beta_1 + \frac{\beta_2 - \beta_1}{z_2 - z_1}(z_x - z_1) \tag{2.11}$$

Now we want to use the pressure instead of the geopotential height in the equation above. This is obtained by inserting (2.6) and (2.7) into (2.11)

$$\beta_x = \beta_1 + \frac{\beta_2 - \beta_1}{\ln p_2 - \ln p_1}(\ln p_x - \ln p_1) \tag{2.12}$$

The advantage of this equation over (2.11) is that it uses pressure instead of geopotential height. In the data processing, it is ensured that all levels have valid pressure values, but this requirement is not made for the geopotential height. This method is of course only applicable when β_1 and β_2 exist and are valid, which is not always the case. Also, note that (2.12) can be used to interpolate the geopotential height. In some cases we only know the geopotential height z_x at the x level, and want to find the parameter β_x using the measured levels p_1 and p_2. Again we can use (2.12) both for $\beta_x = z_x$ to solve for p_x and where β_x is some physical parameter.

When there are invalid values above or below the level being interpolated no attempts are made to interpolate the physical parameters. However, the geopotential height z is interpolated as long as there exists valid temperature measurements at the interpolation levels. Then it is possible to calculate the scalar height for all the layers and use (2.5) to interpolate z. This case arises when the top level in a sounding lacks the geopotential height value. From fig. 2.6b we find that

$$z_n = z_{n-1} + H_{n-1,n} \ln\left(\frac{p_{n-1}}{p_n}\right) \tag{2.13}$$

where the scalar height for the layer $(n-1, n)$ is given by

$$H_{n-1,n} = \frac{R}{g} \cdot \frac{T_{v,n-1} + T_{v,n}}{2} \tag{2.14}$$

The only case when we try to interpolate z without knowing the temperature at the interpolation levels is when the mandatory level 1000 hPa is under the surface. To estimate z we use the scalar height at the surface layer,

[15] Our definition of layers and levels is such that if $(1,2)$ is a layer, with upper boundary 2 and lower boundary 1, then x is a level inside the layer only if $x \in (1,2)$.

$H_{s,s+1}$, and apply it to the imaginary atmospheric layer (p_1, p_s) in order to interpolate at 1000 hPa. From fig. 2.6b we have

$$z_1 = z_s - H_{1,s} \ln\left(\frac{p_1}{p_s}\right) \tag{2.15}$$

where the scalar height is given by

$$H_{1,s} \equiv H_{s,s+1} = \frac{z_{s+1} - z_s}{\ln(p_s/p_{s+1})} \tag{2.16}$$

The interpolation procedure of the radiosonde data is given in detail in A.3.

2.2.3 Mean values

Daily mean

In light of the variable observational times prior to 1972 it was decided to construct daily mean values using all observations available each day. This way the daily values in the time series for the entire period should be mutually comparible given that the daily number of observations are a minimum of two. Since relatively few days have only one observation and the fact that these days are fairly well scattered over the entire period of the data, as pictured in 2.3, we assume that there is a negligible bias introduced when a single observation is taken to be the daily mean, especially when the daily values are used in the calculation of monthly or climatological means. We saw in section 2.1 that the UTC observational hours for each day are evenly distributed over one solar day, and we will see in section 3.1, that diurnal variability is in most cases negligible.

Monthly mean

The requirement for each monthly mean is that at least 20 days are available. Otherwise the monthly mean is assumed missing.

Annual mean

The requirement for each annual mean is that a minimum of 70% data is available for the year[16]. Otherwise the annual mean is assumed missing. This requirement excludes the annual means of the years 1946, 47 and 51. The annual mean time series for the Keflavik radiosonde station can thus only span the period 1952-00 at the most.

[16]This can introduce substantial bias when entire months are missing.

Climatological mean

The climatological mean is based on averaging over a period for each year (e.g. the mean of each day or month of the specified period is calculated). We require about 70-80% of the years, in a specified period, to be valid.

2.3 Precision of radiosonde data

Before we present any results and conclusions it is necessary to have in mind the actual precision in the radiosonde measurements, which will be our measure of significance in the variations detected in the proceeding sections.

The evaluation of radiosonde measurement precision is a complicated matter and is mainly dependant on the measurement apparatus, balloon type, data compilation methods, altitude[17] and weather conditions. We can however assume that the measurement precision has increased over the course of time. Therefore, it is likely that data from 1946 is considerably less precise than contemporary radiosonde measurements. Error considerations are a whole study of its own and necessary when inferencing is made regarding climate changes. In this study we will circumvent the complicated error considerations and start by choosing reasonable error intervals for the entire period 1946-00. Tests of the radiosonde system in use in the United States in the 80s showed the measurement precision (defined as one standard deviation) for pressure, temperature, dewpoint and relative humidity to be about ±2 hPa, ±0.3°C, ±3.5°C, and ±2%, respectively (Elliott and Gaffen, 1991). According to the Fedaral Meteorological Handbook (OFCM, 1997), contamporary radiosonde measurement precision for pressure, temperature, relative humidity, wind speed, wind direction, and geopotential height is about ±1 hPa, ±0.2°C, ±2 %, ±0.8 m/s, ±2 degrees, and ±20 m, respectively. According to Elliott and Gaffen (1991), for most tropospheric temperatures and pressures the measurement precision for specific humidity is less than ±0.5 g/kg.

For the purpose of this study, we assume the precision for temperature, geopotential height, specific humidity, wind speed, wind direction and zonal wind listed in table 2.2. Using the law of combinations of errors

$$\sigma_f^2 = \sum_{i=1}^{n} \left(\frac{\partial f}{\partial x_i} \right)^2 \sigma_i^2 \tag{2.17}$$

for a function $f = f(x_1, x_2, ..., x_n)$ of n variables, we find that for the zonal wind we have

$$\sigma_u^2 \leq \sigma_U^2 + U^2 \sigma_\theta^2 \tag{2.18}$$

[17] Humidity measurements are especially sensitive to high altitudes where the performance degrades in cold, dry regions, because the sensors respond to the number of water molecules present in the atmosphere.

	T	z	q	U	θ	u
Precision:	$\pm 0.5^{\circ}$C	± 30 m	± 0.2 g/kg	± 1 m/s	± 5 degrees	± 1.2 m/s

Table 2.2: Estimated radiosonde measurement precision defined as one standard deviation.

where U, u (A.14) and θ are the wind speed, zonal wind and wind direction, respectively. From the surface to the lower stratosphere we can assume $1 \leq U \leq 50$. Therefore, we can conclude that

$$\sigma_u \leq 1.2 \text{ m/s} \tag{2.19}$$

The precision of a radiosonde measurement is modeled upon a single pointwise measurement. However, most of the results presented in this study are based on temporal averages, e.g. monthly, annual and climatological averages. The uncertainty of these kinds of temporal averages are not quite the same. As a consequence of the so-called *central limit theorem*, repeated N independent measurements of the same quantity $x_1, x_2, ..., x_N$ with a distribution of mean $\mu = \mu_1 = \mu_2 = ... = \mu_N$ and a standard deviation $\sigma = \sigma_1 = \sigma_2 = ... = \sigma_N$ will result in the following standard deviation of the average $\bar{x} = N^{-1} \sum x_i$

$$\sigma_{\bar{x}}^2 = \frac{\sigma^2}{N} \tag{2.20}$$

Although the radiosonde measurements are independent, repeated measurements at a specified level are conducted at continuously varying conditions, i.e. weather conditions. Since the precision of the radiosonde measurement apparatus is dependent on these varied conditions, it is not correct to assume all the measurements have the same standard deviationσ. Therefore, in general for two independent radiosonde measurements x_i and x_j, where $i \neq j$, we have $\sigma_i \neq \sigma_j$. However, in most normal situations we can expect the standard deviations $\sigma_1, \sigma_2, ..., \sigma_N$ to be of the same order. It should be safe to expect the following condition to hold in most normal cases of radiosonde measurements

$$\sigma_{\bar{x}}^2 \gtrsim \frac{\sigma_x^2}{N} \tag{2.21}$$

where $\bar{x}$ can be e.g. the monthly or annual mean of temperature at 100 hPa and σ_x is the estimated standard deviation of a single radiosonde measurement of the physical parameter x as in table 2.2. Even though climatic changes in the order of $\sigma_{\bar{x}}$ in temporal means are in principle significant, the associated effect on climate is insignificant. We will therefore present climate changes in temporal means, such as monthly or annual means, in the order of σ_r, since changes less than this have insignificant impact on the actual weather conditions.

In general, we have to keep in mind that radiosonde measurements are more prone to errors at high altitudes and data availability decreases fast above 100 hPa (Gaffen, 1999).

Chapter 3

Results

In climate studies usually regional or global temperature trends are analyzed. By averaging over large areas the dynamically-forced and natural fluctuations are smoothed, giving a better picture of the long term changes in the atmosphere. In addition, use of mean temporal values over a long time (e.g. a year) removes many of these fluctuations. Since our results are based on a single radiosonde station, time series of temporal means will have more substantial dynamical and natural fluctuations than similar regional temperature time series. Therefore, most time series are not well described by a linear trend, since these fluctuations tend to either increase or decrease the real long term trend we are interested in.

In this chapter we start in section 3.1 by evaluating the diurnal variability in the data. In section 3.2 we examine the climate development since the 50s and relate them to the development in the AO index. In section 3.3 we detect the AO signal over Iceland by using correlations, climatological differences and trends. Finally, in section 3.4 we examine the seasonality of the variance in the wind, temperature, geopotential height and humidity fields.

3.1 Diurnal variability

In our analysis we use all soundings, regardless of the UTC hour, when calculating monthly means. If diurnal variations are important[1], this could possibly introduce a bias in the comparison of periods where observation time convention differ or are not uniformily distributed for each solar day for long periods. As shown in fig. 2.3, days with an odd number of observations (i.e.

[1] Physical related diurnal variations in the lower stratosphere and troposphere are negligible since their characteristic time scales (a measure of atmospheric response time) are in general much longer than one day. Substantial diurnal variations, if any, can only arise due to technical deficiencies in the measurement apparatus.

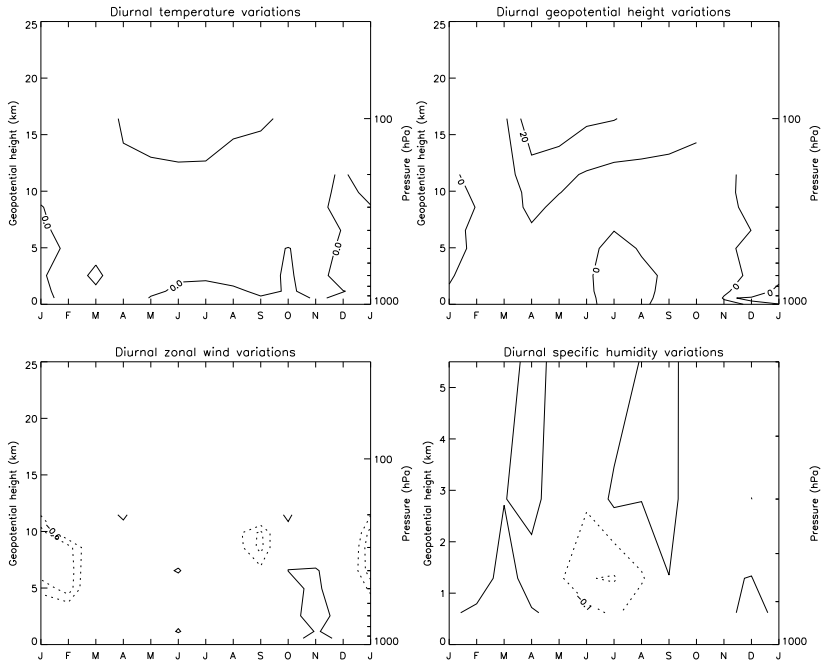

Figure 3.1: Diurnal variations of temperature, zonal wind, geopotential height and specific humidity for all calender months. All contour plots are based on climatological monthly mean data in the period 1957-00 of the 12 and 0 UTC hours from 1000 to 100 hPa (except for specific humidity is based on the period 1980-00 from 1000 to 500 hPa). Contour intervals are 0.5°C (-0.5, 0, 0.5, ...) for temperature, 0.2 m/s (-0.2, 0, 0.2, ...) for zonal wind, 10 m (-10, 0, 10, ...) for geopotential height and 0.1 g/kg (-0.1, 0, 0.1, ...) for specific humidity. Dotted contour lines denote negative values. Note that not enough data is available at the highest levels in the cold months.

1 or 3 observations) are in minority[2] and relatively well distributed over the entire period of the data set. Also, when the number of daily observations are an even number, diurnal effects on daily averages is minimized. As mentioned in section 2.1, nearly all 2-daily observations are conducted at 0 and 12 UTC and 4-daily observations at 3, 9, 15 and 21 UTC or 0, 6, 12 and 18 UTC. Therefore, we expect diurnal variations to have negligible effect on the monthly means. For confirmation, we present the actual diurnal variations in the data by calculating the climatological monthly mean difference between the 12 and 0 UTC hour soundings for temperature, geopotential height, zonal wind and specific humidity in the period 1957-00.

In fig. 3.1[3], we find that there are insignificant day-to-night variations in temperature near the surface. However, there is evidence of a warmer daytime lower stratosphere relative to nighttime (maximum of 0.7°C in July at 100 hPa). This is also reflected in higher geopotential (maximum of 30 m

[2]There are 746 days with odd number of observations and 17.359 days with even number of observations (i.e. 2 or 4 observations). Therefore, days with an odd number of observations are less than 5% of the available data set.

[3]All figures in this chapter are based on the Keflavik radiosonde data.

in April at 100 hPa). A likely expaination is the the well documented solar and infrared radiation problem in thermometers, which is known to cause a significant positive bias in the day-night temperature difference. However, according to Luers and Eskridge (1995) this error is usually less than 0.5°C below 15 km. If this explanation is the main cause of the observed day-night bias, we should expect the apparent warmer daytime to be e.g. less for recent data in the 90s versus older data in the 70s due to improvements in measurement apparatus. It turns out that there are no apparent summer stratospheric diurnal variations for the period 1990-00 (not shown) in contrast to substantial diurnal variations for the period 1973-85 (maximum of 1.5°C in April at 70 hPa). These results support the hypothesis and we conclude that the apparent diurnal variation in the summertime lower stratosphere is due to technical errors in early radiosonde thermometer apparatus.

There seems to be a tendency toward a stronger nighttime upper tropospheric polar vortex in Jan-Feb, between 5 and 10 km (minimum of -1 m/s in January at 300 hPa). At this stage we do not know if this is a real physical effect or just due to technical errors in the data.

Surprisingly, the specific humidity is slightly greater at midnight relative to noon in the warm months (minimum of -0.2 g/kg in July at 850 hPa).

We can therefore safely assume that diurnal effects are unimportant over Iceland and the hourly observational distribution in the data set period minimizes its effect on the monthly means.

3.2 Climate development

3.2.1 The monthly mean anomalies

The color spectrum plots, based on the 10-year running mean of the monthly mean anomalies, in fig. 3.2 and 3.3, depict the development of the geopotential height, temperature, zonal wind, wind speed and specific humidity.

Starting with the geopotential height we see an obvious subdivision between early high anomalies and late low anomalies. This development appears first in the upper troposphere and then later drops abruptly to extremely low anomalies at the surface and lower stratosphere. However, there is evidence of recovery in the troposphere, especially in the upper troposphere.

These changes are also reflected in the temperature development. In a similar way, the temperature development is characterized by early high anomalies followed by extremely low anomalies and a late recovery in the troposphere, again appearing earlier in the upper troposphere.

Both the zonal wind and wind speed show positive trends in the last two decades, especially in the 90s. This increase in wind applies to all levels. However, increase in wind speed is not necessarily reflected in increasing zonal wind and vice versa. For example, the anomalously high tropospheric

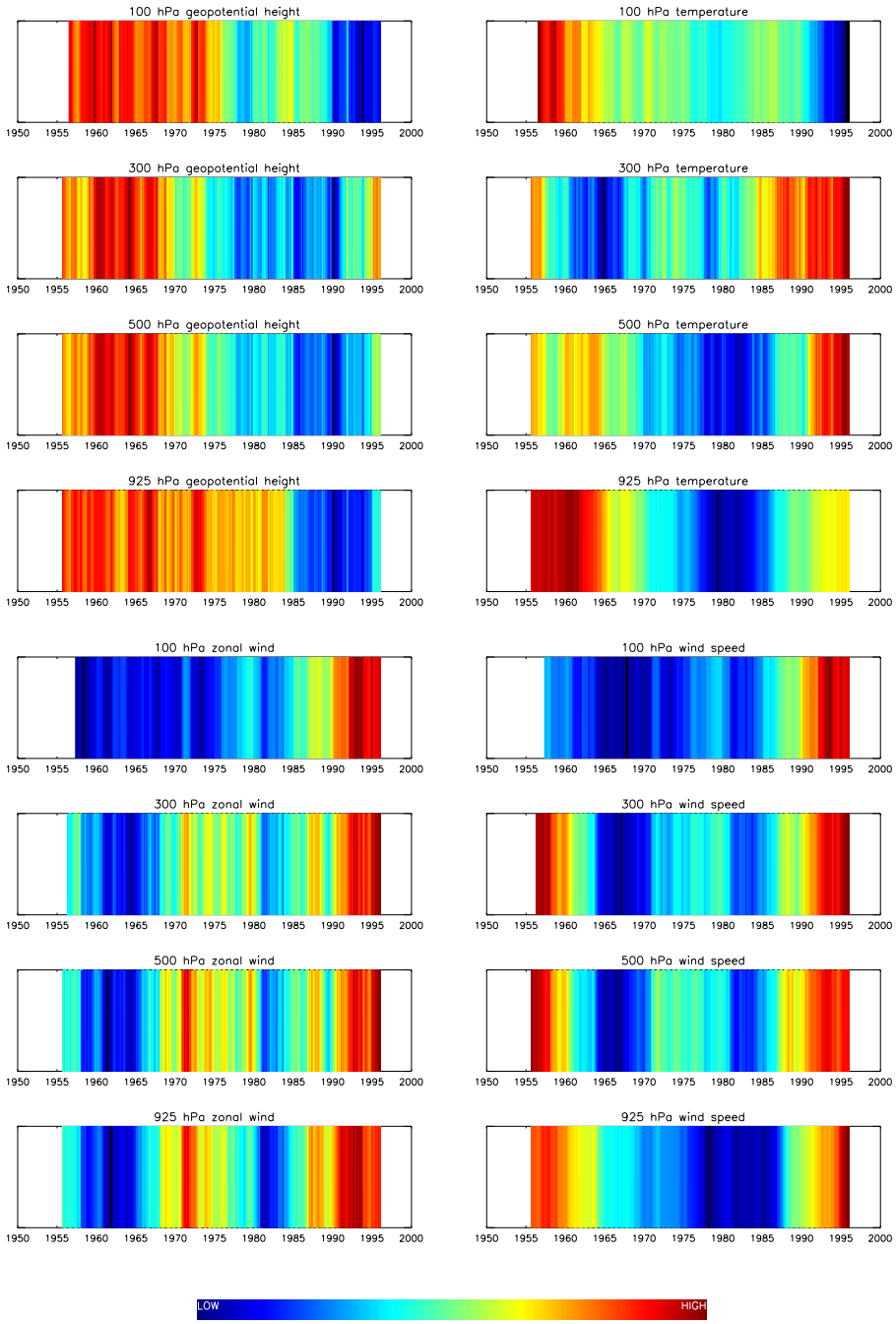

Figure 3.2: Color spectrum of the geopotential height, temperature, zonal wind and wind speed at 925, 500, 300 and 100 hPa. The plots are based on a 10-year running mean of the monthly mean anomaly time series.

wind speeds in the 50s are not as much reflected in the zonal wind as are the strong winds in the 90s. This means that the recent increase in zonal wind is reflected more in wind speed increase than the tendency of the wind direction toward zonal flow. The strong tropospheric winds in the 50s must therefore be reflected in relatively strong meridional wind flow. In addition, the strong winds in the 50s is limited to the troposphere unlike the strong winds in the 90s. The strong wind periods in the 50s and 90s are therefore very different in nature, which is likely due to the fact that the AO index polarity in the former period is relatively low compared with the latter period (fig. 1.14). Also, the strong surface zonal winds in the 70s is not reflected in the wind speed, which must mean a tendancy change in wind direction rather than wind speed. Comparing the wind speed to the temperature, it appears that low wind speeds prevail in cold conditions in the troposphere and vice versa. Furthermore, this connection is reversed in the lower stratosphere where cold conditions are associated with strong winds (strong polar vortex) and vice versa. An even stronger connection can be seen between the geopotential height and the zonal wind, where low geopotential height anomalies are associated with strong zonal winds from the surface to the lower stratosphere.

The specific humidity is highly correlated with the temperature and shows similar features in the troposphere as the temperature. However, the recent negative trend in the specific humidity at the surface is not consistent with the increase in temperature at the same time.

It is tempting to connect these strong observed subdivisions between high and low anomalies, that are evident in all the fields, mutually in relation to the AO index. The early development toward low anomalies in the geopotential height and toward high anomalies in the zonal wind and wind speeds in the 70s at 500 and 300 hPa (also at 925 hPa for the zonal wind) is in conjunction with the turning point of the Jan-Mar mean AO index (fig. 1.15) around its record low value in 1969 and its characteristic high in the 70s. The anomalously high geopotential height at 100 hPa and anomalously low zonal wind (and wind speeds) at all levels in the early 80s is in conjuction with the characteristic depression in the Jan-Mar AO index at the same time.

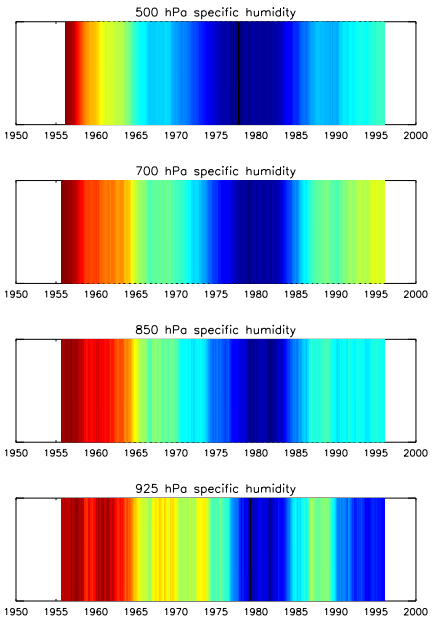

Figure 3.3: Same as fig. 3.2 but for specific humidity at 925, 850, 700 and 500 hPa.

The development toward anoma-

lously low geopotential height and anomalously high zonal wind (and wind speeds) at all levels in the late 80s and 90s is in conjunction with the characteristic high Jan-Mar mean AO index at the same time. The development toward anomalously high geopotential height at all levels (except at 100 hPa) in the 90s is in conjuction with the negative AO trend in the 90s. From these observations, we can conclude that the developments in the geopotential height and wind fields are strongly coupled with the Jan-Mar mean AO index. The relationship between the AO index and temperature, if any, is not as clear. However, the temperature at 300 hPa shows remarkably similar features as the color spectrum of the AO index (fig. 1.14), and consequently as the zonal wind in the troposphere (compare the temperature at 300 hPa with the zonal wind in the troposphere), where low temperatures seem to call for weak zonal winds and vice versa. This apparent relationship appears to reverse in the lower stratosphere, where cold conditions call for strong zonal winds and lower geopotential heights in conjuction with a stronger polar vortex (compare the temperature with the zonal wind and geopotential height at 100 hPa).

Viewing these results in context we can state that the statosphere has abruptly developed toward lower geopotential heights and temperatures, and stronger winds in the last two decades. All these developments are conducive toward a stronger polar vortex. Lower geopotential heights and stronger winds are also developing in the troposphere, however the temperature has been increasing since the 80s. In addition, the development in the AO index is best reflected in the zonal wind at all levels.

3.2.2 The annual and Jan-Mar mean anomalies

The geopotential height plunge seen in the 80s and 90s in fig. 3.2 in the troposphere is mainly due to the anomalously low values in the annual and Jan-Mar mean 1989 and 1990 (fig. 3.4 and 3.6). This dramatic plunge does not appear in the stratosphere where the negative geopotential height trend has been gradual since the mid-80s. The tropospheric geopotential heights have been recovering from the anomalously low values in the early 90s and there is evidence of a later recovery in the stratosphere in the mid-90s.

There are two distinctive peaks in the Jan-Mar mean temperature at 50 hPa, a warm peak in 1989 and a cold peak in 1996 (also seen at the 100 hPa level), which can be linked to known events in the atmosphere (also apparent in the annual mean). The 1989 warm peak is due to a sudden warming event in January (Steenrod et al., 1991; Seol and Yamazaki, 1997) and the 1996 cold peak is due to the unusual tilt of the polar vortex center of action toward the Atlantic region and its above normal strength and prevalence (Newman et al., 1997). As a consequence, the the total column of ozone abundance in 1996 was measured a record low over Iceland. The apparent stratospheric cooling over Iceland is therefore likely due to both the tilt inclination of the

vortex and the strengthening of the vortex. The well known stratospheric cooling is only evident in the 90s, with an apparent recovery later on.

The wind speed and zonal wind have been showing positive trends since in the mid-80s, especially in the stratosphere. The record high value in the Jan-Mar means occurs in 1997 and is in accordance with the well documented 1996/97 record high polar vortex strength (Newman et al., 1997; Hansen and Chipperfield, 1999). Unlike the 1995/96 polar vortex, the 1996/97 vortex had its center of action over the pole and therefore appears to be stronger in the zonal wind and not as cold as the 1995/96 vortex over Iceland. The wintertime stratospheric temperatures over Iceland are therefore strongly dependent on the polar vortex tilt, or its center of action. There are also notable peaks in the tropospheric zonal wind (seen both in the Jan-Mar and annual means) that could possibly be related to the major volcanic eruption El Chichon in 1982 and Mount Pinatubo in 1991. As mentioned in section 1.3.1, Kodera (1994) states that stratospheric anomalies induced by volcanic aerosol can propagate down to the troposphere, producing considerable changes. He further concludes that after major volcanic eruptions, the following winter has stronger zonal-mean zonal winds in the polar region but weaker around 40°N. This dipole type anomaly in the middle and higher latitudes extends from the stratosphere to the troposphere and resembles the AO signal (fig. 1.8). In fact, he continues to describe an AO like signal in the SAT field, where major volcanic eruptions are followed by warm tropospheric temperatures over Europe, Siberia and North America, while cooling occurs over western Asia to North Africa (fig. 1.7). It is highly likely that what their seeing is an AO signal that is induced by major volcanic eruptions. If this is true, then the effect of major volcanic eruptions on climate is best seen over Iceland in the zonal wind field. Both eruptions, El Chichon and Mount Pinatubo, are followed the next winter by anomalously high tropospheric zonal winds and wind speeds. Furthermore, the Jan-Mar AO index shows a substantial jump to higher polarity the following winter only after the Mount Pinatubo eruption (a value of 1.5 standard deviations in the 1992 Jan-Mar mean from the low value 0.2 in 1991). This is in agreement with the apparent Pinatubo signal being stronger than the Chichon signal throughout the atmosphere over Iceland. There is however no obvious signature from the 1963 Agung eruption over Iceland.

The annual specific humidity shows similar features has the annual 925 hPa temperature, devided into a characteristic negative trend period pre-1979 and a positive trend period post-1979. This is also evident in the precipitable water (see section A.5 for definition and calculation methods) calculated by Hrafn Guðmundsson (1999). Therefore, the temperature near the surface is a controling parameter for the humidity concentrations in the lower troposphere. There is however a distinctive discrepancy in the lower tropospheric temperature and specific humidity relationship that occurs in the 90s, seen more clearly in the annual means, where the latter plunges

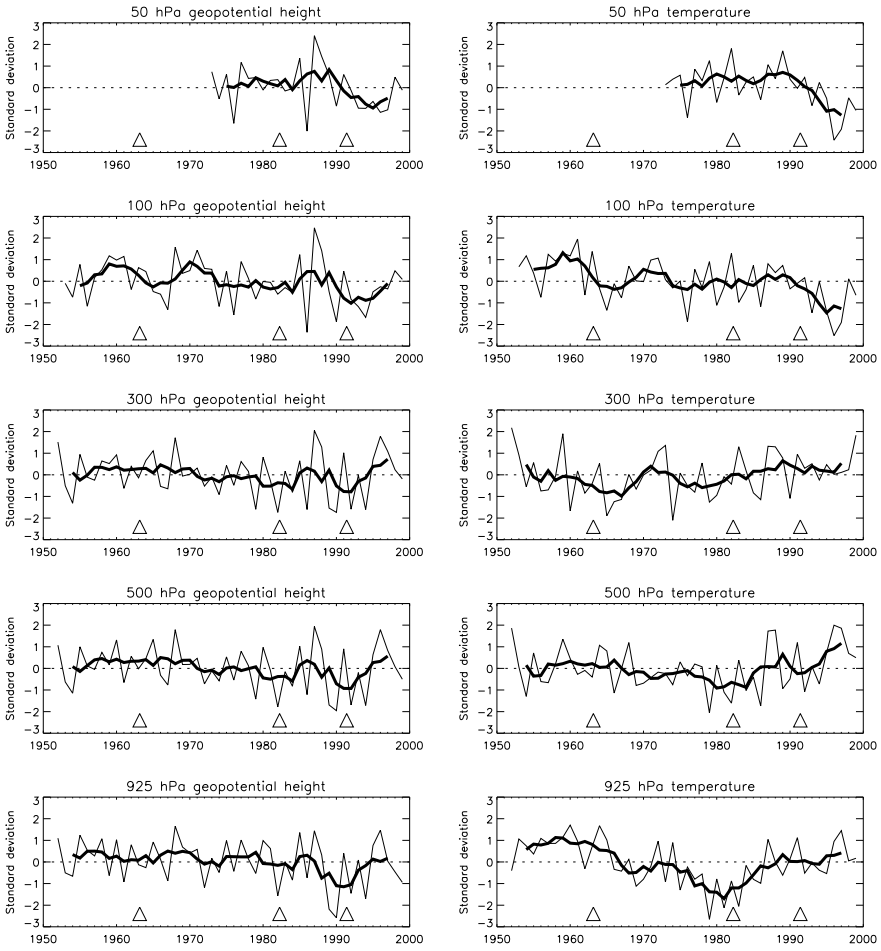

Figure 3.4: Annual mean time series of the geopotential height and temperature at 925, 500, 300, 100 and 50 hPa. The thick line is the 5-year running mean. The triangles mark the events of the major volcanic eruptions of Mt. Agung 1963 in Indonesia, El Chichon 1982 in Mexico and Mt. Pinatubo 1991 in the Philippines.

substantially to anomalously low values, while the former still recovers from the low values in 70s and 80s. This was also mentioned in relation with the spectrum plots above.

We can summarise these developments in conjunction with the Jan-Mar AO index. In fig. 3.9 it is evident that the anomalously low geopotential heights and strong zonal winds at 925, 300 and 100 hPa since the 70s are related to the anomalously high AO values at the same time. The AO-temperature relations, if they exist, are not as clear, although there seems to be an inclination toward colder conditions, especially in the lower stratosphere, when the AO is low.

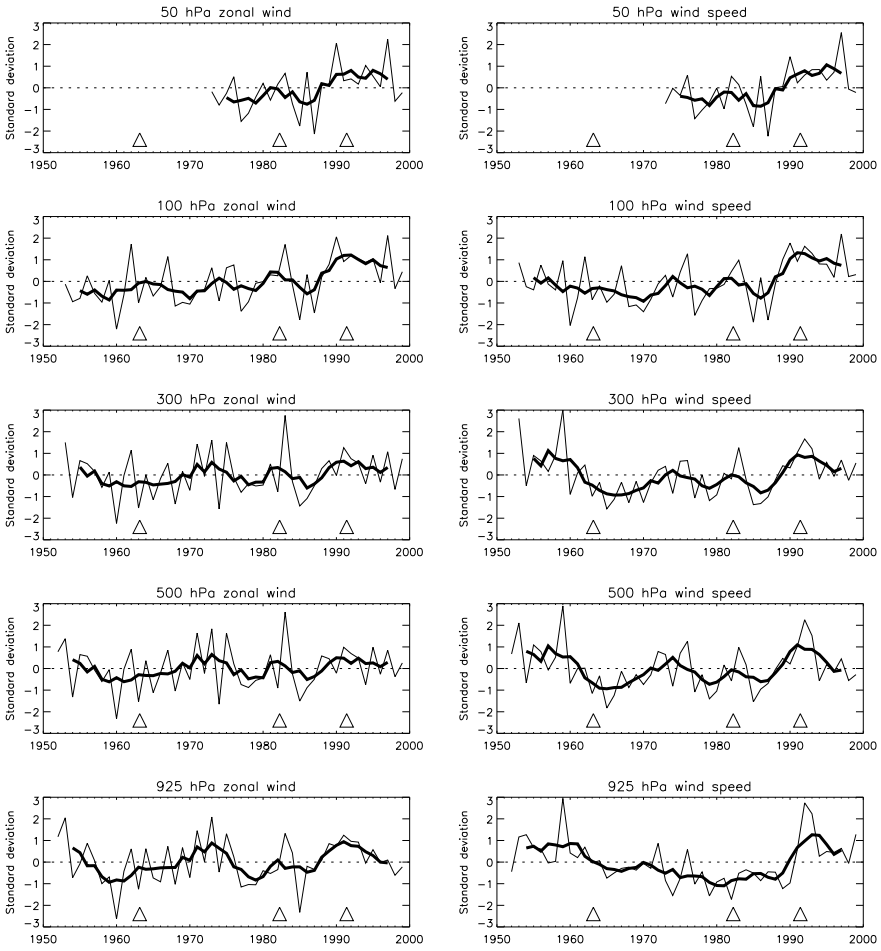

Figure 3.5: Same as in fig. 3.4 but for zonal wind and wind speed.

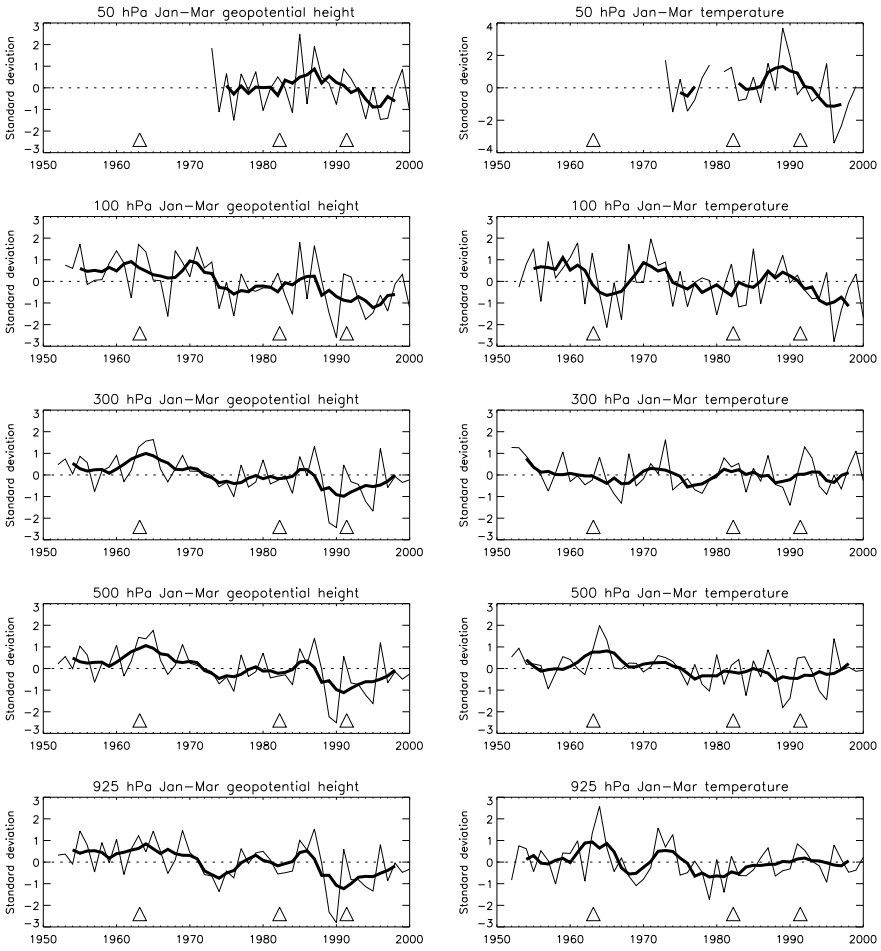

Figure 3.6: Same as for 3.4 but for Jan-Mar averages.

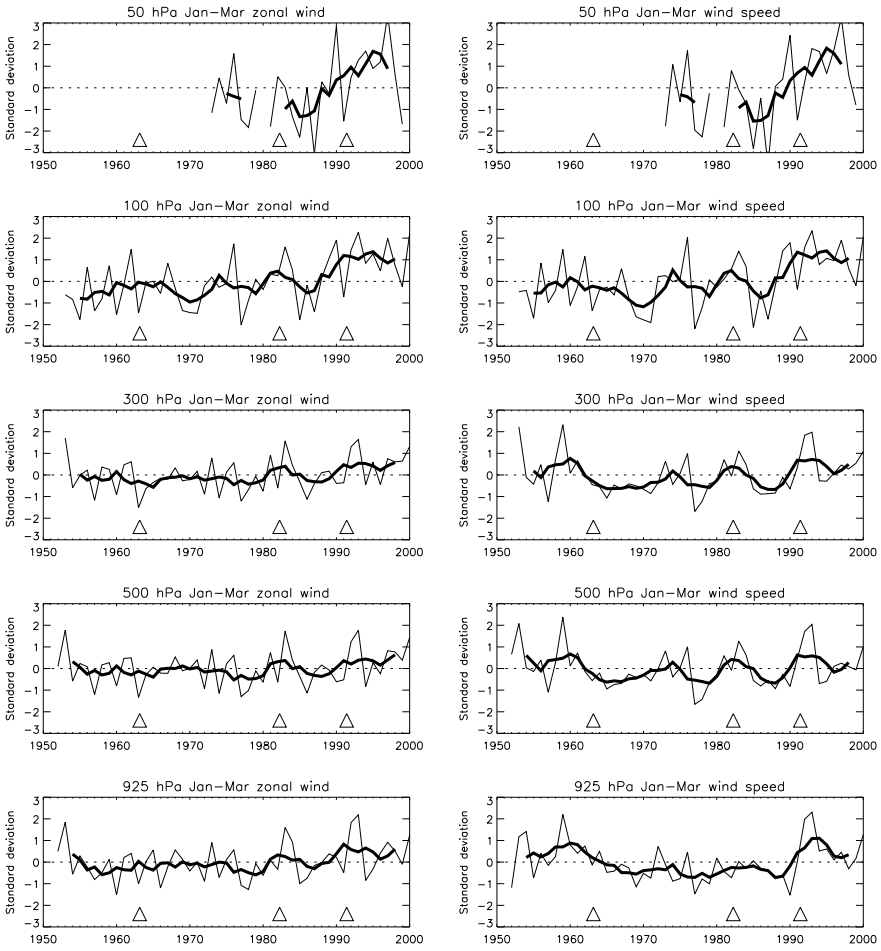

Figure 3.7: Same as fig. 3.4 but for Jan-Mar averages of the zonal wind and wind speed.

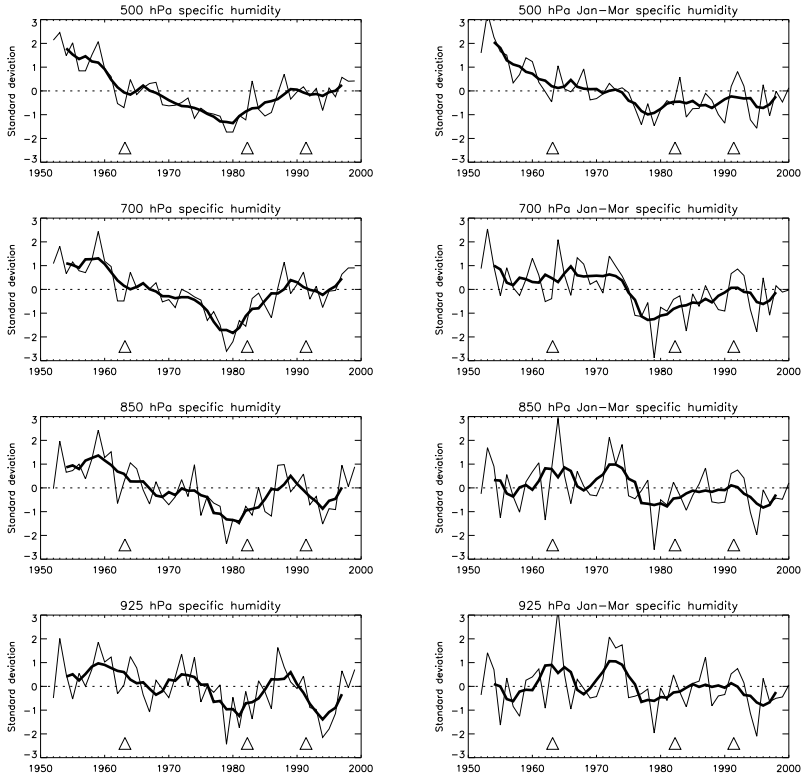

Figure 3.8: Left: Same as in fig. 3.4 but for specific humidity at 925, 850, 700 and 500 hPa. Right: Same as fig. 3.4 but for Jan-Mar averages of the specific humidity at 925, 850, 700 and 500 hPa.

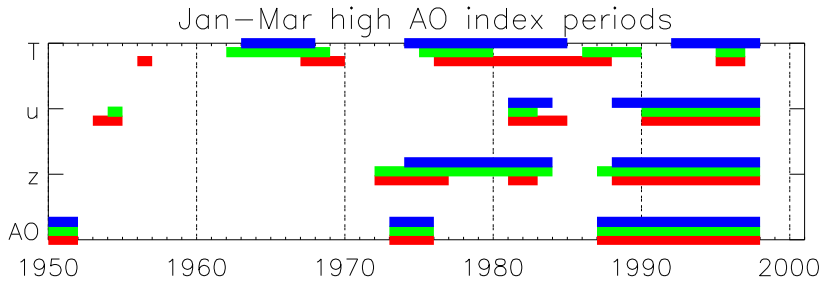

Figure 3.9: Anomalously high and low periods for the geopotential height (z), zonal wind (u) and temperature (T) for 925 (red), 300 (green) and 100 hPa (blue), compared with the AO index. The color bars mark anomalously high periods for the AO and zonal wind and anomalously low periods for the geopotential height and temperature based on the 5-year running mean of the Jan-Mar mean time series.

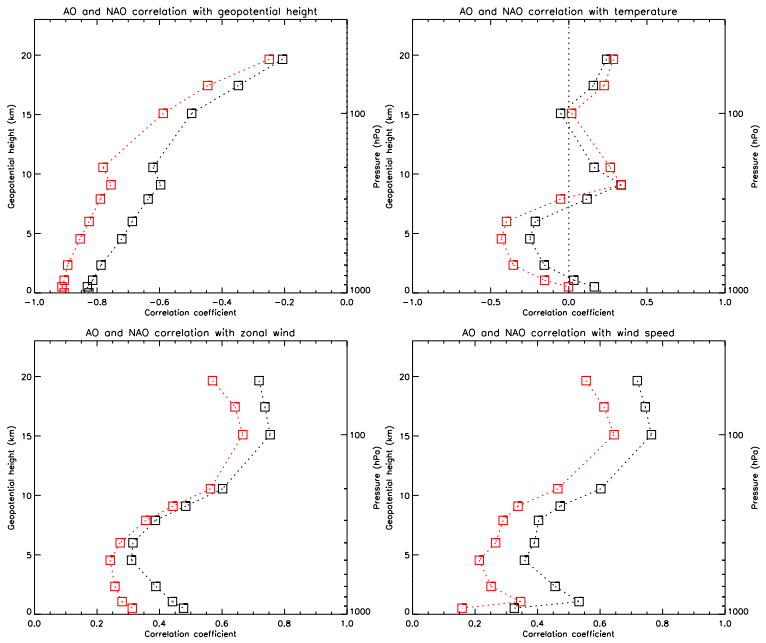

Figure 3.10: The Jan-Mar correlation of the AO (black) and NAO (red) indexes with the geopotential height, temperature, zonal wind and wind speed. The correlations are based on Jan-Mar mean data in the period 1952-00 (except for data above 100 hPa there is only data available for the period 1973-00) from 1000 hPa to 50 hPa. Correlations above 100 hPa are based on at least 20 years of data.

3.3 The AO signal

3.3.1 Correlation

The Jan-Mar correlation[4] between the AO and NAO indexes and the geopotential height, zonal wind, temperature and wind speed is shown in fig. 3.10.

As expected, the correlation between the NAO and geopotential height is slightly greater than for the AO in the entire 1000-30 hPa layer. This is the consequence of the SLP in Iceland being part of the NAO definition. We also see that the correlation is best at the surface, which is reasonable since the definitions of the AO and NAO indexes are both based on SLPs.

The wind correlations with the AO and NAO are highly positive, especially in the lower stratosphere and are at all levels higher for AO relative to NAO. This is a reasonable result since the AO is a better measure of the regional meridional pressure gradient hence the zonal wind strength at mid-latitudes around the entire subpolar region than NAO is. We see that the correlation profile at the 64°N between the AO and the zonal-mean zonal

[4]In the following discussion, we must have in mind when making conclusions, that correlations in the stratosphere (above 100 hPa) are based on the period 1973-00 versus the period 1952-00 between 1000 and 100 hPa. Any features or effects could be caused by this limitation rather than by real physical processes.

wind in fig. 1.8a strongly resembles that of the correlation of the Jan-Mar AO with the zonal wind over Iceland. Both profiles have a characteristic correlation minimum at approximately 500 hPa and a maximum at approximately 100 hPa. The correlation over Iceland is always slightly lower than for the zonal-mean as expected, since the AO is connected to the entire annular flow around the polar cap and not just at a single localized point. In addition, the tropospheric wind speed correlations are slightly greater than for the zonal wind, but there is a notable decrease in wind speed correlation at the surface not seen in the zonal wind.

The temperature shows weak correlation with the AO, although the correlations with the NAO seem to be slightly higher. The tropospheric temperatures tend to be negatively correlated with the AO and NAO, while above 300 hPa the correlations are positive. According to the AO correlations with the zonal-mean temperature at 64°N in fig. 1.9a, we can not expect a strong relationship between the AO and temperature near the surface over Iceland. This conclusion is also supported by the AO signature in the zonal-mean temperature in fig. 1.9b and the SAT in fig. 1.7. However, the negative temperature correlations in the middle troposphere over Iceland are in accordance with the zonal-mean temperature correlations. In the lower stratosphere the agreement between zonal-mean temperature correlations and temperature correlations over Iceland fails. The temperature correlatons over Iceland tend to be positive in contrast to the highly negative correlations in the zonal-mean temperature. This means that the positive AO polarity is not necessarily associated with wintertime stratospheric cooling over Iceland as it is in general for the zonal-mean temperature north of approximately 55°N.

The AO and NAO correlations with the wind speed, zonal wind, geopotential height and temperature for each month is shown in fig 3.11 and support the above conclusions.

The wind speed and zonal wind show similar features in the cold seasons in the stratosphere in both the AO and NAO correlations. In accordance with the regional definition of the AO, its correlation with the wind field is substantially greater for all months in the atmosphere relative to the NAO. Again we see the characteristic minimum in the troposphere, which divides the relatively high correlations in the lower stratosphere and at the surface. Wind speed and zonal wind correlation with the AO, show values above 0.7 in the lower stratosphere in Dec-Feb. In the summer stratosphere, where the zonal flow turns easterly after the polar vortex breakdown, the AO correlation with the zonal wind becomes high. This is also seen in the wind speed as a negative correlation. This means that for a high summertime AO index polarity, one can expect weak stratospheric easterlies. This is somewhat surprising since the AO signature is confined to the troposphere in the summertime in addition to being only about 1/3 of its wintertime

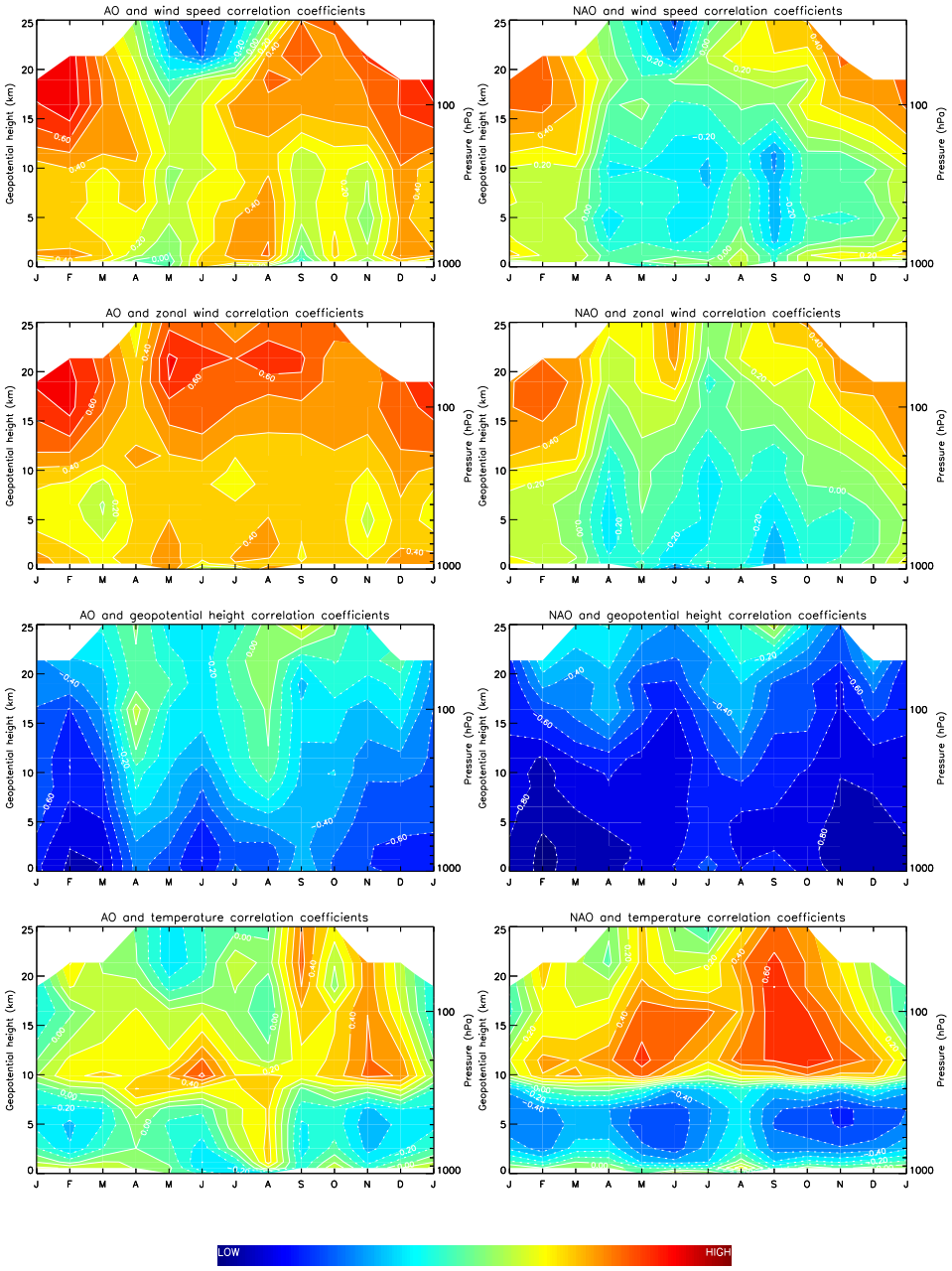

Figure 3.11: AO and NAO correlations with the wind speed, zonal wind, geopotential height and temperature for each month. Contour intervals are 0.1 (-1, -0.9, ..., 1). Correlations above 100 hPa are based on at least 20 years of data.

amplitude[5]. Furthermore, we see that the high stratospheric zonal wind correlation continues into the autumn in Aug-Sep when the polar vortex starts its buildup. These results seem to indicate an AO modulation of the summer stratosphere, which in general is not believed possible. We also see that the AO correlation with the zonal wind is greater than for the wind speed except in the winter troposphere and Jul-Aug troposphere. The AO correlations are distinctively low in the months of the polar vortex breakdown, especially for the wind speed. As in the zonal-mean zonal wind in fig. 1.8a, the maximum wintertime correlation is near 100 hPa.

As expected, the geopotential height is highly correlated with the AO and NAO at the surface. Unlike for the wind, the NAO is more correlated with the geopotential height than AO is. Again, this is because of the definition of the NAO. A notable feature in the AO correlation with the geopotential height is the way the high correlations extend up into the stratosphere in the winter and the high correlations in the lower summer troposphere. This is in accordance with the fact that the AO signal is apparent year-round in the troposphere and amplifies with height upward into the stratosphere in wintertime. Also, there are distinctive low correlations in April and September, which are the months that mark the periods of breakdown and buildup of the polar vortex.

The AO correlation with temperature is weak, although there is a tendency toward positive correlations near and above the tropopause versus negative correlations in the troposphere, as in the Jan-Mar mean temperature correlations in fig. 3.10. This is more striking in the NAO correlation, where the tropopause seems to mark a sharp deviding line between positive and negative correlations in the stratosphere and troposphere, respectively. Furthermore, the positive correlations in the stratosphere appear to reach higher into the stratosphere in the autumn relative to other seasons. We see that the expected wintertime stratospheric cooling associated with a high AO polarity is only apparent in January above 10 km, judging from the correlations. Therefore, the inclination toward positive correlations in the Jan-Mar mean temperature in the lower stratosphere in fig. 3.10, is mainly in Feb-Mar.

Correlations of the AO with the specific humidity (not shown) are in general weak, although there is a tendency toward positive correlation at the surface in wintertime.

3.3.2 High and low AO polarity periods and years compared

When the high and low Jan-Mar AO polarity years are compared in their climatological mean, two main features seem clear: Stronger wintertime winds

[5]We have to keep in mind that even though the stratospheric summertime correlations with zonal wind are of similar magnitude as for the stratospheric wintertime correlations, the summertime winds are much weaker.

and colder stratosphere in January for the high AO polarity relative to the low AO polarity (fig. 3.12). We can also see that the breakdown process is prolonged into April for the high AO polarity, while the polar vortex is on the average completely destroyed at that time above approximately 20 km for low AO years. However, in both cases the polar vortex buildup process begins in August. We can also see that contour lines are considerably denser in the late winter lower stratosphere in the high AO index polarity, meaning a more violent breakdown process. The polar vortex destruction is seen clearly in the zonal wind field and the apparent increase in its contour slopes in Apr-May, seen both in the high and low AO polarity although more pronounced in the former, is seen deep down in the troposphere, indicating a stratosphere-troposphere coupling connected to this destruction, as mentioned in section 1.1. There is a surprising feature in the zonal wind contour lines in Aug-Sep, which are considerably denser throughtout the atmosphere for the low AO polarity relative to the high AO polarity. This is an indication that the buildup process is faster the first month in a low AO polarity year relative to a high AO polarity year. There is a distinctive dipole feature between the late and early winter stratosphere in the low AO polarity seen both in the wind speed and zonal wind fields. More apparent in the zonal wind field, there are distinctive maximum dipole like wind belts in December and February. This means that the polar vortex has the tendency to fail to buildup over the entire active seasons and tends to partially breakdown in January and then recover in February. This rebounding effect is not seen in the high AO polarity, where the polar vortex buildup is gradual over the entire active seasons, reaching a peak value in February with approximately 2 times greater wind speeds relative to the low AO polarity in the lower stratosphere. From the temperature contour plots it is clear that January, the coldest month of the year in the lower stratosphere, is considerably colder in the lower stratosphere for the high AO polarity. However, surprisingly the reverse becomes true in Feb-Mar at the tropopause level and above 20 km. Viewing the specific humidity, high AO years seem to be associated with higher concentrations of humidity in January, relative to low AO years.

From the climatological mean zonal wind fraction of the wind speed in fig. 3.13, it is clear that the high AO years are not only associated with stronger westerlies in the wintertime, but also with larger portions of the wind speed devoted to west-east flow at all levels. The difference in the buildup process mentioned above becomes clearer in the zonal wind fraction of the wind speed. The low AO years are characterized by a relatively fast buildup of the westerlies, reaching the 0.8 mark already in September (approximately a month sooner than in the high AO years). Moreover, this fast shift toward strong westerlies is also apparent in the troposphere. In addition, the violent breakdown of the strong polar vortex in the high AO years appears to cause a delay in the formation of the following easterlies, relative to the low AO years.

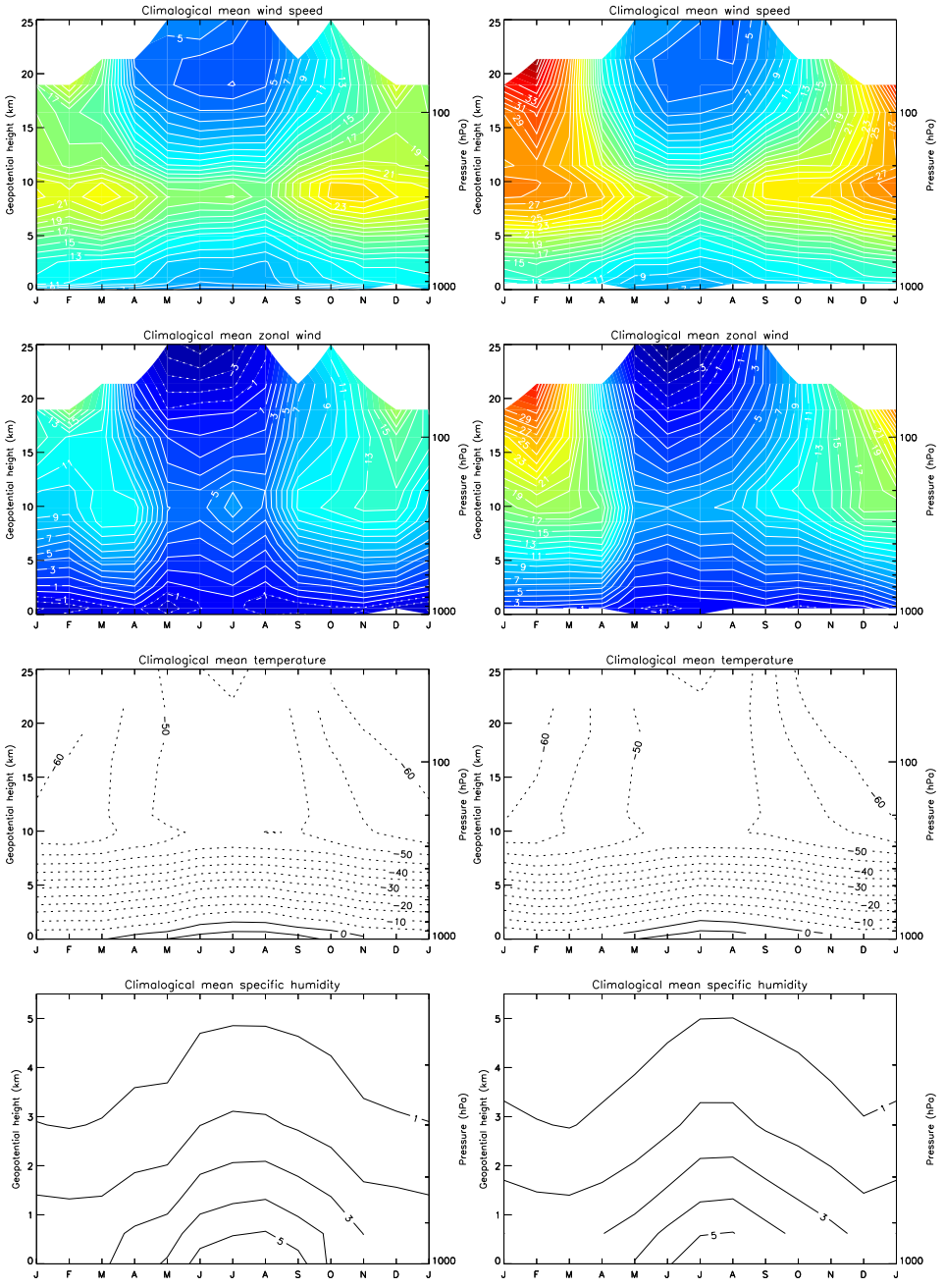

Figure 3.12: Seasonality of the climatological monthly mean wind speed, zonal wind, temperature and specific humidity for the high (right panel) and low (left panel) AO polarity years. Contour intervals are 1 m/s (-1, 0, 1, ...) for the wind speed and zonal wind, 5°C (-5, 0, 5, ...) for the temperature and 1 g/kg (-1, 0, 1, ...) for the specific humidity. The data is based on high and low AO polarity years (Above and below one standard deviation from the Jan-Mar mean AO index) in the period 1947-00 (Except the data above 100 hPa is based on the period 1973-00.)

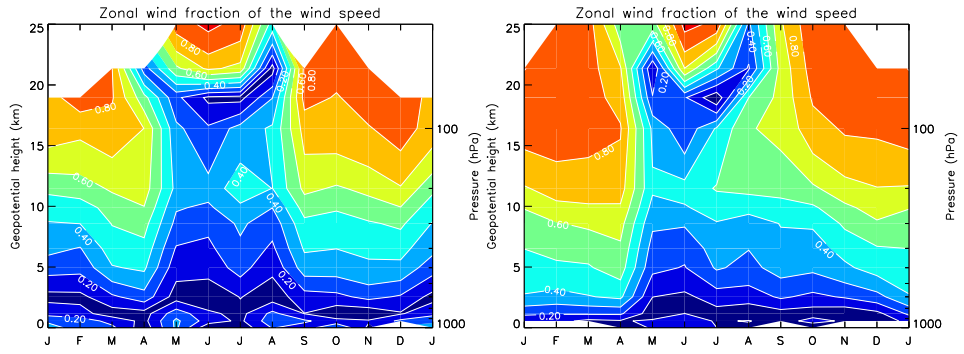

Figure 3.13: Seasonality of the climatological monthly mean zonal wind fraction of the wind speed for high (right) and low (left) AO years based on data between 1000 and 30 hPa. Contour intervals are in fractions 0.1 (0, 0.1, ...,1).

The contrasts between high and low AO years mentioned above become more clear when we calculate their climatological monthly mean difference (fig. 3.14). The following conclusions are the main features that apply to high AO years, relative to low AO years:

- Stronger wind speeds and zonal winds at all levels (except in autumn for the zonal wind), mainly in Dec-Apr
- Lower geopotential heights, mainly in Jan-Mar at all levels
- Colder lower stratosphere, mainly in January
- Warmer tropopause in Feb-Mar
- Warmer stratosphere above 20 km in Feb-Mar
- Colder troposphere in Feb-Apr
- Higher humidity concentrations near the surface in Jan-Feb

The maximum difference between high and low AO periods in the wind and geopotential fields are in February below 20 km and in January above 20 km. The observed AO amplitude in the zonal wind over Iceland is substantial compared to the climatological mean polar vortex, or about 70%. The negative difference in the springtime wind fields, seen best in the zonal wind in September above 15 km, is in accordance with the buildup process being faster in the low AO years, relative to the high AO years (fig. 3.13).

In fig. 3.15 the climatological monthly mean difference of high and low AO years has been normalized with respect to the difference between the associated mean Jan-Mar high and low AO index. Therefore, the amplitudes shown for each parameter correspond to anomaly values in that field that occur in association with a one standard deviation anomaly in the Jan-Mar AO

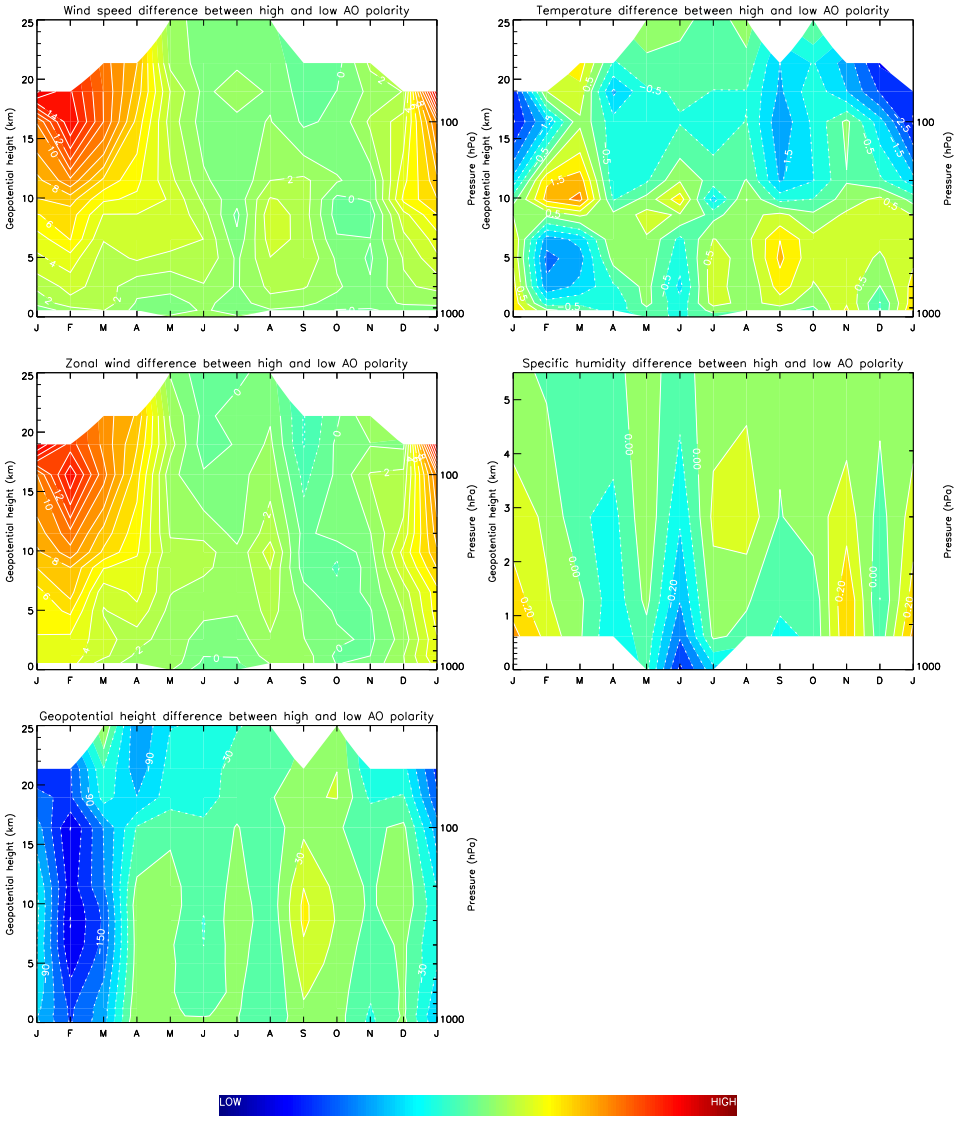

Figure 3.14: Seasonality of the climatological monthly mean difference between high and low AO years for the wind speed, zonal wind, geopotential height, temperature and specific humidity. The data is based on 8 (7 above 100 hPa) high and 13 (4 above 100 hPa) low AO years in the period 1947-00. Contour intervals are 1 m/s (-1, 0, 1, ...) for wind speed and zonal wind, 0.5°C (-0.5, 0, 0.5, ...) for temperature, 30 m (-30, 0, 30, ...) for geopotential height and 0.1 g/kg (-0.1, 0, 0.1, ...) for specific humidity.

index time series and are comparable to the AO amplitudes in fig. 1.6, 1.7, 1.8 and 1.9. The zonal wind amplitude over Iceland is considerably greater than the zonal-mean zonal wind amplitude in fig. 1.8b at the 64°N, especially in the troposphere. The mean Jan-Mar geopotential height amplitude over Iceland is in excellent agreement with fig. 1.6 (table 3.1). There is however some discripancy in the stratospheric levels where the estimated geopotential height amplitude in this study is considerably smaller than in fig. 1.6. In fig. 1.7 we see that Iceland lies between positive and negative SAT anomalies in the AO amplitude. This is in accordance with the SAT signature in fig. 3.15. However, the negative temperature amplitude in the upper troposphere and lower stratosphere seen in fig. 1.9b is not as strong over Iceland.

hPa	B1999	H2001
100	-80 m $\pm 20m$	-45 m $\pm 5m$
200	-40 m $\pm 20m$	-40 m $\pm 5m$
300	-45 m $\pm 15m$	-43 m $\pm 5m$
500	-40 m $\pm 10m$	-40 m $\pm 5m$
700	-40 m $\pm 10m$	-37 m $\pm 5m$
1000	-45 m $\pm 10m$	-35 m $\pm 5m$

Table 3.1: Comparison of the AO signatures in the geopotential height at 100, 200, 300, 500, 700 and 1000 hPa obtained in this study (H2001) with that from Baldwin and Dunkerton (1999) (B1999). The error intervals for B1999 are estimated from the contour intervals in fig. 1.6 and for H2001 are estimated from eq. (2.21).

We will now see that the strong AO signals in the wind, temperature and geopotential fields show strong resemblance to the main climatic changes observed over Iceland in recent decades. We must ask ourselfs what the climate changes over Iceland in the second half of the century are actually like. In other words, in terms of the available data, we would like to know if the first half of the period 1952-00 is significantly different from its second half in the main meteorological fields. We know that the entire NH climate has undergone dramatic changes in this period, which is best reflected in the Jan-Mar mean AO index (fig. 1.15). But are these hemispheric changes also reflected in the climate over Iceland? At least we know from the above results that there is a great difference in the climate over Iceland between high and low AO years. Since the AO is the main mode of variability in the NH (after the seasonal variability), the climatic development in the period 1952-00 is most likely characterized by the AO signal seen in fig. 3.14.

The climatological difference between the second and first half of the period 1952-00 (the difference between the periods 1976-00 and 1952-76) is shown in fig. 3.16 (left panel). All the main AO features mentioned above are evident except the high humidity concentrations in January does not reveal itself in this case. As expected, when we narrow down on the high and low AO periods, 1988-00 and 1955-71, respectively, in fig. 3.16 (right panel), we get an even better agreement with the AO signatures in fig. 3.14

To understand better the nature of the differences between these high and low AO years, we examine the climatological daily mean development of the zonal wind, geopotential height and temperature at 100 hPa (fig. 3.18).

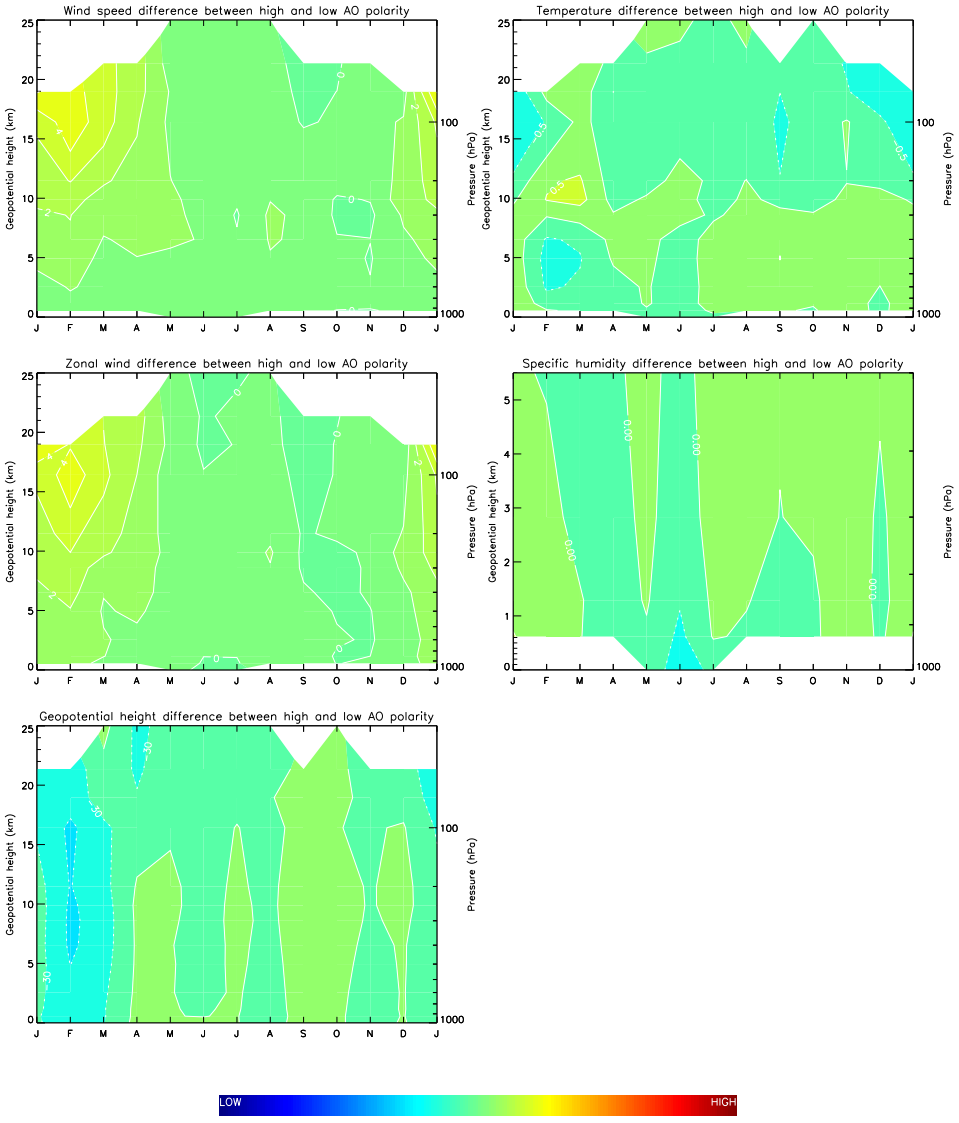

Figure 3.15: Same as in fig. 3.14 but normalized with to the Jan-Mar AO index. The amplitudes shown for each parameter therefore correspond to anomaly values in that field that occur in association with a one standard deviation anomaly in the Jan-Mar AO index time series and can thus be considered typical amplitudes.

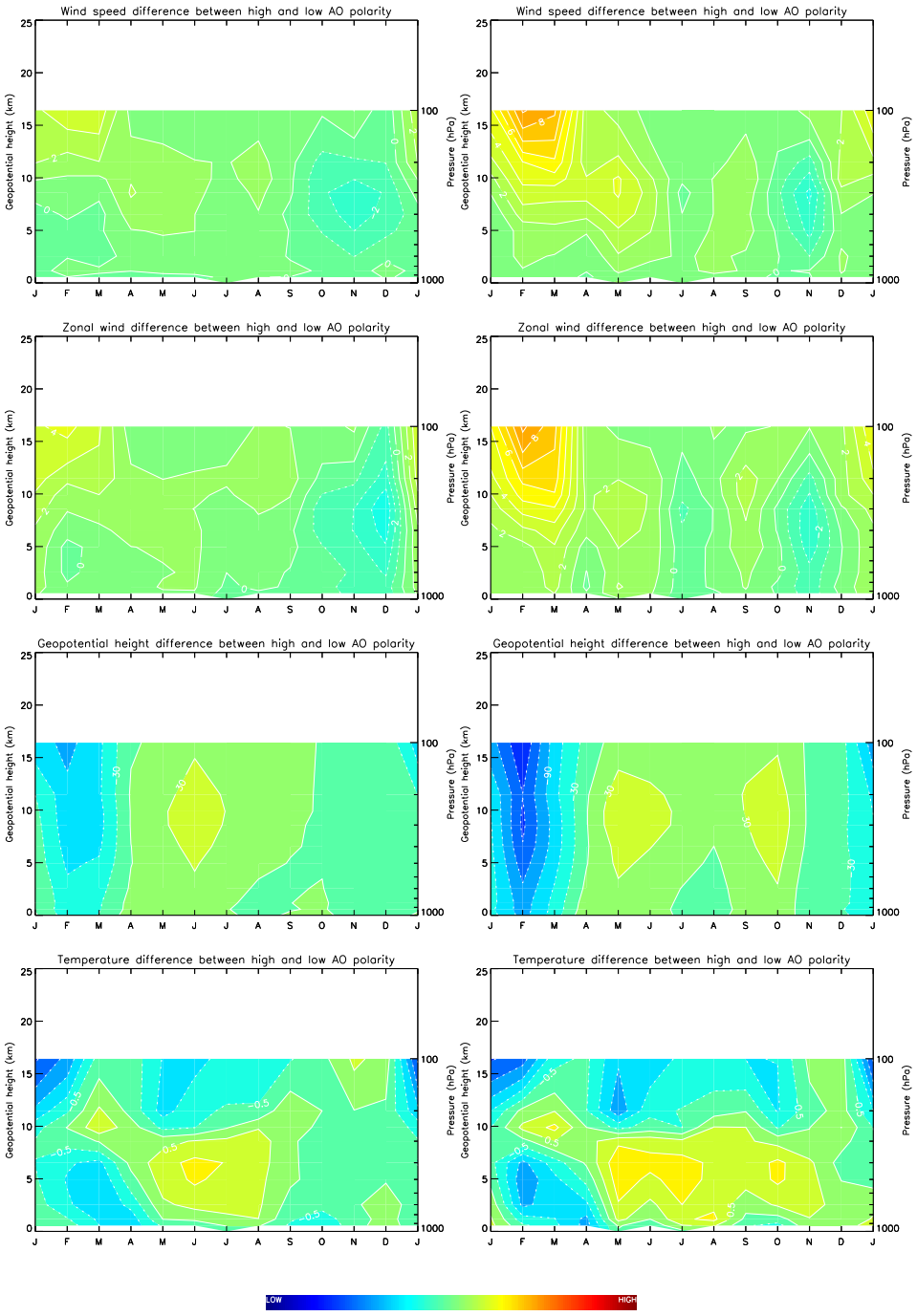

Figure 3.16: Seasonality of the climatological monthly mean difference between high and low AO periods between 1000 and 100 hPa. The left panel shows the difference between the high and low AO index periods 1976-00 and 1952-76 and the right panel the periods 1988-00 and 1955-71, respectively. Contour intervals are 1 m/s (-1, 0, 1, ...) for the wind speed and the zonal wind and 0.5°C (-0.5, 0, 0.5, ...) for the temperature, 30 m (-30, 0, 30, ...) for the geopotential height.

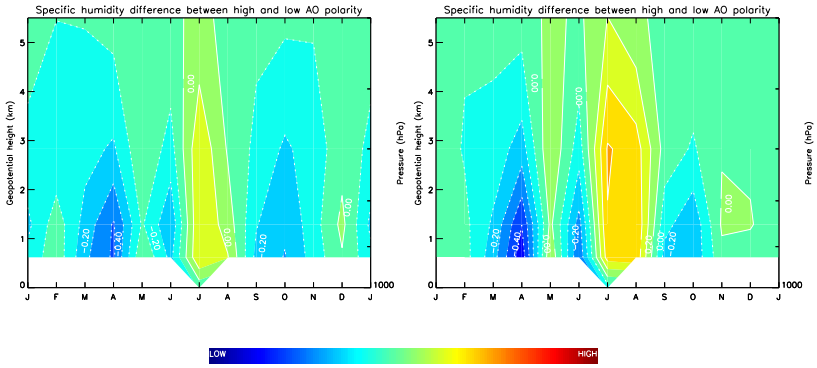

Figure 3.17: Same as fig. 3.16 but for specific humidity with contour intervals 1 g/kg (-0.1, 0, 0.1, ...).

The difference between the high and low AO years in the zonal wind is greatest in Jan-Mar, when the polar vortex strength is at its peak. In accordance to the denser contour lines during the breakdown of the polar vortex seen in fig. 3.12 for the high AO years, the breakdown at 100 hPa of the high AO years is substantially more violent compared to the low AO years. The polar vortex for the low AO years reaches its peak in December, while the zonal wind continues to rise for high AO years until its peak is reached in February. Breakdown speed, measured from the polar vortex peak to the 1st of May amounts to a decrease of 1 m/s in 3.5 days and 1 m/s in 7.2 days for the high and low AO years, respectively. This means that the breakdown process is roughly two times faster for the high AO years relative to the low AO years.

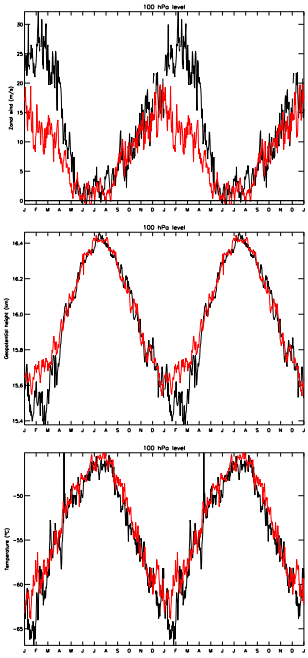

Figure 3.18: Seasonality of the climatological daily mean of high (black) and low (red) AO years at 100 hPa for the zonal wind, geopotential height and temperature. The data is based on years where the Jan-Mar mean AO index is above and below one standard deviation. Each climatological daily mean value is based on at least 7 years.

Also a measure of the polar vortex strength is the geopotential height depression. The main difference is in Jan-Mar, where the high AO years have a deeper polar vortex than the low AO years.

The temperature also shows considerably colder conditions in the Dec-Mar for the high AO years relative to the low AO years in accordance with the above findings. The warm peaks situated on both sides of the polar vortex peak,

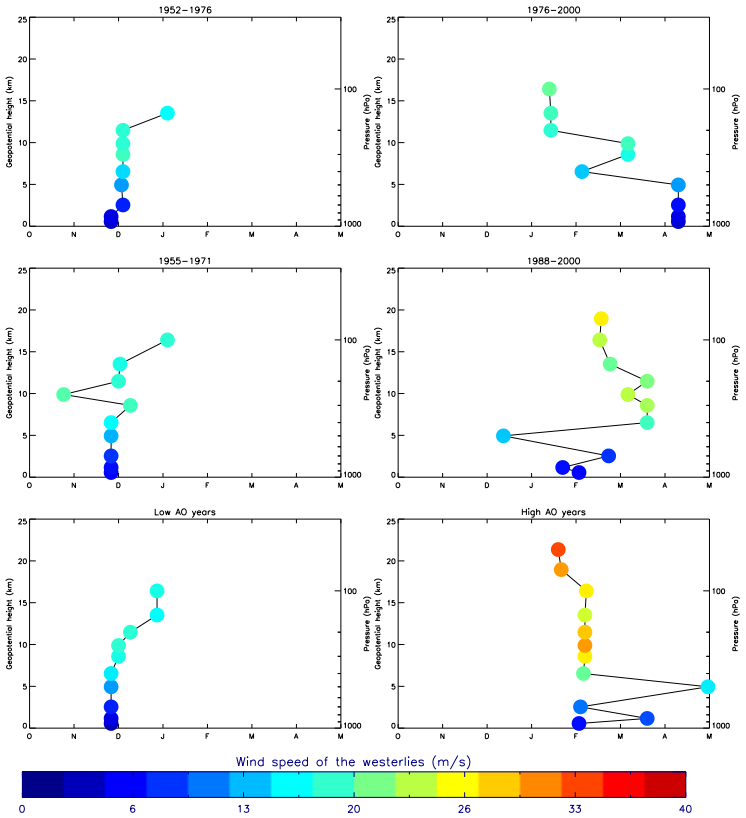

Figure 3.19: The polar vortex peak of the climatological daily mean for high and low AO polarity at various levels. Each period has at least 340 climatological daily means valid. Each climatological daily mean is based on at least 80% of the available years in the period.

also apparent at 50 hPa in fig. 1.5, are a measure of the frequency of sudden stratospheric warmings. There seems to be a tendancy of a delayed early and late winter sudden warmings in the high AO years, relative to the low AO years. Whether this is a consequence of high AO polarity remains a question.

From fig. 3.19 we see that not only is the polar vortex substantially stronger when the AO is high, relative to low AO, but also has a tendency to reach its peak a few months later. The strength of the polar vortex has considerable effect on the tropospheric winds, where strong polar vortex means strong zonal winds in the upper troposphere. For low AO polarity (fig. 3.19, left panel), the tropospheric zonal winds tend to reach there climatological peaks in late November or early December and the lower stratospheric zonal winds peak a month later in late December early January. In contrast, in high AO polarity (fig. 3.19, right panel), the climatological peak of the tropospheric zonal winds are in Feb-Apr and the lower stratospheric zonal winds peak in Jan-Feb.

As we saw in the climatological monthly means of the zonal wind field, there is a distinctive fall in the tropospheric westerlies in Apr-May (seen best in the zonal wind fraction of the wind speed in fig. 3.13 in the high AO years), which could possibly be linked to the polar vortex destruction in

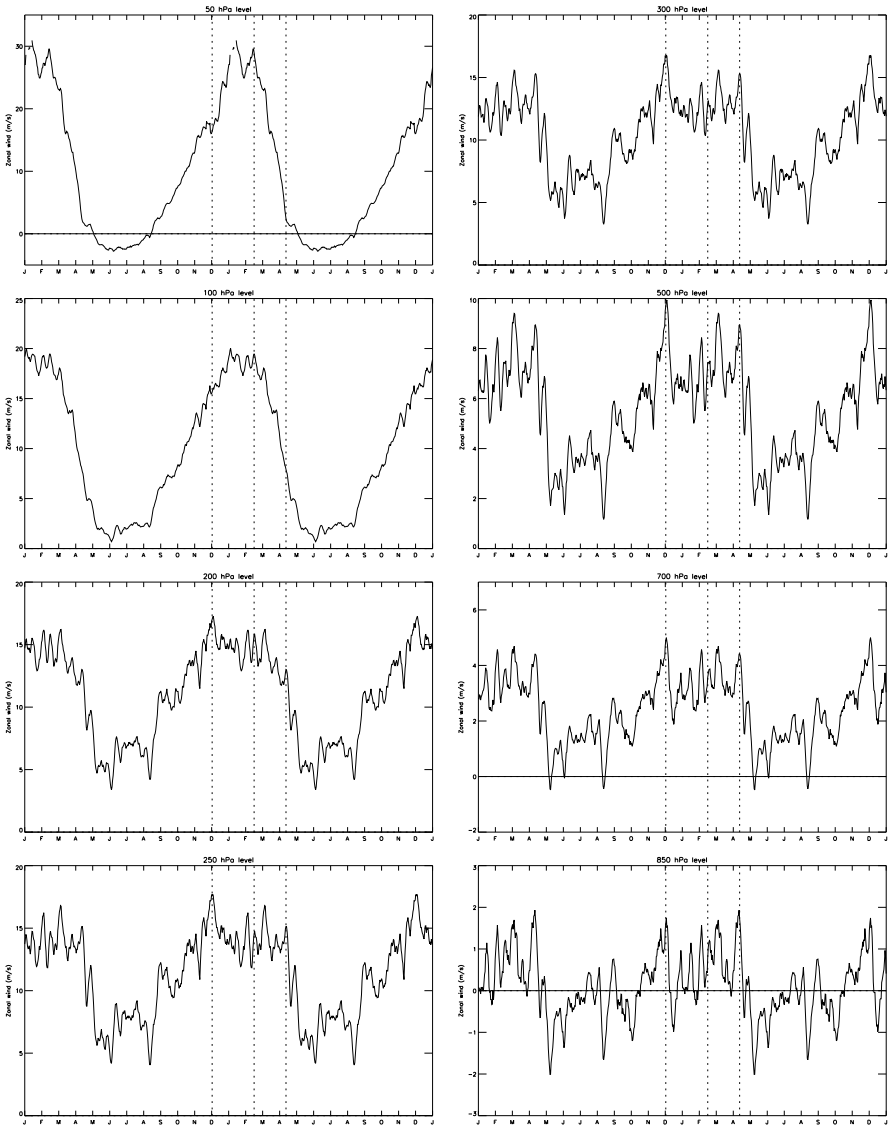

Figure 3.20: Seasonality of the climatological daily mean zonal wind at various levels. The vertical lines mark notable dates in the zonal wind development as described in the main text. The data is based on the period 1952-00 (except 1973-00 at 50 hPa) and the climatological daily means are based on at least 40 years (except 20 at 50 hPa). The climatological daily means are smoothed with a 7-day running mean.

the stratosphere. In fig. 3.20 we see that this zonal wind collapse seems to start in early April and end in early March. The vertical lines mark notable features in the development of the zonal wind. Starting from the early stages of the polar vortex buildup process, the first notable feature is the apparent tropospheric peak in early December. December is the first month where the buildup process recedes at all levels (note the distinctive ridge at 50 hPa). This is, as mentioned before in section 1.2.1, most likely due to increase in stratospheric sudden warming events. This is supported in the climatological daily mean geopotential height and temperature at 50 hPa in fig. 1.5, which both display distincive peaks in December. The interesting result here is that, if stratospheric sudden warmings are the cause, they seem to affect the troposphere also. The first signs of the polar vortex dissipation or breakdown process in seen in mid-February at 50 hPa and approximately two months later in early April the tropospheric zonal winds start to collapse in a course of 2-3 weeks.

3.3.3 Positive and negative AO trend periods compared

Since the first half of the period 1952-00 is characterized by low AO anomalies and the second half by high anomalies, we should expect the trend over the entire period to show strong resemblence to the climatological difference between its second (1976-00) and first (1952-76) half periods (fig. 3.16) and also to the climatological difference between the high and low AO periods (fig. 3.14). This expectation is confirmed in fig. 3.21 (left panel) of the 1952-00 trends in wind speed, zonal wind, geopotential height and temperature. The Feb-Mar wind trends above 10 km, the Feb-Mar geopotential trends at all levels, the January cooling trend above 10 km and the Feb-Apr cooling trend in the troposphere (nearly 0.5°C/dec) are all at the 95% confidence level and are all seen in the high-low AO contrast in fig. 3.14. Therefore, we conclude that these trends are mainly, if not entirely, due to the AO trend in the last few decades. This certifies that the change from negative to positive AO polarity in the period 1952-00 is the main mode of variability over Iceland. In addition, we see again that the zonal wind change penetrates deeper into the troposphere, relative to the wind speed (compare to wind in fig. 3.14). In order to view the trends further up in the stratosphere, we calculate the trends in the period 1973-00 (fig. 3.21, right panel). All the trends for this period exceed the 1952-00 trends as expected in the period of positive AO trend, although their significance are decreased since they depend on a shorter period. There is a notable negative trend in the tropospheric zonal wind in April that is at the 95% confidence level below 5 km. This could be caused by the increasing effectiveness of the downward propagation of the polar vortex breakdown in high AO polarity, observed in fig. 3.20. The stratospheric cooling trend above 10 km in the warm months is also at the 95% confidence level, but whether it's related to the trend in the AO and/or

to anthropogenic influences (e.g. GHG increases) remains uncertain.

To understand further the development of the meteorological parameters in response to AO increases or decreases, we view the characteristic positive and negative AO trend periods 1969-00 and 1952-69, respectively (fig. 3.22). The positive AO trend period is associated with:

- Increasing wind speeds, mainly in Jan-Mar, extending into the spring
- Increasing zonal winds, mainly in Jan-Mar, extending into the spring
- Decreasing lower tropospheric zonal winds in April
- Decreasing geopotential height, mainly in February
- Tropospheric cooling in March
- Tropospheric warming in May-Nov
- Stratospheric cooling for all months

On the contrary, the negative AO trend period is associated with wind speed and zonal wind decreases in most months and geopotential height increases in Dec-Feb. Surprisingly, there is evidence of substantial zonal wind increases and geopotential height decreases in March, and cooling in the winter stratosphere[6]. In addition, these trends are greater than seen for the positive AO trend period. Although the positive AO trend period is associated with stratospheric cooling for all months, the winter stratospheric cooling in the negative AO trend period is in comparison much greater. Therefore, the winter stratospheric cooling and late winter zonal wind increases and geopotential height falls are not necessarily entirely connected to the AO.

The shorter periods 1977-90 and 1989-00, characterized by positive and negative AO tends, respectively, confirm the main conclusions above. And yet again we have a surprisingly strong cooling trend in the winter stratosphere in the negative AO trend period[7]. The only discrepancy is the substantial wintertime stratospheric warming in the positive AO trend period[8]. We can therefore with considerable confidence say that when the wintertime AO increases, we can expect increases in zonal winds, geopotential decreases and tropospheric cooling. Also, when the wintertime AO decreases, we can expect the opposite for most months and also extreme wintertime stratospheric cooling, something we would have expected for the positive AO trend period. However, from fig. 3.15 we can be quite sure that high AO polarity

[6]The stratospheric cooling for the period 1952-69 is due to anomalously low temperatures followed by the Agung eruption in 1963, seen best in the Jan-Mar mean temperature at 100 hPa in fig. 3.6.

[7]This is due to the fact that the stratospheric cooling is greatest in the 90s as seen in fig. 3.6.

[8]This is due to the sudden warming in 1988/89 as seen in fig. 3.6 at 50 hPa.

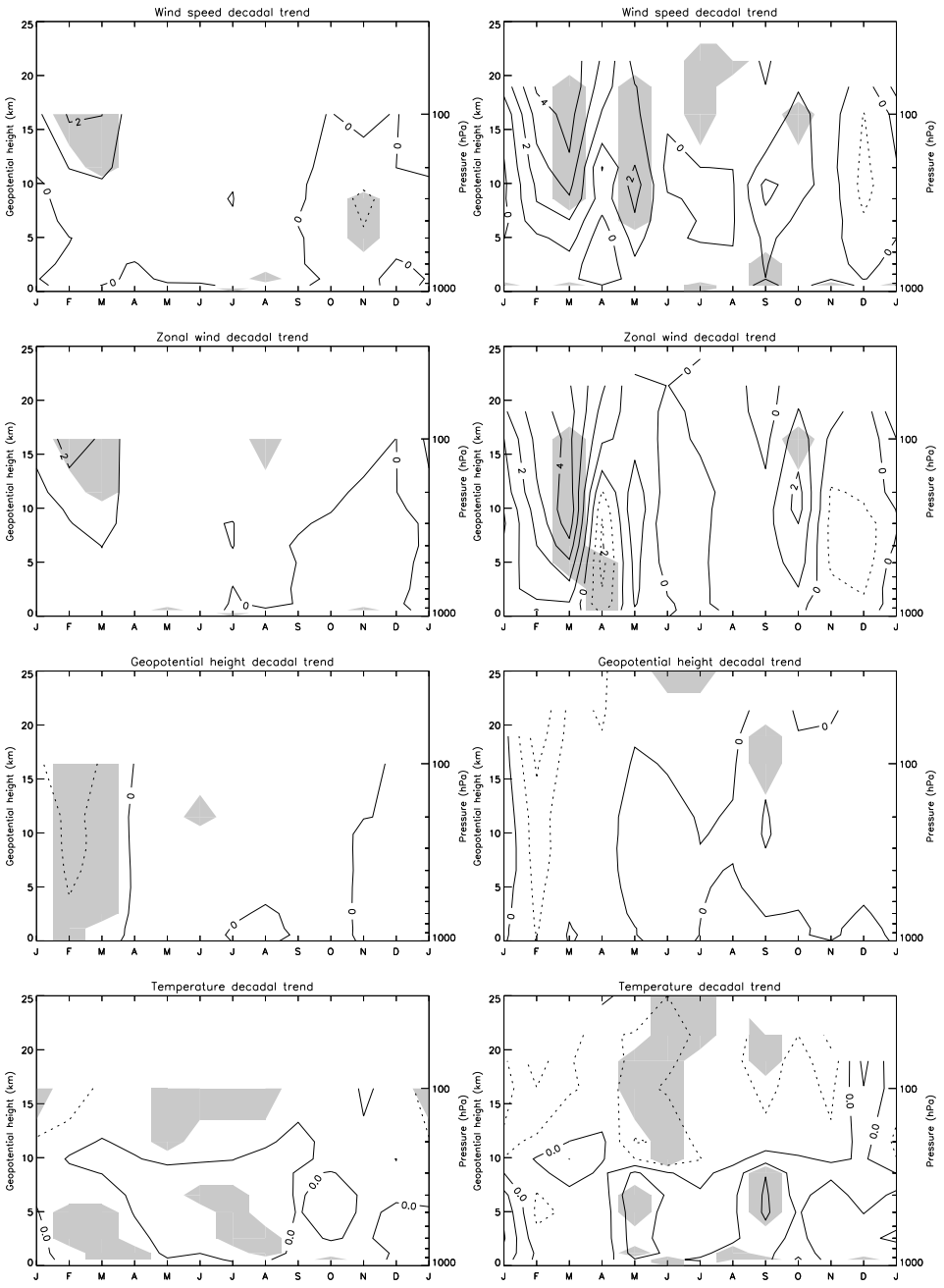

Figure 3.21: Decadal trends in wind speed, zonal wind, geopotential height and temperature for the periods 1952-00 (left panel) and 1973-00 (right panel) between 1000 and 100 hPa and between 1000 and 30 hPa, respectively. Shaded areas denote trends at the 95% confidence level. All trends are based on at least 45 years for 1952-00 and 27 years for 1973-00.

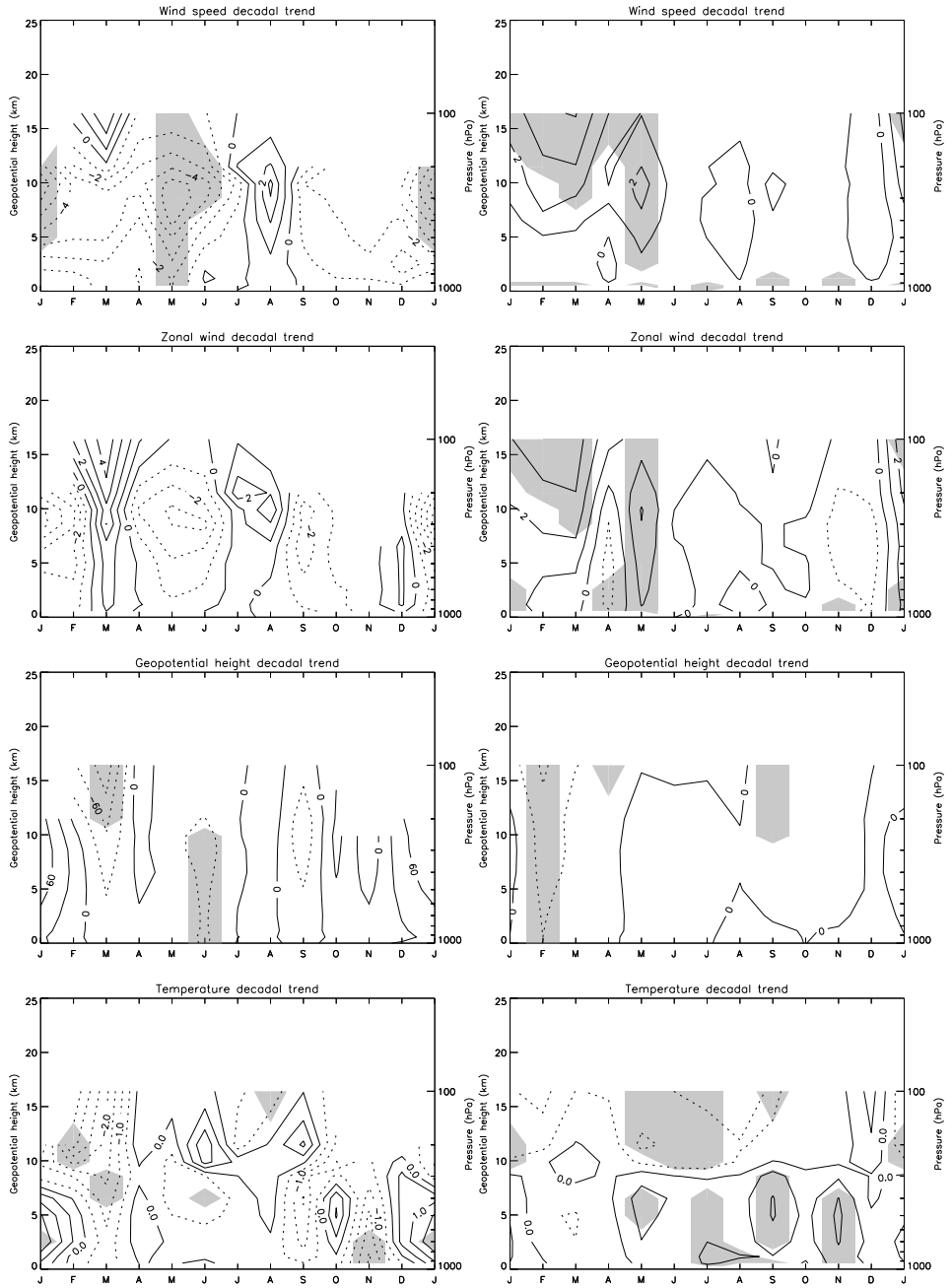

Figure 3.22: Same as in fig. 3.21 but for the periods 1952-69 (left panel) and 1969-00 (right panel) and the shaded areas denote trends at the 90% confidence level. All trends are based on at least 17 years for 1952-69 and 30 years for 1969-00.

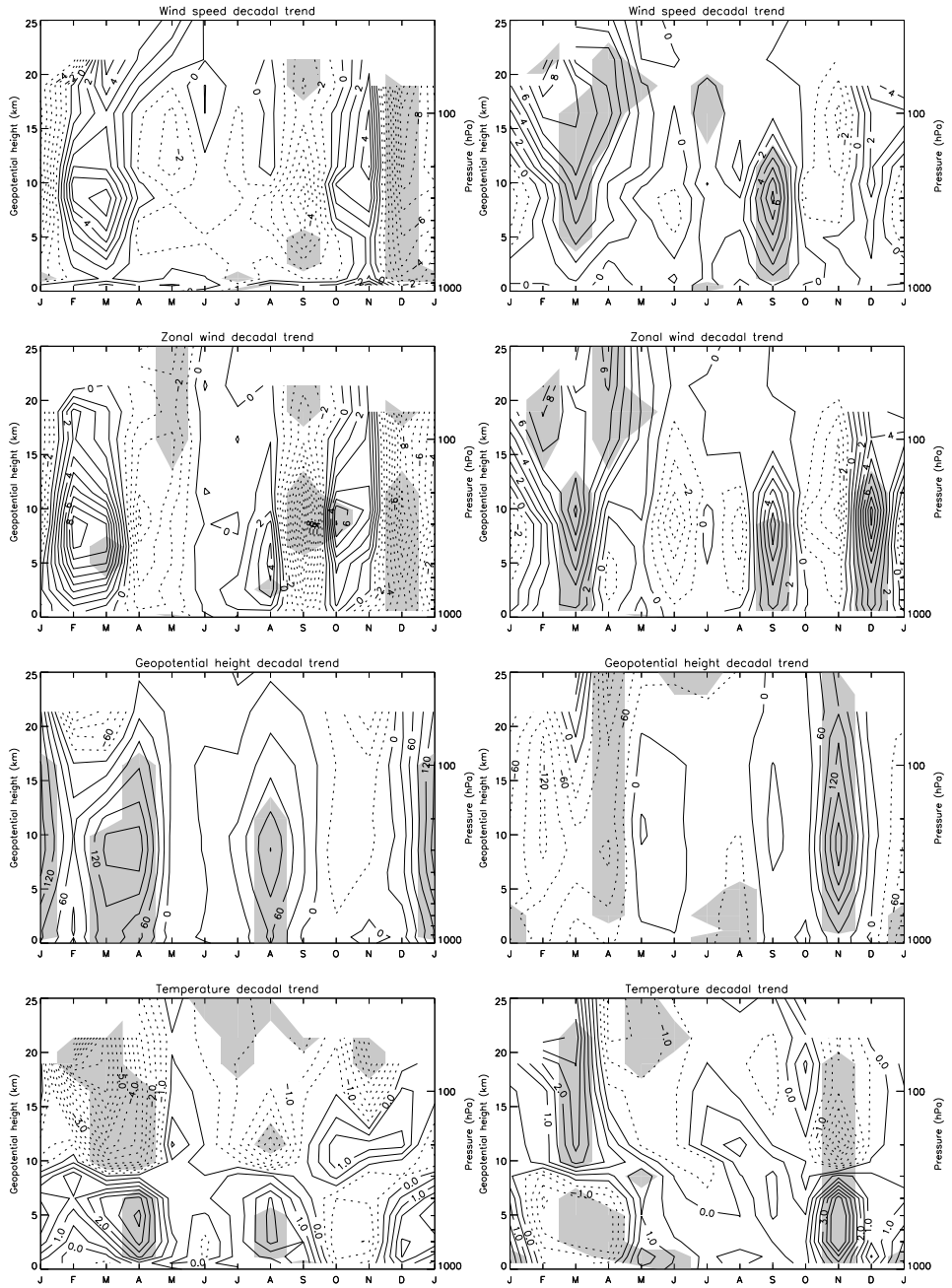

Figure 3.23: Same as in fig. 3.21 but for the periods 1989-00 (left panel) and 1977-90 (right panel) and the shaded areasdenote trends at the 80% confidence level. All trends are based on at least 11 years for 1977-90 and 13 years for 1989-00.

is associated with stratospheric cooling mainly in January but the apparent warmer conditions in Feb-Mar for high AO polarity support the above conclusions, that low AO polarity is associated with colder stratospheric conditions in late winter relative to high AO polarity. The correlations in fig. 3.11 support these conclusions also.

3.4 Inactive and active seasons

The scatter plots of the daily mean time series in fig. 3.24 and 3.25 for the wind speed, zonal wind, geopotential height temperature exhibit distinct active and inactive seasons in the lower stratosphere and troposphere. This is especially apparent in the stratosphere where the amplitude of the fluctuations is greater and the subdivisions clearer than in the troposphere. The active season is at its peak in Jan-Mar when the stratospheric polar vortex is strongest.

In the lower stratosphere the positive geopotential height anomalies during most of the active season are a measure of episodic warmings, which are responsible for most of the variability (50 hPa level shown in 3.25, left panel). On the contrary, negative anomalies are a measure of the polar vortex strength variability. There is however an apparent non-symetric distribution about the vertical line (maximum climatological polar strength) for both positive and negative anomalies (somewhat more so for negative anomalies, in agreement with Thompson and Wallace (2000) findings for the daily mean 50 hPa height averaged over the region poleward of 70°N for the period 1958-97). This feature reflects the occurences of sudden warmings (positive anomalies) versus the delays of the final breakdown, or prevailing polar vortex (negative anomalies). Judging from these features it can be tempting to conclude that there is a tendency toward a prevailing stronger polar vortex at the end of the active season. These variability characteristics are also apparent in the temperature, wind speed and zonal wind at 50 hPa. Note that contrary to the height and temperature, the positive wind anomalies represent a strong polar vortex.

Other notable features in the variability is that the distinction (or subdivision) between the active and inactive seasons become quite unclear in the upper troposphere (300 hPa level shown here) for the temperature and wind fields. In addition, the distribution of the temperature at 925 hPa shows a tendency toward cold extreme conditions, reflected in the greater variability in the negative anomalies.

In the troposphere the specific humidity also displays an annual march (levels 700 and 500 hPa fig. 3.26). However, unlike for height and temperature, its variability is greatest in the warm months Jun-Sep. Statistically speaking this is maybe not surprising since the abundance of water vapor in the atmosphere is substantially greater in the warm seasons. But the

tendency toward extreme values is perhaps an indication of increasing temperatures in recent decades. The annual march however nearly disappears near the surface (925 hPa level shown in fig. 3.26).

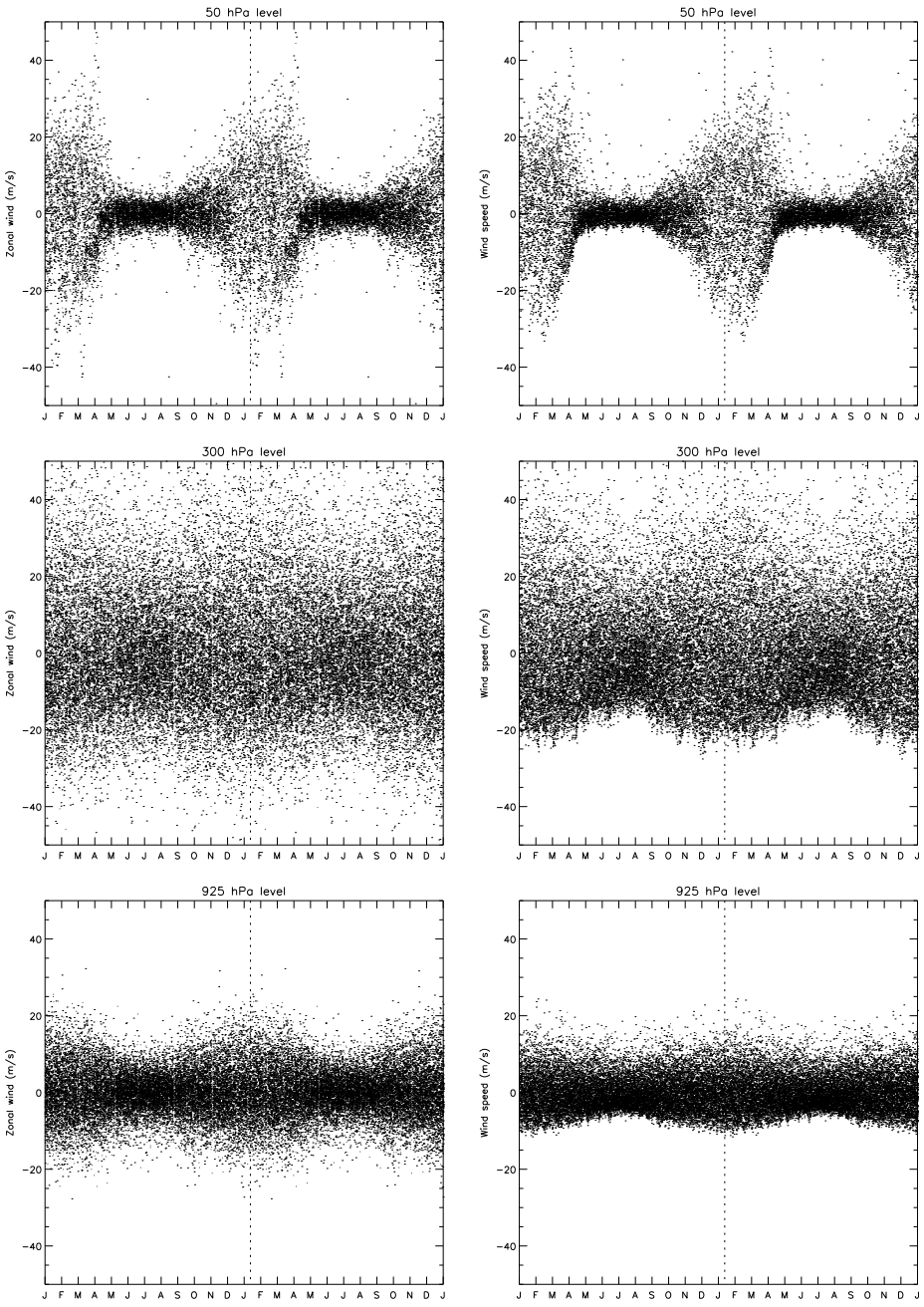

Figure 3.24: Scatter plots of the daily mean wind speed and zonal wind at 50, 300 and 925 hPa for the periods 1973-00 (50 hPa) and 1946-00 (300 and 925 hPa) plotted as a function of calander day. Note that the annual cycle is repeated. The vertical line is located approximately where the polar vortex is at its climatological peak strength.

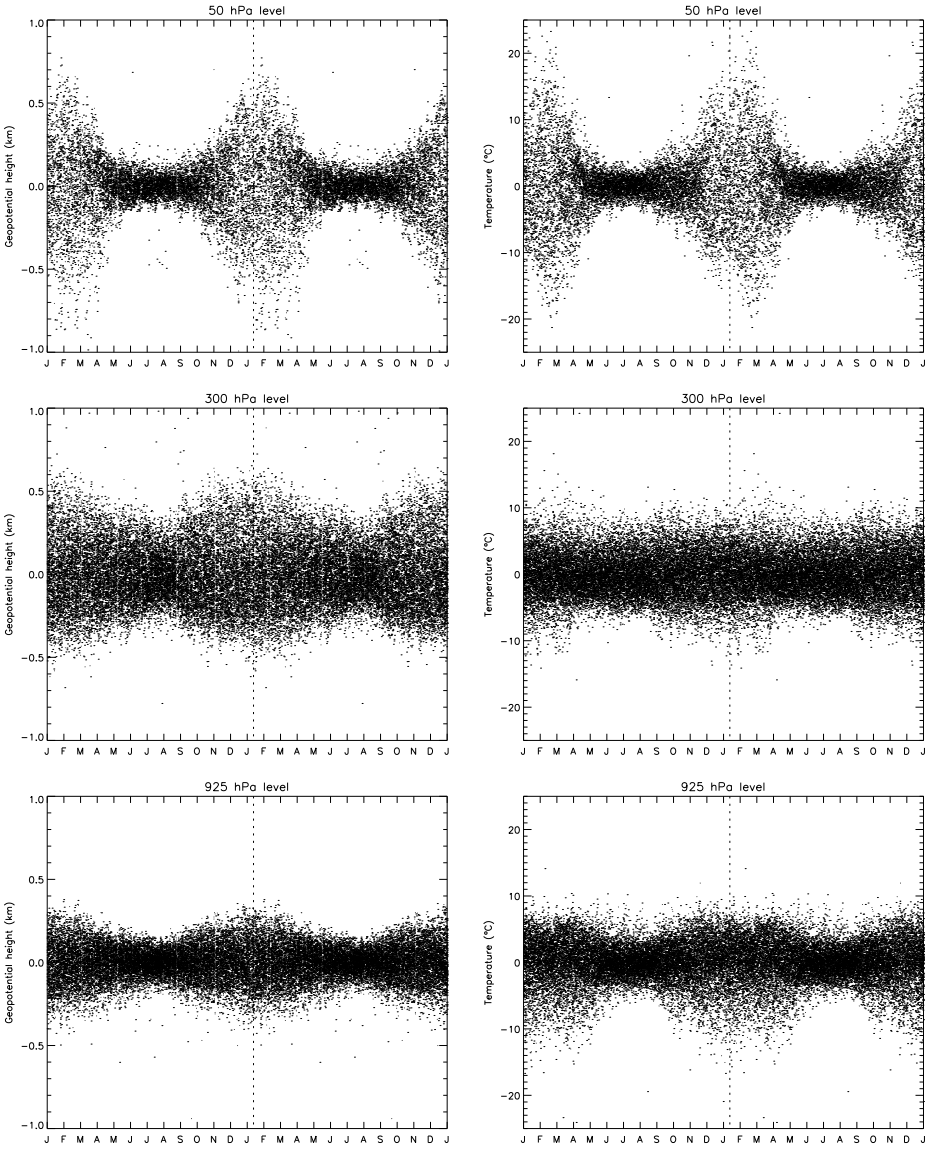

Figure 3.25: Same as in fig. 3.24 but for geopotential height and temperature.

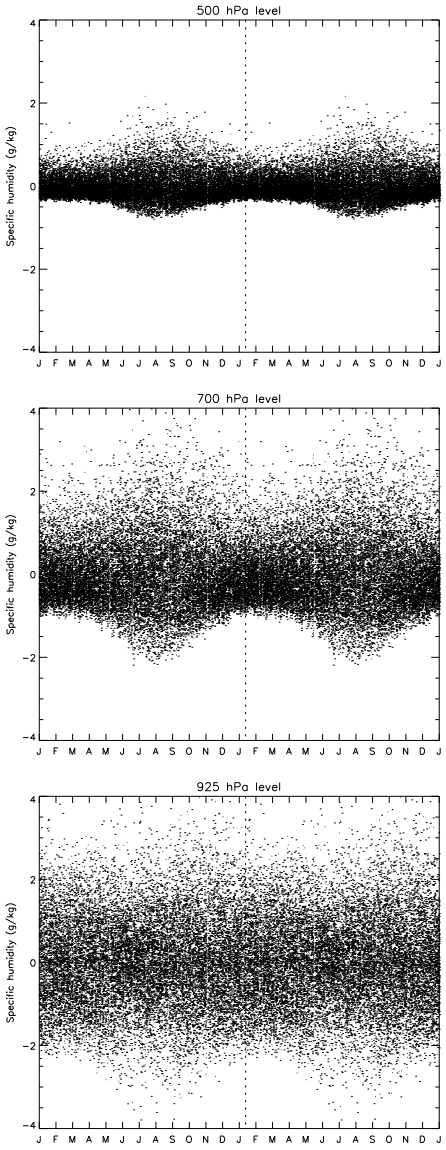

Figure 3.26: Same as in fig. 3.24 but for specific humidity at 500, 700 and 925 hPa

Chapter 4

Summary and discussion

In this study we have interpreted the radiosonde data from Iceland in terms of the variability in the global weather patterns associated with an internal mode of variability at various heights. As an indicator of large scale dynamical variability we use a predefined index termed as the "Arctic Oscillation (AO)" index. Inherent in this index is the characteristics of dynamical variability in the atmosphere northward of 20°N. The commonly used "North Atlantic Oscillation" index can be considered as a subset of the AO index. It is more representative for the northern part of the North Atlantic. Since our goal is to link local changes in meteorological field variables to global processes we prefer using the AO.

Being the dominant mode of variability in the Northern Hemisphere (NH), apart from seasonal variability, both modelling efforts and analysis of assimilated data sets show that its maximum amplitude in both geopotential height and zonal-mean zonal wind fields is located right above Iceland at the lower height levels in the troposphere. As a consequence, the Keflavik radiosonde station provides a unique opportunity for detecting and studying the AO signal locally in the past and the present and thus evaluating its real effect on the climate in general.

The results reveal great consistency between the AO and the radiosonde data. We have confirmed the recently detected stratospheric cooling, strengthening of the westerlies and drop in the geopotential, all of which are related to the strengthening and deepening of the polar vortex. In addition, these trends have been linked to AO signatures during the winter from the surface to the lower stratosphere. Furthermore, compelling evidence of a stratospheric modulation of tropospheric processes and volcanic influences on the AO polarity reinforces our conclusion that the AO is the main mode of variability in the atmosphere over Iceland.

To summarise, in an atmosphere with high AO polarity relative to low AO polarity we find:

- stronger wind speeds and zonal winds at all levels in the stratosphere,

mainly for the time period December-April in the stratosphere

- lower geopotential heights, mainly in January-March at all levels
- colder lower stratosphere, mainly in January
- colder troposphere in February-April
- stronger polar vortex with the breakdown process being delayed into late winter ("late stratospheric warmings").

The currently revised and combined Keflavik radiosonde database along with an associated software package developed in this study offers a wide range of opportunities in climate studies. Low frequency oscillation detection with spectral analysis and calculations of various energy budget parameters using energy budget models (Hrafn Guðmundsson, 1998) are some of many exciting applications. The software can also be applied to a network of radiosonde stations to the benefit of more extensive global climate research.

It is not yet known what physical processes are most desicive in controling the AO. Climate models have recently shown that observed long term AO trends can be induced by increased greenhouse effect and/or ozone depletion. Currently, this is the only plausible explanation of the trends. Therefore, recent changes in the AO suggest a profound anthropogenic effect on the atmosphere. Remarkably for us, the effect on dynamical field variables northward of 20°N maximizes in the lower atmosphere over Iceland. The present study supports this conlusion.

Chapter 5

Acknowledgments

I thank my supervisor Þór Jakobsson at the Icelandic Meteorological Office and the rest of my master committee, Professors Sven Þ. Sigurðsson and Þorsteinn Ingi Sigfússon at the University og Iceland, for their constructive criticism throughout my work and seemingly endless tolerance. My father, Guðmundur G. Bjarnason, for sharing his intuition on the subject and providing valuable motivation. Örnólfur Einar Rögnvaldsson at the Force Technology Inc. in Denmark for his useful guidance in the IDL programming language. Ólafur Rögnvaldsson and Haraldur Ólafsson at the Institute for Meteorological Research and Mats Carlsson and Torben Leifsen at the Institute for Theoretical Astrophysics, University of Oslo for providing access to IDL and computation recources. Trausti Jónsson at the Icelandic Meteorological Office for helpful comments and patience during the final stages of my work. The Icelandic Meteorological Office for providing facilities necessary for completing this work. The staff at the Department of Weather Services for excellent companionship and allowing me to make extra strong coffee.

In addition, I want to thank Þór, Sven, Guðmundur, Haraldur and Trausti for their crucial guidance concerning my lecture preparation.

And finally, I thank my loving fiancee, Elinborg B. Harðardóttir, for her encouragement and endless understanding.

Hrafn Guðmundsson, January 2001

Appendix A

Appendix

A.1 The thermal wind

In the simple situation when the pressure gradient and Coriolis force are in approximate balance, the horizontal velocity field is said to be in geostrophic balance and can be written

$$\mathbf{V}_g = \mathbf{k} \times \frac{1}{\rho f} \nabla_z p = \mathbf{k} \times \frac{1}{f} \nabla_p \Phi \tag{A.1}$$

where $\mathbf{V}_g \equiv \mathbf{i}u_g + \mathbf{j}v_g$ is called the geostrophic wind, $f = 2\Omega \sin\theta$ is the Coriolis parameter and Φ is the geopotential. The hydrostatic equation can be written in the form

$$\frac{\partial \Phi}{\partial p} = -\alpha = -\frac{RT}{p} \tag{A.2}$$

Differentiating (A.1) with respect to pressure and applying (A.2) we obtain the so called thermal wind equation

$$\frac{\partial \mathbf{V}_g}{\partial \ln p} = -\frac{R}{f} \mathbf{k} \times \nabla_p T \tag{A.3}$$

which gives the relationship for the vertical wind shear.

A.2 Virtual temperature

A convenient measure of the mean temperature in a layer bounded by two predetermined pressures is the geopotential height difference between these two pressure surfaces (the thickness of the layer), which depends on the density of the air in the layer. The density is largely a function of the mean temperature in the layer but also depends on the moisture content. This dependence on both temperature and moisture is expressed by the *virtual temperature* T_v, which is the temperature that dry air would have if it had

the same density as moist air at the same pressure

$$T_v \equiv \frac{p}{\rho R_d} = \frac{p}{\rho R} \cdot \frac{R}{R_d} = T \cdot \frac{R}{R_d} = (1 + 0.608q)T \tag{A.4}$$

Computed heights of the pressure surfaces depend on the vertical density distribution between the pressures, not just the density at particular pressure levels. and so the thickness of the layer reflects conditions of the entire layer. Therefore, the temperature obtained from the thickness is the mean layer virtual temperature $< T_v >$, rather than the mean layer temperature $< T >$, which would be measured by a thermometer. Because$< T_v >$ is also a function of the moisture distribution in a layer, any change in moisture could be interpreted as a change in mean temperature of the layer.

The mean layer temperature can be calculated using two methods. We can simply use the measured temperatures at each level in the specified layer or we can derive the temperature from the layers geopotential heights. The former method depends on the available temperature measurements at the layer's boundaries and inside the layer, while the latter requires the pressure[1], geopotential height at the layer's boundaries and the mean layer specific humidity $< q >$.

Let (p_1, p_2) be a layer in the sounding. The scalar height for the layer is given by

$$H_{1,2} = \frac{z_2 - z_1}{\ln p_1/p_2} = \frac{R_d < T_v >}{g} \tag{A.5}$$

The virtual temperature in (A.4) is often approximated with

$$T_v \approx T + Aq \tag{A.6}$$

where A is a constant between 0.16 K and 0.18 K depending on$T$. To obtain an estimate of $< q >$ we simply calculate the mean

$$< q >= \frac{1}{n} \sum_{i=1}^{n} q_i \tag{A.7}$$

where n is the number of measured levels in the layer (including the boundaries).

From these considerations, we see that for tropospheric levels where moisture content is mostly concentrated, it can be treacherous to assume the layer thickness is equivalent to the mean layer temperature. According to Elliott et al. (1994), real changes in mean layer specific humidity of up to 50% would couse changes in mean layer virtual temperature of less than 1°C, except in the tropical boundary layer, where the high moisture content would lead to larger virtual temperature changes. Therefore, the effect of humidity changes is negligible in polar regions and most pronounced in the tropics.

[1]The pressure is always valid. This is guaranteed in the data processing.

A.3 The interpolation procedure

The objective of the interpolation procedure is to replace, if possible, all dummy values in the available data sets with usable physical values.

We assume all pressure measurements to be valid in each sounding. That leaves us with the geopotential height, temperature, dew point temperature, wind direction and speed that are interpolated if necessary. We use the interpolation procedures discussed in section 2.2.2 but in the following we utilize in detail the interpolation process.

The procedure starts by checking if the sounding has a valid surface measurement. This information is crucial when parameters are to be interpolated at the surface. Also, we should note that the surface level is not necessarily the first level in the sounding since the standard level 1000 hPa is frequently under the surface. In addition, some soundings have a substantial portion of the lower profile of the measurement missing in which case no valid surface level exists. Finally, cases have been detected where more than one level has been labeled surface levels, but differing by only a few hectopascals. In these cases the calculations are performed with the first surface level as the true surface level.

The interpolation process can be divided into the following two procedures:

1. **Linear interpolation with respect to pressure**

   We start the interpolation process from the surface level (or first level from surface if the surface measurement is missing). Let$p = (p_1, p_2, ..., p_n)$ be the levels in the sounding and $\beta = (\beta_1, \beta_2, ..., \beta_n)$ be the corresponding physical parameters or geopotential height of the sounding. If β_s is the surface measurement then we find $j \geq s$ such that β_j is the first non-dummy from the surface β_s (fig. 1). Next we find k such that β_{j+k} is the first dummy from β_j. Then we find l such that β_{j+k+l} is the first non-dummy from β_{j+k}. We can then interpolate $\beta_{j+k}, \beta_{j+k+1}, ..., \beta_{j+k+l-1}$ using

   $$\beta_{j+k+i} = \beta_{j+k-1} + \frac{\beta_{j+k+l} - \beta_{j+k-1}}{\ln p_{j+k+l} - \ln p_{j+k-1}} (\ln p_{j+k+i} - \ln p_{j+k-1}) \quad \text{(A.8)}$$

   for $i = 0, ..., l-1$. After interpolation we set $j+k+l \rightarrow j$ and continue the above procedures until the top level is reached.

2. **Interpolation of the geopotential height at the surface and top levels**

   In cases when the geopotential height at the surface and top levels are missing, there is a possibility to interpolate with the hydrostatic equation if temperature measurements are available at these levels. We require at least two temperature measurements to be valid, at

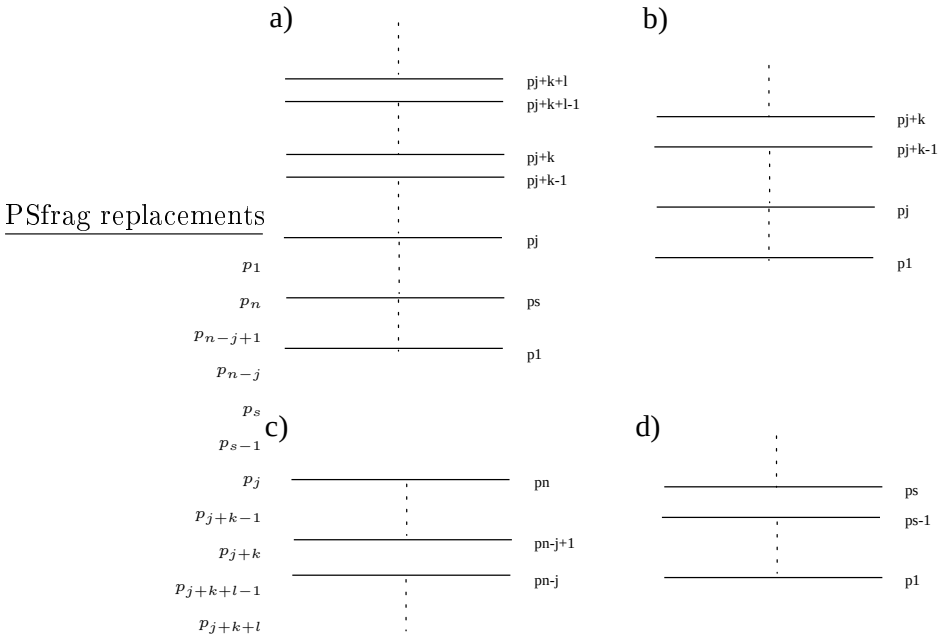

Figure A.1: Sounding levels with missing data: The interpolation procedure. (a) Interpolation of intermediate levels, (b) surface levels, (c) top levels and (d) levels under the surface. p_s is the surface level, n is the number of levels in the sounding and the dotted vertical line between levels denotes unspecified number intermediate levels.

the missing levels, for the scalar height estimation. We let p_j be the surface level, or in the case where the surface level is lacking, the first level from the surface (fig. 1 b)). Then we find k such that p_{j+k} is the first non-dummy from p_j. Then the geopotential height at levels $p_j, p_{j+1}, ..., p_{j+k-1}$ can be interpolated using

$$z_{j+k-i} = z_{j+k} - H_{j+k-i,j+k} \cdot \ln\left(\frac{p_{j+k-i}}{p_{j+k}}\right) \tag{A.9}$$

for $i = 1, ..., k$ where

$$H_{j+k-i,j+k} = \frac{R}{g} \cdot \frac{T_{j+k-i} + T_{j+k}}{2} \tag{A.10}$$

For the top levels we find j such that p_{n-j} is the first non-dummy from p_n (fig. 1 c). Then the geopotential height at levels$p_{n-j+1}, p_{n-j+2}, ..., p_n$ can be interpolated using

$$z_{n-j+i} = z_{n-j} - H_{n-j,n-j+i} \cdot \ln\left(\frac{p_{n-j}}{p_{n-j+i}}\right) \tag{A.11}$$

for $i = 1, ..., j$ where

$$H_{n-j,n-j+i} = \frac{R}{g} \cdot \frac{T_{n-j} + T_{n-j+i}}{2} \tag{A.12}$$

When the manditory level 1000 hPa is under the surface we use (2.15) and (2.16) in the more genaral case where more levels than the 1000 hPa are accounted for under the surface level. Assume $p_1, ..., p_{s-1}$ are levels under the surface level p_s. Then we interpolate the geopotential heights at these levels using

$$z_{s-i} = z_s - H_{s-i,s} \cdot \ln\left(\frac{p_{s-i}}{p_s}\right) \tag{A.13}$$

for $i = 1, ..., s$.

A.4 Wind speed and direction

Meteorological convention specifies the wind direction as that from which the wind blows. A 360 degree compass oriented clockwise from north is used; thus a wind blowing from the west is given a 270 degree direction, and from the south a 180 degree direction. Therefore, the u-component (east-west zonal wind) of the wind is given by

$$u = -U \sin\theta \tag{A.14}$$

and the v-component (north-south) by

$$v = -U \cos\theta \tag{A.15}$$

where $U = \sqrt{u^2 + v^2}$ is the wind speed and θ the direction. By definition, the westerlies have $u > 0$ and the easterlies have $u < 0$.

A.5 Precipitable water

The precipitable water PW_i between the height levels z_i and z_{i+1} can be calculated as

$$\mathrm{PW}_i = \int_{z_i}^{z_{i+1}} \rho_v dz \tag{A.16}$$

where ρ_v is the water vapor density, which can be calculated using the hydrostatic relation for density

$$\rho_{v_i} = \rho_{v_i} \exp\left(-\frac{z_{i+1} - z_i}{H_{i,i+1}}\right) \tag{A.17}$$

where

$$H_{i,i+1} = \frac{z_{i+1} - z_i}{\ln\left(\rho_{v_i}/\rho_{v_{i+1}}\right)} \tag{A.18}$$

is the scalar height for water vapor density. Inserting this equation into (A.16) and integrating, we find

$$\mathrm{PW}_i = \rho_{v_i} H_{i,i+1} \left[1 - \exp\left(-\frac{z_{i+1} - z_i}{H_{i,i+1}}\right)\right] \tag{A.19}$$

To obtain the total precipitable water PW between 1000 and 500 hPa, we must sum over each contributing layer in the sounding

$$\mathrm{PW} = \sum_{i=1}^{n-1} \mathrm{PW}_i \tag{A.20}$$

where n is the number of levels between 1000 and 500 hPa. To find ρ_v in terms of the measured parameters, pressure p, temperature T and dew point T_d, we use the definition of the specific humidity

$$q = \frac{\rho_v}{\rho} = \frac{\epsilon e}{p - (1-\epsilon)e} \tag{A.21}$$

where ρ_v is the vapor density, ρ is the air density, e is the vapor pressure, p is the total air pressure and $\epsilon \equiv R_d/R_v \approx 0.622$. From this equation we obtain the desired relation

$$\rho_v = \rho q = \frac{p}{RT}\frac{\epsilon e}{p-(1-\epsilon)e} = \frac{p}{RT}\frac{\epsilon e_s(T_d)}{p-(1-\epsilon)e_s(T_d)} \tag{A.22}$$

where from the Clausius-Clapeyron equation 2.1 we have

$$e_s(T_d) = e_{s0} \exp\left[\frac{l_v}{R_v}\left(\frac{1}{T_0} - \frac{1}{T_d}\right)\right] \tag{A.23}$$

The reference temperature T_0 can be any arbitrary level. For $T_0 = 273$ K we have $e_{s0} = e_s(T_0) = 6.11$ hPa. The enthalpy of vaporization of water at 0°C is $l_v = 2.5 \cdot 10^6$ Jkg^{-1} and the gas constant for water vapor is $R_v = 461.5$ Jkg^{-1}K^{-1}.

We can also use another equivalent method by noting that the precipitable water PW_i between the pressure levels p_i and p_{i+1} can be calculated as

$$\mathrm{PW}_i = -\frac{1}{g}\int_{p_i}^{p_{i+1}} q dp \tag{A.24}$$

We calculate the integral by approximating the specific humidity q between levels $i+1$ and i with the average value $\bar{q} = (q_{i+1} + q_i)/2$. To obtain the total PW between 1000 and 500 hPa, we must sum over each contributing layer in the sounding

$$\mathrm{PW} = \sum_{i=1}^{n-1} \mathrm{PW}_i = \frac{1}{2g}\sum_{i=1}^{n-1}(q_{i+1} + q_i)(p_i - p_{i+1}) \tag{A.25}$$

A.6 Observation frequency

The information given in the following tables for the IRIS, IMO, NCDC and Combined data sets are: total monthly observations (Jan-Dec), total annual observations (Obs) and total missing days (Miss).

A.6.1 IRIS

Year	Jan	Feb	Mar	Apr	May	Jun	Jul	Aug	Sep	Oct	Nov	Dec	Obs	Miss
1946	46	0	0	0	0	0	61	61	55	48	55	44	370	158
1947	60	51	54	51	0	0	0	0	0	0	0	0	216	250
1948	0	0	0	0	0	0	0	0	0	0	0	0	0	366
1949	0	0	0	0	0	0	0	0	0	0	0	0	0	365
1950	0	0	0	0	0	0	0	0	0	0	0	0	0	365
1951	0	0	0	0	0	0	0	0	60	97	120	121	398	243
1952	118	116	123	117	123	120	124	124	111	116	86	124	1402	8
1953	122	111	119	119	122	120	124	123	113	123	117	122	1435	0
1954	124	112	123	120	124	111	124	123	119	124	114	122	1440	0
1955	122	112	124	118	124	120	123	122	118	124	120	120	1447	0
1956	123	116	123	120	123	120	123	124	120	121	115	118	1446	0
1957	121	111	123	119	123	119	124	124	120	123	119	122	1448	0
1958	123	111	122	120	124	120	124	123	117	124	120	121	1449	0
1959	124	111	123	120	124	120	124	124	120	124	1	1	1216	59
1960	124	115	123	120	121	119	123	124	119	124	120	123	1455	0
1961	124	112	124	120	124	119	124	124	118	123	115	122	1449	0
1962	121	108	123	119	120	120	123	123	119	124	115	120	1435	0
1963	124	108	123	119	121	119	122	123	120	121	118	123	1441	0
1964	113	114	121	120	124	120	121	120	117	121	120	115	1426	0
1965	117	101	113	116	121	119	124	123	118	122	117	123	1414	0
1966	119	112	122	119	123	120	124	122	119	123	120	120	1443	0
1967	123	83	114	118	124	112	118	117	118	121	114	120	1382	0
1968	122	114	121	119	119	108	123	122	120	105	120	123	1416	0
1969	122	111	122	118	122	117	124	123	114	123	119	124	1439	1
1970	124	108	120	104	120	118	118	122	116	120	112	106	1388	2
1971	118	107	62	60	61	60	62	61	58	61	58	62	830	0
1972	62	54	62	59	60	60	61	61	60	62	58	59	718	1
1973	62	56	62	58	61	60	62	62	59	62	60	61	725	0
1974	61	55	61	60	61	60	60	61	60	62	60	60	721	0
1975	60	54	62	60	62	60	62	62	60	62	60	62	726	0
1976	62	55	62	60	62	59	62	62	60	62	60	59	725	0
1977	61	55	62	60	61	60	62	62	60	62	60	62	727	0
1978	62	56	62	60	62	60	62	62	60	61	60	62	729	0
1979	60	55	59	60	61	60	62	62	60	62	60	59	720	0
1980	58	58	59	60	62	60	62	62	60	62	60	60	723	1
1981	61	54	61	60	62	60	62	62	60	62	60	62	726	1
1982	62	55	61	60	61	60	62	62	60	62	0	0	605	61
1983	0	0	0	0	0	0	0	0	0	0	0	0	0	365
1984	0	0	0	0	0	0	0	0	0	0	0	0	0	366
1985	61	56	62	60	62	60	0	62	60	0	57	62	602	62
1986	62	56	62	60	62	60	62	62	60	61	59	61	727	0
1987	62	54	62	59	62	60	61	62	59	62	59	62	724	0
1988	61	58	62	59	61	60	0	62	60	0	59	61	603	62
1989	58	51	59	59	62	58	62	62	0	62	59	49	641	34
1990	28	26	16	0	0	0	0	0	0	0	0	0	70	322
1991	0	0	0	0	0	0	0	0	0	0	0	0	0	365
1992	0	0	0	0	0	0	0	0	0	0	0	0	0	366
1993	0	0	0	60	60	6	5	5	0	0	57	62	255	234
1994	61	38	55	60	62	58	51	61	0	0	0	0	446	135

Total observations: 40698

A.6.2 IMO

Year	Jan	Feb	Mar	Apr	May	Jun	Jul	Aug	Sep	Oct	Nov	Dec	Obs	Miss
1993	59	54	63	60	62	60	62	61	58	62	60	61	722	1
1994	62	56	63	60	62	60	51	62	60	62	59	61	718	4
1995	62	56	61	60	62	60	61	60	59	60	59	60	720	0
1996	62	57	62	58	62	59	62	61	59	59	60	60	721	0
1997	121	111	63	59	62	60	62	56	60	62	60	59	835	3

```
1998  60  56  58  59  62  60  62  62  59  61  60  58  717    0
1999  60  56  62  59  62  60  62  60  59  61  60  61  722    2
2000  60  56  62  59  57  59  61  10   0   0   0   0  424  150
Total observations: 5579
```

A.6.3 NCDC

```
Year Jan Feb Mar Apr May Jun Jul Aug Sep Oct Nov Dec  Obs Miss
1973  51  52  54  54  60  57  60  57  58  60  48  56  667   10
1974  61  52  54  59  57  60  58  59  60  57  54  55  686    3
1975  59  45  60  48  62  60  62  62  59  60  59  62  698    4
1976  62  53  62  60  62  58  61  60  57  61  59  59  714    1
1977  61  55  62  59  61  60  62  63  60  60  53  61  717    0
1978  61  56  62  60  62  60  61  62  60  60  57  62  723    0
1979  58  55  59  57  61  59  62  61  59  62  60  58  711    0
1980  57  58  57  60  62  59  62  62  59  62  60  60  718    2
1981  62  53  61  60  60  59  62  61  57  61  60  61  717    1
1982  61  54  57  60  60  59  61  61  60  62  60  62  717    0
1983  55  56  60  61  54  59  61  62  60  61  59  61  709    2
1984  57  58  62  60  62  60  62  62  57  62  60  61  723    1
1985  61  56  62  59  61  60  61  62  60  61  57  62  722    0
1986  62  56  62  60  60  60  62  62  60  60  59  61  724    0
1987  62  54  62  59  48  60  61  62  59  62  59  62  710    7
1988  61  54  60  59  61  60  61  62  60  62  59  61  720    1
1989  58  52  60  58  62  57  62  62  60  62  58  61  712    1
1990  62  55  58  57  62  59  60  62  59  62  58  59  713    0
1991  59  55  62  59  62  59  62  61  61  61  60  64  725    0
1992 123  53  63  60  61  59  62  62  61  60  59  61  784    0
1993  59  54  62  61  62  61  62  61  58  62  60  62  724    1
1994  61  55  62  60  63  60  52  63  60  63  59  62  720    4
1995  63  56  62  59  62  61  64  60  60  61  59  61  728    0
1996  60  57  62  58  62  59  63  61  59  59  60  61  721    0
1997 121 109  63  59  63  58  62  60  60  61  59  59  834    1
1998  60  54  59  58  62  59  61  62  59  62  59  59  714    0
Total observations: 18751
```

A.6.4 Combined

```
Year Jan Feb Mar Apr May Jun Jul Aug Sep Oct Nov Dec  Obs Miss
1946  46   0   0   0   0   0  61  61  55  48  55  44  370  158
1947  60  51  54  51   0   0   0   0   0   0   0   0  216  250
1948   0   0   0   0   0   0   0   0   0   0   0   0    0  366
1949   0   0   0   0   0   0   0   0   0   0   0   0    0  365
1950   0   0   0   0   0   0   0   0   0   0   0   0    0  365
1951   0   0   0   0   0   0   0   0  60  97 120 121  398  243
1952 118 116 123 117 123 120 124 124 111 116  86 124 1402    8
1953 122 111 119 119 122 120 124 123 113 123 117 122 1435    0
1954 124 112 123 120 124 111 124 123 119 124 114 122 1440    0
1955 122 112 124 118 124 120 123 122 118 124 120 120 1447    0
1956 123 116 123 120 123 120 123 124 120 121 115 118 1446    0
1957 121 111 123 119 123 119 124 124 120 123 119 122 1448    0
1958 123 111 122 120 124 120 124 123 117 124 120 121 1449    0
1959 124 111 123 120 124 120 124 124 120 124   1   1 1216   59
1960 124 115 123 120 121 119 123 124 119 124 120 123 1455    0
1961 124 112 124 120 124 119 124 124 118 123 115 122 1449    0
1962 121 108 123 119 120 120 123 123 119 124 115 120 1435    0
1963 124 108 123 119 121 119 122 123 120 121 118 123 1441    0
1964 113 114 121 120 124 120 121 120 117 121 120 115 1426    0
1965 117 101 113 116 121 119 124 123 118 122 117 123 1414    0
1966 119 112 122 119 123 120 124 122 119 123 120 120 1443    0
1967 123  83 114 118 124 112 118 117 118 121 114 120 1382    0
```

```
1968 122 114 121 119 119 108 123 122 120 105 120 123 1416    0
1969 122 111 122 118 122 117 124 123 114 123 119 124 1439    1
1970 124 108 120 104 120 118 118 122 116 120 112 106 1388    2
1971 118 107  62  60  61  60  62  61  58  61  58  62  830    0
1972  62  54  62  59  60  60  61  61  60  62  58  59  718    1
1973  62  56  62  58  61  60  62  62  59  62  60  61  725    0
1974  61  55  61  60  61  60  60  61  60  62  60  60  721    0
1975  60  54  62  60  62  60  62  62  60  62  60  62  726    0
1976  62  55  62  60  62  59  62  62  61  62  60  59  726    0
1977  61  55  62  60  61  60  63  63  60  62  60  62  729    0
1978  62  56  63  60  62  60  62  62  61  61  60  62  731    0
1979  60  55  60  60  61  60  62  62  61  62  60  59  722    0
1980  58  58  59  60  62  60  62  62  60  62  61  60  724    1
1981  62  54  61  60  62  60  62  63  60  62  60  63  729    1
1982  62  55  61  60  61  60  62  62  60  62  60  62  727    0
1983  55  56  60  61  54  59  61  62  60  61  59  61  709    2
1984  57  58  62  60  62  60  62  62  57  62  60  61  723    1
1985  61  56  62  60  63  60  61  62  60  61  57  62  725    0
1986  62  57  62  60  62  60  62  62  60  62  59  61  729    0
1987  62  54  62  59  62  60  61  62  59  62  59  62  724    0
1988  61  58  62  59  61  60  61  62  60  62  59  61  726    0
1989  58  52  60  59  62  58  62  62  60  62  59  61  715    1
1990  62  56  63  57  62  59  60  62  59  62  58  59  719    0
1991  59  55  62  59  62  59  62  61  61  61  60  64  725    0
1992 123  53  63  60  61  59  62  62  61  60  59  61  784    0
1993  62  57  63  62  62  61  65  83  61  66  60  64  766    1
1994  63  56  64  60  63  61  52  63  61  63  59  62  727    4
1995  63  57  62  61  62  61  65  60  60  63  59  61  734    0
1996  62  57  63  58  62  59  63  61  60  59  60  61  725    0
1997 121 111  63  59  63  60  62  62  61  62  60  62  846    1
1998  63  58  60  61  64  61  62  63  60  62  60  60  734    0
1999  60  56  62  59  62  60  62  60  59  61  60  61  722    2
2000  60  56  62  59  57  59  61  10   0   0   0   0  424  150
Total observations: 49720
```

A.7 The FSL format

Each column in the data files represents a specific physical property of the sounding measurements except the first column, which identifies the type of each measured level in the sounding. The first level in each sounding is of type 9 (surface level). The preceding levels are ordered in ascending order with respect to the height. It should be noted that the manditory level $1000hPa$ is frequently below the surface level. When this is the case, all physical parameters are missing (since no measurements can take place below ground level) and the geopotential height is often the only information we have for that level. After data syncronization has taken place, the final form of the FSL format will have the following properties for each column:

- Column 1: LINTYP (line type). Only valid identification data.
- Column 2: Pressure (10^{-1}hPa). Only valid measured data[2].

[2]We require all levels to have valid pressure measurements in the data processing and exclude them otherwise.

- Column 3: Height (m). Derived data (see (2.5)).
- Column 4: Temperature ($10^{-1}{}^{\circ}C$). Measured data[3].
- Column 5: Dew point temperature ($10^{-1}{}^{\circ}C$). Measured data.
- Column 6: Wind direction (degrees). Measured data.
- Column 7: Wind speed ($10^{-1}m/s$). Measured data.

The FSL data format comes in to different forms, the so called original and new formats. These formats are identical except for these differences:

1. Dummy values[4]: 32767 in original format and 99999 in new format.
2. Pressure units: $1hPa$ in original format and $10^{-1}hPa$ in new format.

The official FSL data format is similar to the format used by the National Severe Storms Forecast Center (NSSFC) in Kansas City. The first four lines of the sounding are identification and information lines. All additional lines are data lines. An entry of 32767 (original format) or 99999 (new format) indicates that the information is either missing, not reported, or not applicable.

The official FSL data format is similar to the format used by the National Severe Storms Forecast Center (NSSFC) in Kansas City. The first 4 lines of the sounding are identification and information lines. All additional lines are data lines. An entry of 32767 (original format) or 99999 (new format) indicates that the information is either missing, not reported, or not applicable.

		---COLUMN NUMBER---				
1	2	3	4	5	6	7
LINTYP						
			header lines			
254	HOUR	DAY	MONTH	YEAR	(blank)	(blank)
1	WBAN#	WMO#	LAT	LON	ELEV	RTIME
2	HYDRO	MXWD	TROPL	LINES	TINDEX	SOURCE
3	(blank)	STAID	(blank)	(blank)	SONDE	WSUNITS
			data lines			
9	PRESSURE	HEIGHT	TEMP	DEWPT	WIND DIR	WIND SPD
4						
5						
6						
7						

[3]Data, other than pressure and height are not required to be valid at all levels since measurements of particular physical parameters frequently extend further up into the atmosphere than others, e.g. humidity measurements are not reliable above approximately $500hPa$ (Elliott and Gaffen, 1991).

[4]Dummy values occur in data when information is either missing, not reported or not applicable. In the current data processing when dummy values are encountered, various interpolation methods are often applicable so they can be replaced with physicaly valid values.

```
      8

                                    LEGEND

LINTYP: type of identification line
        254 = indicates a new sounding in the output file
          1 = station identification line
          2 = sounding checks line
          3 = station identifier and other indicators line
          4 = mandatory level
          5 = significant level
          6 = wind level (PPBB) (GTS or merged data)
          7 = tropopause level (GTS or merged data)
          8 = maximum wind level (GTS or merged data)
          9 = surface level

HOUR:   time of report in UTC
LAT:    latitude in degrees and hundredths
LON:    longitude in degrees and hundredths
ELEV:   elevation from station history in meters
RTIME:  is the actual release time of radiosonde from TTBB. Appears in GTS data
        only.
HYDRO:  the pressure of the level to where the sounding passes the hydrostatic
        check (see section 4.3).**
MXWD:   the pressure of the level having the maximum wind in the sounding.  If
        within the body of the sounding there is no "8" level then
        MXWN is estimated (see section 3.2).
TROPL:  the pressure of the level containing the tropopause. If within the
        body of the sounding there is no "7" level, then TROPL is estimated
        (see section 3.3)**
LINES:  number of levels in the sounding, including the 4 identification lines.
TINDEX: indicator for estimated tropopause. A "7" indicates that sufficient
        data was available to attempt the estimation; 11 indicates that data
        terminated and that tropopause is a "suspected" tropopause.
SOURCE: 0 = National Climatic Data Center (NCDC)
        1 = Atmospheric Environment Service (AES), Canada
        2 = National Severe Storms Forecast Center (NSSFC)
        3 = GTS or FSL GTS data only
        4 = merge of NCDC and GTS data (sources 2,3 merged into sources 0,1)
SONDE:  type of radiosonde code from TTBB. Only reported with GTS data
        10 = VIZ "A" type radiosonde
        11 = VIZ "B" type radiosonde
        12 = Space data corp.(SDC) radiosonde.
WSUNITS:wind speed units (selected upon output)
        ms = tenths of meters per second
        kt = knots

PRESSURE: in whole millibars (original format)
          in tenths of millibars (new format)
HEIGHT:   height in meters (m)
TEMP:     temperature in tenths of degrees Celsius
DEWPT:    dew point temperature in tenths of a degree Celsius
WIND DIR: wind direction in degrees
WIND SPD: wind speed in either knots or tenths of a meter per second
          (selected by user upon output)
```

An example of fortran format statements necessary to read output raw-insonde data, according to LINTYP, is as follows:

```
LINTYP
   254    (3i7,6x,a4,i7)
     1    (3i7,2f7.2,2i7)
     2    (7i7)
```

```
                    3    (i7,10x,a4,14x,i7,5x,a2)
              4,5,6,7,8,9    (7i7)
```

A.8 Station history

```
UPPER AIR STATION HISTORY
Comprehensive Aerologicial Reference Data Set


*** Station History ***
     CARDS# Station Name                  ST CN  Ob Count   Year Range
     ------------------------------------------------------------------------------
     040180 KEFLAVIK (USN)                   IC  50088      1946-1998


*** Location History ***
     Begin     End       Latitude   Longitude  Elevation
     ------------------------------------------------------------------------------
     196707    999912    63.95000   -22.61700   38.0
     196202    196707    63.96700   -22.60000   58.0
     195109    196202    63.95000   -22.61700   49.0
     194801    195108    63.95000   -22.61700   49.0
     194601    194704    63.95000   -22.61700   49.0


*** Auxiliary Information ***
      Year/Month  Event
      ------------------------------------------------------------------------------
      194406      MISCELLANEOUS
                  Independence: 17 June 1944 (from Denmark)

      194601      STATION OPENED


      194704      STATION CLOSED


      194801      STATION OPENED


      195108      STATION CLOSED


      195109      STATION OPENED


      195400      CHANGE SONDE MODEL                    UNKNOWN SONDE                          VIZ (Generic)


      196000      USING SONDE MODEL                     VIZ AN/AMT 4B
                  Derived from WMO (1965)

      196202      STATION CLOSED


      196202      STATION OPENED


      196707      STATION CLOSED


      196707      STATION OPENED


      197600      USING SONDE MODEL                     VIZ AN/AMT MOD
                  Derived from SPACKMAN (1977)

      198200      USING RADIAT. CORR.                   NO RAD. CORRECTION
                  Derived from WMO (1982)

      198200      USING SONDE MODEL                     VIZ 1392
                  Derived from WMO (1982)

      198600      USING RADIAT. CORR.                   NO RAD. CORRECTION
                  Derived from D MET O 1/6/1/15

      198600      USING SONDE MODEL                     VIZ 1392
```

```
          Derived from D MET O 1/6/1/15

198900    USING SONDE MODEL                  VIZ (Generic)
          Derived from KITCHEN (1988)

199000    CHANGE SONDE MODEL                 VIZ (Generic)                  VAISALA RS80

199212    USING RADIAT. CORR.                VAISALA RS80 1986

199212    USING SONDE MODEL                  VAISALA RS80
```

Bibliography

Angell, J. K. (1988). Variations and trends in tropospheric and stratospheric global temperatures, 1958-87. *J. Climate*, 1:1296–1313.

Angell, J. K. (1991). Stratospheric temperature change as a function of height and sunspot number during 1972-89 based on rocketsonde and radiosonde data. *J. Climate*, 4:1170–1180.

Angell, J. K. (1999). Variation with height and latitude of radiosonde temperature trends in North America, 1975-94. *J. Climate*, 12:2551–2561.

Baldwin, M. P. (2000). The Artic Oscillation and its role in stratosphere-troposphere coupling. *Stratospheric Processes and their Role in Climate*, 14:10–14.

Baldwin, M. P. and Dunkerton, T. J. (1999). Propagation of the Artic Oscillation from the stratosphere to the troposphere. *J. Geophys. Res.*, 104:30937–30946.

Bohren, C. F. and Albrecht, B. A. (1998). *Atmospheric thermodynamics*. Oxford Universal Press, 1 edition.

de F. Forsters, P. M. and Shine, K. (1999). Stratospheric water vapour changes as a possible contributer to observed stratospheric cooling. *Geophys. Res. Lett.*, 26:3309–3312.

Elliott, W. P. and Gaffen, D. J. (1991). On the utility of radiosonde humidity archives for climate studies. *Bull. Amer. Meteor. Soc.*, 72:1507–1520.

Elliott, W. P., Gaffen, D. J., Kahl, J. D. W., and Angell, J. K. (1994). The effect of moisture on layer thickness used to monitor global temperatures. *J. Climate*, 7:304–308.

Eskridge, R. E., Alduchov, O. A., Chernykh, I. V., Panmao, Z., Polansky, A. C., and Doty, S. R. (1995). A comprehensive aerological reference data set (CARDS): Rough and systematic errors. *Bull. Amer. Meteor. Soc.*, 76:1759–1775.

Fyfe, J. C., Boer, G. J., and Flato, G. M. (1999). The Arctic and Antarctic Oscillations and their projected changes under global warming. *Geophys. Res. Lett.*, 26:1601–1604.

Gaffen, D. J. (1999). Radiosonde observations and their use in SPARC-related investigations. *Stratospheric Processes and their Role in Climate*, 12:17–21.

Gillett, N. P., Hegerl, G. C., Allen, M. R., and Stott, P. A. (2000). Implications of changes in the Northern Hemisphere circulation for the detection of anthropogenic climate. *Geophys. Res. Lett.*, 27:993–996.

Graf, H.-F., Kirchner, I., and Perlwitz, J. (1998). Changing lower stratospheric circulation: The role of ozone and greenhouse gases. *J. Geophys. Res.*, 103:11251–11261.

Hansen, G. and Chipperfield, M. P. (1999). Ozone depletion at the edge of the Arctic polar vortex 1996/1997. *J. Geophys. Res.*, 104:1837–1845.

Hartley, D. E., Villarin, J. T., Black, R. X., and Davis, C. A. (1998). A new perspective on the stratosphere and troposphere. *Nature*, 391:471–474.

Hartmann, D. L., Wallace, J. M., Limpasuvan, V., Thompson, D. W. J., and Holton, J. R. (2000). Can ozone depletion and global warming interact to produce rapid climate change? 97:1412–1417.

Hrafn Guðmundsson (1998). The energy budget model Ebba. Technical Report 31, The Icelandic Meteorological Office; The European Subpolar Ocean Programme-2. This report was supported by the Commision of the European Communities under Contract MAS3-CT95-0015 of the MAST3 Programme.

Hrafn Guðmundsson (1999). Radiosonde observations over Iceland since 1946. Technical report, The Icelandic Meteorological Office. This report was supported by the Icelandic Student Funding for Innovative Studies (*Ice.* Nýsköpunarsjóður Námsmanna).

Kerr, R. A. (1999). A new focus in high-latitude climate. *Science*, 284:241–242.

Kodera, K. (1994). Influence of volcanic eruptions on the troposphere through stratospheric dynamical processes in the Northern Hemisphere. *J. Geophys. Res.*, 99:1273–1282.

Kodera, K. and Yamazaki, K. (1994). A possible influence of recent polar stratospheric coolings on the troposphere in the northern hemisphere winter. *Geophys. Res. Lett.*, 21:809–812.

Limpasuvan, V. and Hartmann, D. L. (1999a). Eddies and the annular modes of climate variability. *Geophys. Res. Lett.*, 26:3133–3136.

Limpasuvan, V. and Hartmann, D. L. (1999b). Wave-maintained annular modes of climate variability. *J. Climate*. In press.

Luers, J. K. and Eskridge, R. (1995). Temperature corrections for the viz and vaisala radiosondes. *J. Appl. Meteor.*, 34:1241–1253.

Marshall, J. and Kushnir, Y. (1997). Atlantic climate variability. White paper; Online at: http://geoid.mit.edu/accp/avehtml.html.

NCDC (1998). *Data documentation for TD 6200 NCDC upper air digital files*. National Climatic Data Center, 151 Patton Ave. Asheville, NC 28801-5001 USA.

Newman, P. A., Gleason, J. F., McPeters, R. D., and Stolarski, R. S. (1997). Anomalously low ozone over the Arctic. *Geophys. Res. Lett.*, 24:2689–2692.

OFCM (1997). *Federal meteorological handbook no. 3: Rawinsonde and Pibal observations*. Office of the Federal Coordinator for Meteorology, Available online at: http://www.ofcm.gov/fmh3/text/.

Peixoto, J. P. and Oort, A. H. (1992). *Physics of climate*. American Institute of Physics, 1 edition.

Seol, D. I. and Yamazaki, K., editors (1997). *Stratospheric sudden warming in 1989 from the viewpoint of atmospheric angular momentum*, number 11 in 21. NIPR Symposium on Polar Meteorology and Glaciology.

Shindell, D. T., Miller, R. L., Schmidt, G. A., and Pandolfo, L. (1999). Simulation of recent northern winter climate trends by greenhouse-gas forcing. *Nature*, 399:452–455.

Shindell, D. T., Rind, D., and Lonergan, P. (1998). Increased polar stratospheric ozone losses and delayed eventual recovery owing to increasing greenhouse-gas concentrations. *Nature*, 392:589–592.

Smagorinsky, J. (1953). The dynamical influence of large-scale heat sources and sinks on the quasi-stationary mean motions of the atmosphere. *Quart. J. Roy. Meteor. Soc.*, 79:342–366.

Steenrod, S. D., Rood, R. B., Lamich, D. J., Rosenfield, J. E., and Govindaraju, R. C. (1991). The minor stratospheric warming of january 1989: Results from STRATAN, a stratospheric-tropospheric data assimilation system. *Mon. Wea. Rev.*, 120:221–229.

Thompson, D. W. J. and Wallace, J. M. (1998). The Arctic Oscillation signature in the wintertime geopotential height and temperature fields. *Geophys. Res. Lett.*, 25:1297–1300.

Thompson, D. W. J. and Wallace, J. M. (2000). Annular modes in the extratropical circulation. Part I: Month-to-month variability. *J. Climate*, 13:1000–1016.

Thompson, D. W. J., Wallace, J. M., and Hegerl, G. C. (2000). Annular modes in the extratropical circulation. Part II: Trends. *J. Climate*, 13:1018–1036.

Wallace, J. M. and Hobbs, P. V. (1977). *Atmospheric science; An introductory survey.* Academic Press, 1 edition.

Wang, J. and Ikeda, M. (2000). Arctic Oscillation and Arctics Sea-Ice Oscillation. *Geophys. Res. Lett.*, 27:1287–1290.

Wilks, D. S. (1995). *Statistical methods in the atmospheric sciences* Academic Press, 1 edition.

Zurek, R. W., Manney, G. L., Miller, A. J., Gelman, M. E., and Nagatani, R. M. (1996). Interannual variability of the north polar vortex in the lower stratosphere during the UARS mission. *Geophys. Res. Lett.*, 23:289–292.